Model Uncertainty of Non-Linear Finite Element Analysis of Reinforced Concrete Beams without Shear Reinforcement

Examining the Effect of Modelling Strategies and Modes of Failure

Tihitina Tilahun Teshome

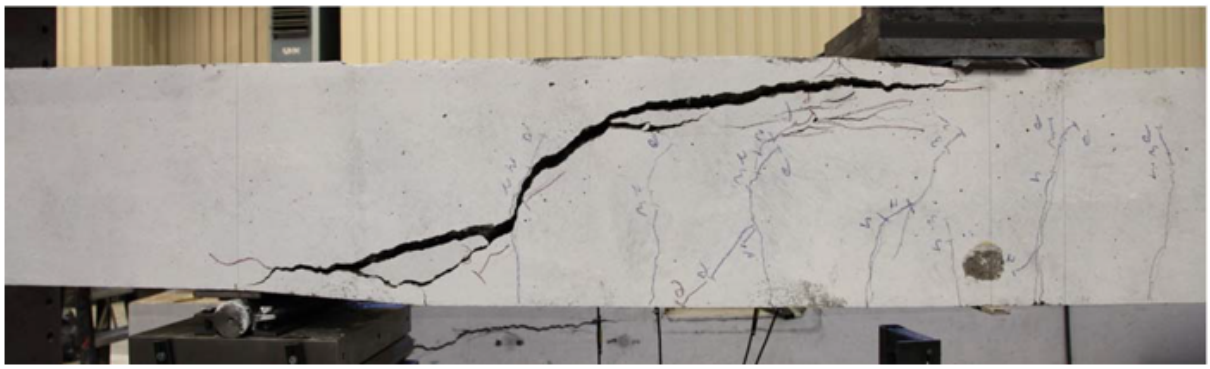

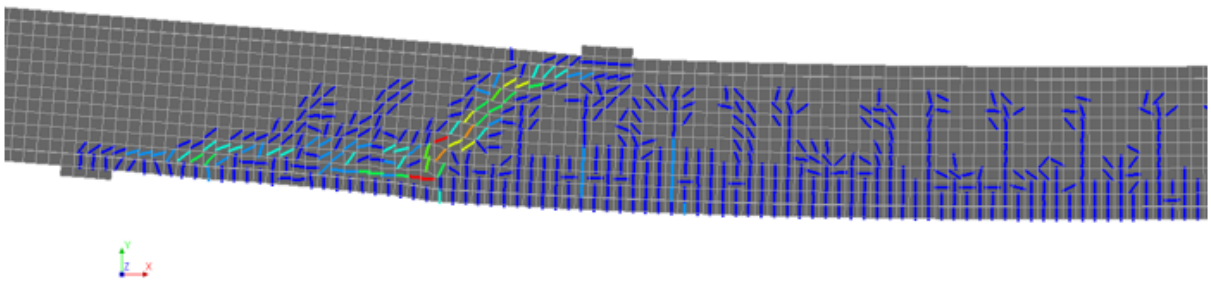

$$\theta = \frac{R_{\text{experimental}}}{R_{\text{numerical}}}$$

TU Delft

Model Uncertainty of Non-Linear Finite Element Analysis of Reinforced Concrete Beams without Shear Reinforcement

Examining the Effect of Modelling Strategies and Modes of Failure

by

Tihitina Tilahun Teshome

to obtain the degree of Master of Science
at the Delft University of Technology,
to be defended publicly on Thursday August 29 at 11:30 AM.

Student number:	4721845	
Project duration:	December 1, 2018 – August 29, 2019	
Thesis committee:	Dr. ir. Max A.N. Hendriks,	TU Delft, Chair
	Prof. dr. ir. Jan G. Rots,	TU Delft
	Dr. ir. Morten Engen,	NTNU
	Dr. ir. Yuguang Yang,	TU Delft

An electronic version of this thesis is available at http://repository.tudelft.nl/.

TU Delft

Preface

This thesis project is part of my 2 years master program in civil engineering at Delft university of technology. The past two years have been the most difficult and rewarding years of my life. This experience has helped me discover who I am as a person and both my strengths and weaknesses which I believe I would not have realised if it were not for the the experience of studying and living at Delft. Studying at TU Delft, I have witnessed the growth in my knowledge and skill as an engineer and discovered there is even more to learn which further inspires me.

I would like to express my immense gratitude to the Delft Global Initiative for awarding me with the Sub-Saharan Africa excellence scholarship and enabling me to study at one of the best universities in the world.

I would also like to express my deep appreciation and gratitude to the chair of my masters thesis committee Max Hendriks for his invaluable insights and critical remarks. I would like to thank him for being collaborative and supportive throughout my thesis project. In addition I would like to thank Jan Rots, Yuguang Yang and Morten Engen for agreeing to join my committee and for their critical comments and assistance through out my thesis project. Our meetings and discussions have been motivating and inspiring in more than one occasion.

I would like to thank God for His continued blessings and my parents who are my role models for their love . I also would like to thank my two sisters and all my close friends and family for their continued support throughout my masters program. It has been quite an unforgettable journey.

Tihitina Tilahun Teshome
Delft, August 2019

Abstract

The aim of this thesis project is to investigate the model uncertainty of non-linear finite element analysis of reinforced concrete structures at ultimate limit state. The study of this model uncertainty is conducted by focusing on the approaches to model concrete cracking, concrete-reinforcement interaction and mesh size. Based on these two aspects of non-linear finite element analysis of reinforced concrete structures, eight different finite element modelling strategies are developed and used to examine model uncertainty.

A set of sixty-seven experiments on reinforced concrete beams without shear reinforcement are chosen to serve as benchmark for the study on the model uncertainty of the eight modelling strategies. Flexural, shear and mixed failure modes are observed in the benchmark experiments with the beams having varying reinforcement ratio, concrete compressive strength and depth. The measure of model uncertainty of all eight finite element modelling strategies is performed firstly by making quantitative comparison of the predicted ultimate capacity using the ratio of experimental to numerical failure load and secondly, by making qualitative comparison of the predicted failure behaviour with that observed in the benchmark experiments. For the quantitative comparison of the failure load, the deviation of values form 1 indicates high model uncertainty with values lower than 1 representing non-conservative predictions and values higher than 1 representing conservative predictions.

The eight modelling strategies are categorized into three groups. The first group of modelling strategies is used primarily to select the shear retention model to be used for the fixed total strain based crack concept and secondly to study the behaviour of both fixed and rotating crack concepts when implemented in combination with embedded reinforcement. Four of the eight modelling strategies are found in this group and only nine representative benchmark experiments are analysed using these modelling strategies. The damage based and aggregate-size based shear retention models are investigated resulting in a mean model uncertainty ratio of 0.86 and 0.82 respectively. This indicates that on average both predict higher ultimate capacity when compared to experimental results with the aggregate size based shear retention model exhibiting higher model uncertainty. Subsequently, based on the qualitative comparison of predicted failure modes, the aggregate size based shear retention model was not capable of predicting shear and mixed mode failure types while the damage based shear retention predicted accurate failure modes for seven out of the nine experiments. On the other hand, the rotating crack model with embedded reinforcement shows failure due to delamination of the concrete cover for all nine experiments which is different from any failure mode observed in the experiments. Replacement of the perfectly bonded embedded reinforcement by reinforcement with bond-slip demonstrated to be able to avoid delamination of the concrete cover and predict the failure modes accurately.

Based on the exploratory findings of the first group, the second group comprises of two modelling strategies and all sixty-seven benchmark experiments are analysed using both modelling strategies. The modelling strategies are fixed crack model with damage based

shear retention model and embedded reinforcement, which is referred to as **F-EB-2-D** and rotating crack model with bond-slip reinforcement named **R-BS-2**. Both modelling strategies, **F-EB-2-D** and **R-BS-2**, have 50 mm mesh size and result in mean model uncertainty ratio of 1.11 and 1.06 respectively. This implies that both modelling strategies on average give conservative predictions of the ultimate capacity with **R-BS-2** showing on average a better prediction. Examination of model uncertainty with respect to failure mode shows that both modelling strategies give higher model uncertainty for experiments with shear failure with **F-EB-2-D** and **R-BS-2** predicting accurate failure modes for 48% and 51% of the experiments respectively. The analyses of the beams with reinforcement ratio of lower than 0.6% showed on average less model uncertainty in both **F-EB-2-D** and **R-BS-2**.

Following the study on **F-EB-2-D** and **R-BS-2**, a third group of modelling strategies is composed by modifying the two modelling strategies to study the effect of mesh refinement on model uncertainty. The mesh size of **F-EB-2-D** and **R-BS-2**, is refined from 50 mm to 25 mm in a critical section of the beams to formulate the modelling strategies **F-EB-3-D** and **R-BS-3** of this group. Sixteen of the benchmark experiments are reanalysed using these modelling strategies and a significant improvement of failure mode prediction is observed with both modelling strategies predicting accurate failure modes for 81% of the 16 experiments. A lowered mean model uncertainty ratio of 0.93 and 0.95 is recorded for **F-EB-3-D** and **R-BS-3** respectively. However, the results of the refined mesh models show slightly non-conservative predictions of the capacity as most of the beams behaved more stiff than when a coarser mesh is used.

The correlation between model uncertainty and numerical failure mechanism is made using a ductility index which is defined as the ratio of the plastic dissipated energy in the reinforcement to the plastic dissipated energy in the system. The relation between model uncertainty and the ductility of the numerical failure mode is studied using 16 of the benchmark experiments analysed using **F-EB-3-D**. The majority of the analyses show that numerical ductile flexural failure modes have model uncertainty ratios close to 1, however the ductility index should be used together with model uncertainty if it is verified that the correct equations are solved accurately.

Contents

List of Figures

List of Tables

1 Introduction

Non-linear analysis of reinforced concrete is an advanced alternative for prediction of the capacity and behaviour of reinforced concrete structures. The need for the application of non-linear principles to analyse the mechanisms that occur in reinforced concrete structural elements arises due to the importance of optimization of resources and the growing complexity of civil structures. Non-linear analysis accounts for the response of structures beyond the linear material and geometric deformations and allows for an elevated use of construction materials.

On the other hand, the complexity of the material properties of concrete after the elastic regime has led to the application of simplified principles of linear elastic analysis. Many building codes provide analytical models that are formulated based on linear elastic theories and empirical relations developed through calibration of large number of experiments.

Analytical methods of analysis of reinforced concrete are approximated due to several factors. Firstly, cracking of concrete and the progressive loss of tensile strength is not directly included in the analytical models. The interaction of concrete and reinforcement further adds to the challenge of analytical formulation. Moreover, the inclusion of multiaxial stress conditions leads to cumbersome and complex analytical models and thus is rarely considered. As a result, analytical models can give close approximations but are not able to provide detailed depiction of actual stress transfer mechanisms.

Analysis of structures using finite element method involves a series of numerical approximations and material models which make it possible to attain reasonable predictions of the behaviour of different load carrying structures. In the past few decades, there has been continuous improvement of this method of numerical simulation.

Non-linear finite element analysis (NLFEA) of reinforced concrete has proved to be an important tool with the growing number of complex and ageing structures among other reasons. NLFEA consists of setting up an idealized mechanical model of the structure, selecting and assigning material models and performing non-linear computations. The accuracy of the predictions using NLFEA is heavily dependent on choices with regards to theses aspects. The non-linear computation can include both physical and geometrical non-linear effects. It involves gradual application of the load and employing an iterative procedure to closely approximate the progressive change of stiffness of the structure.

Although analyses using finite element method have shown considerably satisfying results, the susceptibility of the finite element method to the implemented material models,

solution procedures, the expert making the model and even to the type of software used have made engineers sceptical about the use of NLFEA. The lack of coverage of non-linear analysis in building codes has also contributed to its limited use in the professional engineering world.

The study on the improvement of NLFEA of reinforced concrete structures thus becomes understandably important. It entails the identification and quantification of error in prediction of capacity and behaviour of structures. In addition, standardization of modelling techniques by providing guidelines to help obtain a certain level of uniformity of results from different experts is beneficial.

Model uncertainty of NLFEA of reinforced concrete is the contrast between experimental results and computational predictions. Comparison of numerical predictions with experimental results is used to better understand and improve kinematic compatibility, constitutive models as well as procedures for solving equilibrium equations in numerical simulation of reinforced concrete. In addition, model uncertainty also takes into account the material uncertainty and error due to set-up and measurement of experiments. For this reason, it is important to separate the uncertainty in numerical simulation from other material and physical uncertainties.

1.1. Background

As the field of civil and structural engineering evolves together with advancement of technology, more intricate structures are possible and are being desired. The rising popularity of structures such as shells, slender bridges, cantilevers and presence of dynamic loading conditions requires the knowledge of non-linearity. Majority of these structures are made of reinforced concrete. Thus understanding the non-linear material and geometrical properties of reinforced concrete is crucial for design and analysis of complex structures. Forensic engineering and reassessment of growing number of ageing buildings and infrastructure also require application of non-linear analysis.

To harness the advantages of non-linear effects, analytical and numerical computational methods are being used. However, material uncertainties coupled with the lack of adequate knowledge has left non-linear analysis unpopular in the past. In recent years, the advancement of computational tools such as finite element method, has enabled structural engineers to design and predict the capacity of structures using the principles of non-linearity.

An important computational tool is the finite element method which is applicable to solve continuum problems. Finite element method, as its name implies, functions by dividing the geometry of a structure into discrete elements bounded by nodes. Complex displacement field of the structure is then calculated at these nodal points and interpolated within the elements, creating a continuous displacement field throughout the structure. The approximated displacement field in combination with constitutive models is used to generate strain and stress fields. Many complex structures can thus be analysed in this manner of close approximation. As a result it was able to garner attention from the academic and professional world.

Albeit remarkable accomplishments in recent years, application of finite element method to perform analysis and design of reinforced concrete still faces some challenges. The precise prediction of the failure capacity and mechanism is affected by different aspects of the finite element analysis.

The error in numerical prediction of the capacity of a structure is known as model uncertainty. In the paper by Engen [2], the modelling uncertainty is quantified as the ratio of experimental failure load (R_{exp}) to the numerically predicted failure load (R_{num}) which is described in equation (1.1). The closer the value of θ to 1, the more accurate the numerical prediction is with respect to the experimental outcome and values lower than 1 indicate non-conservative predictions while values higher than 1 show conservative predictions.

$$\theta = \frac{R_{\text{experimental}}}{R_{\text{numerical}}} \tag{1.1}$$

The Fib Model code 2010 [4], specifies the need to verify numerical simulations of non-linear analysis using benchmark experiments. It also provides safety formats applicable for non-linear numerical simulations. The Fib model code 2010 puts forth three different safety formats for NLFEA. The partial factor method, the global resistance method and the probabilistic method. These safety formats incorporate a safety factor that accounts for model uncertainty. These three safety formats are based on different levels of implementation of probabilistic theory.

In all the above mentioned safety formats, a model uncertainty global safety factor is included to account for the mismatch between NLFEA predictions of resistance and the experimentally predicted resistance of concrete structures. This model uncertainty as defined in equation (1.1) includes the physical and numerical uncertainties. Thus, a global safety factor for model uncertainty takes into consideration uncertainties such as spatial variability of concrete strength, different batches of concrete used during construction, the variability in concrete properties due to different suppliers as well as parameters of NLFEA such as idealization of geometry, application of boundary conditions and effects of implemented material models. Model uncertainty is also believed to be dependent on the approaches used during finite element analysis. The set of modelling choices which are necessary for the idealization, discretization and analysis of a physical problem is referred in this report as modelling strategy. A quantified model uncertainty allows us to compare between different modelling strategies.

Development of reliable safety formats that can have wide-spread application is a huge advantage for main-stream use of NLFEA. Fib Model code 2010 [4] states that numerical simulation of concrete structures needs to be validated by the use of benchmark experiments and subsequently the model uncertainty safety factor recommended in the code can be verified or revised.

1.2. Motivation

The pressing issue of sustainability has been of interest to our generation for some time. By understanding that the construction industry is one of the major contributors to climate change, several efforts to improve construction methodology and to optimize the use of construction materials are underway. One alternative for optimized use of construction materials is reduction of the size of structural elements by further exploiting the capacity or resistance of materials for example by utilizing the capacity of materials and structural members beyond their linear elastic regime.

In the past, due to several factors the capacity of structural elements and more importantly concrete structures has been limited to the linear elastic regime. However, this highly conservative and simplified assumption of material and structural behaviour results

in large sizes of structural members and uneconomical design methodologies.

The motivation for this MSc. project is the contribution of non-linear analysis towards optimized use of reinforced concrete. The application of non-linear material and geometric properties aids not only in predicting resistance of structures closest to reality but also allows us to benefit from a higher utilization of material and physical capacity.

1.3. Scope

The scope of this research is limited to model uncertainty of NLFEA of reinforced concrete structures under ultimate loading conditions. In this thesis project only the effects of physical non-linearity are considered with quasi-static loading conditions. The finite element models are developed in 2D work environment with varying concrete crack models, concrete-reinforcement bond models and mesh sizes. To study this model uncertainty, a set of experiments conducted on reinforced concrete beams without shear reinforcement are selected to serve as benchmark.

To assist with numerical simulation of the benchmark experiments, a study of the behaviour of reinforced concrete beams without shear reinforcement is carried out. The governing methods of stress transfer and redistribution along with the role of longitudinal reinforcement and interaction between concrete and reinforcement on the failure characteristics are investigated.

The approaches to model cracking of concrete and concrete-reinforcement interaction are given priority and are studied in detail. Different variants of the concrete crack model as well as the reinforcement model are analysed. For fixed crack concept, two shear retention models are investigated based on accuracy of failure load and failure mechanism predictions.

For this thesis, the multi-purpose software Diana version 10.2 is used to perform the finite element analysis of the benchmark experiments. Among the concrete crack models available in Diana, the total strain based crack model with fixed and rotating crack orientations is considered. Similarly from the methods used to model concrete-reinforcement interaction, the embedded and bond-slip interface reinforcement models are applied. In addition to crack and reinforcement models, the study of the effect of mesh refinement on numerical predictions is also performed.

1.4. Research Objectives

The main objective of this thesis work is to investigate the accuracy of NLFEA in predicting the ultimate capacity of reinforced concrete structures. To fulfil this objective the following series of questions are posed.

• To what extent does the applied modelling strategy influence the model uncertainty?

Firstly different modelling strategies will be established to perform NLFEA of the benchmark experiments. Subsequently, using the collected data from the analysis a link between modelling strategy and model uncertainty is investigated. The model uncertainty will be assessed based on the accuracy of the predicted capacity and the failure mode at ultimate limit state.

• Does the failure mechanism affect the model uncertainty?

In this study, a large number of benchmark experiments are used which exhibit different failure mechanisms, enabling in-depth study into the extent of the contribution of failure

mechanism into modelling uncertainty.

• What is the most robust modelling strategy for reinforced concrete beams without shear reinforcement?

After post-processing of analysis results using different modelling strategies, a study of which modelling choices resulted in better predictions of the behaviour and capacity of reinforced concrete beams without shear reinforcement is performed and possible recommendations are made.

• Is it possible to recommend a modelling strategy that will minimize the model uncertainty for a specific failure mechanism?

The model uncertainty is related with the failure mechanism and a comparison between different modelling strategies on how well they can predict a specific failure mode is made.

1.5. Research Approach

After general understanding of the topic of research, the work plan is divided into four main blocks of activities in order to achieve the above mentioned research objectives and answer the research questions.

• Literature Review

In the past, research efforts have been made to define and quantify modelling uncertainty of NLFEA. For this thesis, some of these researches are studied to get insight into the sources of imperfect predictions when applying NLFEA. In addition, theories behind implemented material models are studied to understand the fundamental concepts as well as have realistic expectations of results. Once the benchmark experiments are chosen, literature on the behaviour of the experiments were reviewed.

• Selection of Benchmark Experiments

To quantify the model uncertainty of a specific finite element model, it is necessary to pick reference structures that serve as a measure of the accuracy of the model. For this purpose, experiments conducted at Delft University of Technology by Yuguang Yang [10] in 2016 on simply supported reinforced concrete beams without shear reinforcement are chosen. Sixty seven out of the one hundred and seven experiments carried out by Yuguang Yang are selected for this thesis.

• Finite element analysis and modelling uncertainty computation

For this thesis project the finite element software Diana version 10.2 is used. Considering the benchmark experiments, eight different modelling strategies are developed to serve the purpose of this research. The large number of benchmark experiments selected required a semi-automated process of creating the finite element models and analysing them. To accomplish this, a parametrized script in python is developed and implemented. Following this, an excel spreadsheet is used to calculate the model uncertainty of each modelling strategy per benchmark experiment.

• Interpret results and perform statistical analysis

Once the model uncertainty is calculated, careful observations and relevant comparisons between the results with respect to the goal of the research are done. Probabilistic distribution of the modelling uncertainty from the obtained results is studied to understand trends.

• Ductility Index Computation

To associate the brittle or ductile nature of the predictions with the computed model

uncertainty 'Theta - θ', ductility index is used. This is also used to highlight the effect of the degree of ductility of a failure mechanism on the precision of the finite element model. The ductility index is defined as the ratio between the plastic dissipated energy in the reinforcement to the total plastic dissipated energy in the system. Diana 10.2 does not have a result output of the plastic dissipated energy. Thus, a series of unloading and manipulating stresses and strains is necessary. A separate python script is developed to assist in computing the plastic dissipated energy.

1.6. Report Outline

The structures of this report is aimed to help the reader understand the decisions made during this thesis project to meet the research objectives and answer the research questions. In this section the contents of each chapter is briefly stated to give an overview of the report.

• Following this introductory chapter, in *Chapter 2* the description of the benchmark experiments used for this thesis project is written. In this, an overview of experimental results and a brief discussion of the failure modes observed in the experiments is provided to help familiarize the reader with the behaviour of the selected set of benchmark experiments.

• *Chapter 3* introduces the reader to the chosen modelling strategies and the aspects of the finite element analysis that are the focus of this thesis. The concrete crack models and concrete-reinforcement interaction models were given precedence among the different aspects of NLFEA and are discussed in this chapter. Subsequently, the three groups of modelling strategies applied in this thesis are introduced.

• In *Chapter 4*, the analysis results and discussion of the first group of modelling strategies that are used to analyse a selected few of the benchmark experiments are presented.

• In *Chapter 5*, a second group of the modelling strategies is established and used to analyse the entire set of benchmark experiments. The analyses results and observed trends are presented and discussed in terms of model uncertainty and failure mode.

• A study on mesh refinement to develop a robust finite element model that can closely simulate the failure behaviour of reinforced concrete beams without shear reinforcement is presented in *Chapter 6* and the results of this study are discussed.

• In *Chapter 7*, the study of the correlation between the numerically predicted failure load and failure mechanism is performed. The method of calculation of ductility index is described and the results of the ductility index of one modelling strategy is analysed with respect to modelling uncertainty.

• Finally, the main *Conclusions* of the study are drawn and *Recommendations* are made for future work.

2

Benchmark Experiments by Yang and Koekkoek [10]

A series of experiments on reinforced concrete beams without shear reinforcement were conducted in Delft university of Technology from April 2015 to August 2016. These experiments were conducted by Yuguang Yang for a study on the transition from flexural to shear failure of reinforced concrete beams without shear reinforcement. Three main types of failure modes were observed in this series of experiments. These are flexural, shear and mixed failure. To study the modelling uncertainty of NLFEA, experiments that have high precision in setup and data recording as well as proper measurement of material properties are chosen. To study the modelling uncertainty due to the finite element computation it is appropriate to reduce the error in the experiments to pinpoint the computational methods that are leading to inaccuracies. However, when working with concrete, material uncertainty is an inevitable aspect that can bring variations in the expected outcomes of experiments. To take these variations into account, repeated experiments are useful. Considering these issues, the experiments done by Yuguang Yang proved to be ideal for a study such as this. In addition, the experimental setup of the support and load condition are such that accurate idealization into a finite element model could be done with ease. Out of 107 experiments carried, 67 are selected for this thesis project, with some experiments being repeated. The purpose for which these experiments were conducted also made them compelling from the perspective of understanding the effect of failure mechanisms on accurate numerical prediction. Originally, these experiments were carried out to study the shear capacity of concrete beams and the mechanisms involved in brittle shear failures. The transition from flexural to shear failure is also studied to determine the critical shear span to depth ratio responsible for shear failure. In these experiments, different failure mechanisms are observed as the position of the point load was altered.

2.1. Description of Benchmark Experiments

The 67 benchmark experiments were conducted on 16 simply-supported reinforced concrete beams without shear reinforcement. The geometric and material properties of these 16 specimens are summarized in table 2.1. Numerous experiments were carried out on each beam.

The benchmark experiments are classified into three series of tests named A, B and C.

This classification is based on geometrical and material characteristics of the beam specimens. The A and B-series experiments are comprised of beams having a concrete grade of C65 while the C-series has C30 grade concrete. In addition, the beams in the B-series experiments have a height (H) of 500mm while the A and C-series have 300mm height (H). All the beams have a width of 300mm and a length of 8m with a constant clear span of 5m. The reinforcement ratio (ρ) of the beams varies from 1.2% to 0.45% with same top and bottom reinforcements and effective depth (d).

To identify each of these experiments, a nomenclature was established. The example below illustrates this nomenclature as described in the experimental report [10].

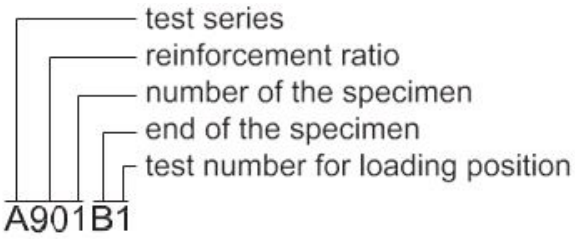

Figure 2.1: Nomenclature of benchmark experiments [10]

Table 2.1: Properties of 16 reinforced concrete beams without shear reinforcement used for the benchmark experiments

No.	Name	$f_{c,cubic}$ (MPa)	Reinforcement	H (mm)	d (mm)	ρ (%)
1	A121	77.5	$3\phi20$	300	269.5	1.17
2	A122	78.2	$3\phi20$	300	270.5	1.16
3	A123	79.2	$3\phi20$	300	270	1.16
4	A901	78.5	$1\phi12 + 2\phi20$	300	274	0.9
5	A902	78.5	$1\phi12 + 2\phi20$	300	276	0.9
6	A751	78.5	$3\phi16$	300	274.5	0.73
7	A752	78.5	$3\phi16$	300	273	0.74
8	A601	78.5	$1\phi10 + 2\phi16$	300	275.5	0.58
9	A602	78.5	$1\phi10 + 2\phi16$	300	272.5	0.59
10	B701	81	$3\phi20$	500	471.5	0.67
11	B702	81.7	$3\phi20$	500	471.5	0.67
12	B501	81.8	$1\phi16 + 2\phi20$	500	471.5	0.59
13	B502	81.9	$1\phi16 + 2\phi20$	500	472.5	0.59
14	C901	23.7	$1\phi12 + 2\phi20$	300	271.5	0.91
15	C751	23.7	$3\phi16$	300	270	0.74
16	C451	23.7	$3\phi12$	300	272.5	0.42

The aim of these experiments is to study the transition between flexural and shear failure in reinforced concrete beams without shear reinforcement. The 67 experiments were conducted by moving the location of a point load applied at the top of the beams. As a result the shear span designated as 'a' in figure 2.4a varies for each experiment. All the benchmark experiments were performed using displacement-controlled loading.

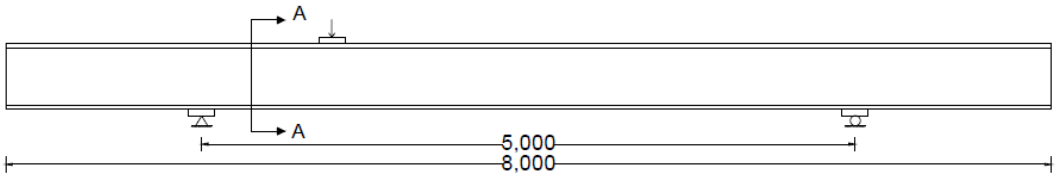

Figure 2.2: Longitudinal view of a typical beam used for benchmark experiments

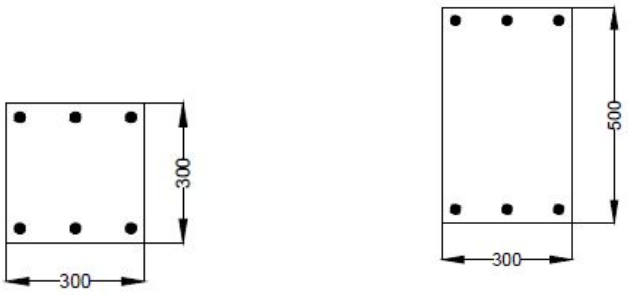

(a) A and C series (b) B series

Figure 2.3: Section A-A view of beams in benchmark experiment

2.2. Experimental Program

The experiments were conducted to make the utmost use of the beams. As a result up to five experiments were conducted on each of the 16 beams. This was made possible by utilizing both ends of the beam.

As illustrated in figure 2.4, the first experiment has a long shear span with the target of obtaining flexural failure. The following experiment has a reduced shear span in an effort to obtain shear failure. Once shear failure is obtained, the shear crack is strengthened as shown in figure 2.4(c) and the position of the load is moved to test a different shear span in order to check the point of transition of failure mode. The supports are also shifted to make use of the remaining undamaged section of the beam end. When one end of the beam can no longer be used, the position of the load is shifted to the other end of the beam and a similar procedure is followed.

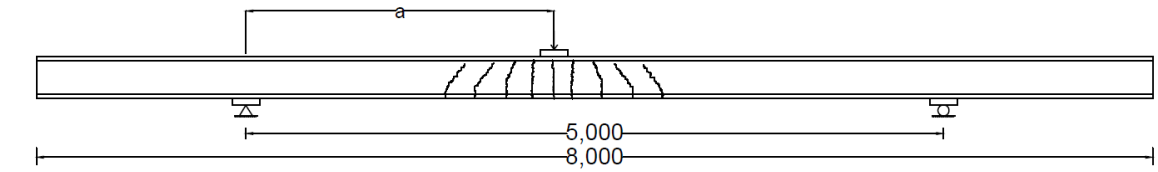

(a) First test

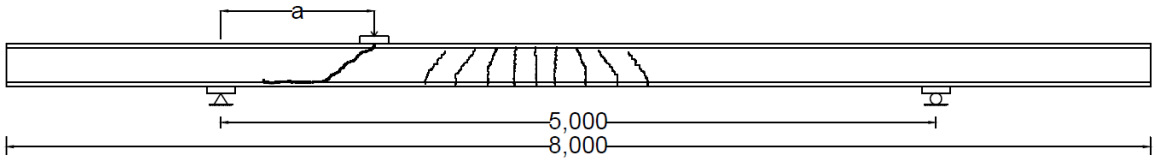

(b) Second test

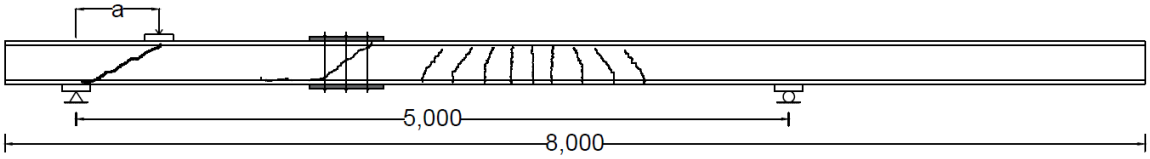

(c) Third test

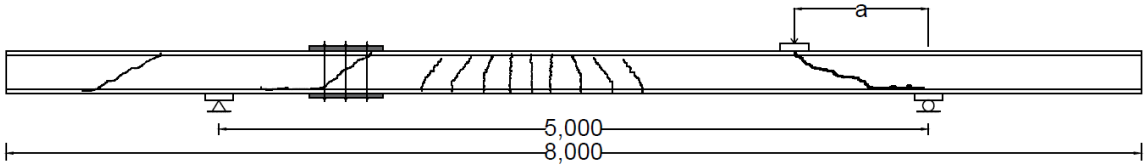

(d) Fourth test

Figure 2.4: Illustration of the experimental approach

2.3. Overview of Experimental Results

Three types of failure modes are observed in the benchmark experiments. These are flexural failure, shear failure and mixed (flexural/shear) failure. Based on the following observations, failure mechanisms were identified and peak loads were measured in these experiments.

A. Flexural failure: identified by the yielding of the reinforcement. In this type of failure, the peak load is sustained for a considerable amount of deflection of the beam before a complete loss of capacity is observed. Primary or flexural cracks precede the yielding of the reinforcement.

B. Shear failure

B.1 Flexural shear failure: This mode of failure is identified as the loss of capacity of the beam due to formation of secondary cracks along the reinforcement in the tensile and compressive zone before yielding of the reinforcement. This is the shear failure recorded in the experiments.

B.2. Shear compression failure: this occurred in few experiments where the point load

is located close to the support. A compression strut from the point load to the nearby support is created and failure of the beam is caused because of crushing of the compressive strut.

C. Mixed(Flexural/Shear) failure: this is the case when reinforcement yields just before flexural shear cracks occur. The peak load is sustained for a short period before the beam undergoes a brittle failure. Two load levels are recorded in Yang's experiments for this type of failure. First at the yielding of reinforcement and second just before shear failure.

The mode of failure and the respective peak load of each benchmark experiments is given in the table 2.2 with the shear slenderness of experiments.

Table 2.2: Experimental failure load and failure mechanism of 67 benchmark experiments

Name	a/d	Exp. Failure Load(KN)	Exp. Failure Mode
A121A1	5.57	115.3	Flexure
A121A2	4.66	138.8	Flexure
A121A3	3.71	144.6	Shear
A121B1	3.71	160.6	Flexure+ shear
A122A1	2.77	194.7	Flexure+ shear
A122B1	3.7	152.3	Shear
A123A1	3.7	136.5	Shear
A123A2	2.96	139	Shear
A123B1	4.63	134.9	Flexure
A123B2	4.26	148.9	Flexure+ shear
A901A1	4.56	105.6	Flexure
A901A2	3.65	123.9	Flexure
A901A3	2.74	145	Shear
A901B1	3.21	127.5	Shear
A901B2	2.74	124.2	Shear
A902A1	3.61	120.7	Shear
A902A2	3.26	136	Flexure
A902A3	2.9	149.4	Shear
A902B1	3.99	121.5	Flexure
A902B2	3.62	124.2	Shear
A751A1	3.64	97.1	Flexure
A751A2	2.73	118.4	Shear
A751B1	2.91	106.7	Shear
A751B2	3.1	110.1	Flexure+ shear
A752A1	3.3	108.7	Flexure
A752A2	3.11	119	Shear
A752A3	3.11	121.6	Flexure+ shear
A752B2	2.56	141.9	Flexure+ shear
A601A1	3.63	80.3	Flexure
A601A2	2.72	102.1	Flexure
A601B1	2.54	118.7	Flexure+ shear
A601B2	2.18	123.2	Flexure with shear cracks
A602A1	2.75	98.8	Flexure
A602A2	2.57	112.8	Flexure
A602A3	2.55	114.2	Flexure+ shear
A602B1	5.5	58	Flexure
A602B2	2.39	110.9	Flexure+ shear
B701A1	4.77	175.5	Flexure
B701A2	4.24	179.5	Flexure
B701A3	3.71	185.7	Flexure
B701B1	3.61	193.6	Flexure
B701B2	3.18	202.4	Shear
B702A1	2.65	183.2	Shear
B702B1	3.08	164.9	Shear
B501A1	4.24	168.5	Flexure
B501A2	3.71	166.4	Shear
B501B1	3.82	165.7	Shear
B502A1	4.02	166.9	Flexure
B502A2	3.81	175.1	Flexure
B502A3	3.6	173.6	Shear
B502B1	3.6	173.2	Shear
C901A1	4.6	98.5	Flexure
C901A2	3.68	103.4	Shear
C901A3	3.68	84.1	Shear
C901B1	4.6	101.7	Shear
C751A1	4.63	76.5	Flexure
C751A2	3.7	84.5	Shear
C751A3	3.7	86.7	Shear
C751B1	3.7	82.8	Flexure+ shear
C451A1	4.59	41.4	Flexure
C451A2	3.67	58.6	Flexure
C451A3	2.75	73.5	Flexure+ shear
C451A4	2.75	70.9	Shear
C451B1	3.12	58.5	Flexure
C451B2	2.94	70.6	Flexure+ shear
C451B3	2.94	67.1	Flexure
C451B4	2.57	77.2	Shear

2.4. Description of Failure Modes in Benchmark Experiments

Flexural, shear and mix mode failure types were observed in the benchmark experiments. Understanding the method of transfer and redistribution of stresses at failure is important to set up a robust finite element model. The two observed fundamental failure modes were flexure and shear. Thus, the governing mechanisms involved in flexural and shear failure are discussed in this section.

A. Flexural Failure

Flexural failure is the loss of strength of reinforced concrete beam due to high bending moment acting on its cross-section. Flexural failure is characterized by the development of compressive and tensile stresses along the height around the neutral axis of the beam. The tensile stresses in reinforced concrete are carried by the reinforcement once the concrete reaches its tensile strength. Following this, the compressive forces in the cross-section are equilibrated with the tensile forces in the reinforcement. Depending on the amount of the reinforcement either the concrete crushes or the reinforcement yields with progressive loading.

The formation and propagation of the flexural cracks formed due to cracking of concrete affect the load-displacement graph of the reinforced concrete beams. Initiation and spacing of flexural cracks is governed by the interaction between concrete and reinforcement.

With cracking of concrete, the tensile forces will be transferred to the reinforcements and this causes the development of bond stresses along the reinforcement. The bond stress and diameter of the reinforcement govern the spacing and width of the subsequent cracks. After the crack formation stage, the reinforcement is assumed to solely carry the tensile forces with significant increase in the stresses resulting in the yielding of the reinforcement. This is then known as flexural failure since it is an outcome of a predominant bending moment acting on a cross-section. For under-reinforced or ductile beams this failure is fairly easy to predict as the material uncertainty of the reinforcement is lower than that of concrete. In addition, factors involved in the interaction between concrete and reinforcement are more or less understood in this case.

B. Shear Failure

The failure of beams due to large shearing forces and formation of diagonal cracks along the span is known as shear failure. Shear failure is a brittle phenomena unlike flexural failure especially in concrete beams without shear reinforcement. It can be classified into two types based on the stresses that result in the diagonal shear cracks. These are flexural shear failure and shear compression failure. The former, as the name implies, is formed when flexural cracks gradually incline as a result of high shear stresses. The latter, on the other hand, is a product of the formation of diagonal cracks due to formation of a strong compressive strut between the point of loading and the nearby support. Shear compressive failure is defined by the crushing of concrete due to this compressive strut.

In concrete beams without shear reinforcement the transfer of shear stress is governed by three components. These are, direct shear transfer in the compressed part of the cross-section, aggregate-matrix interlock in the cracked section and dowel action of longitudinal reinforcement. These three methods of shear transfer are depicted in figure 2.5.

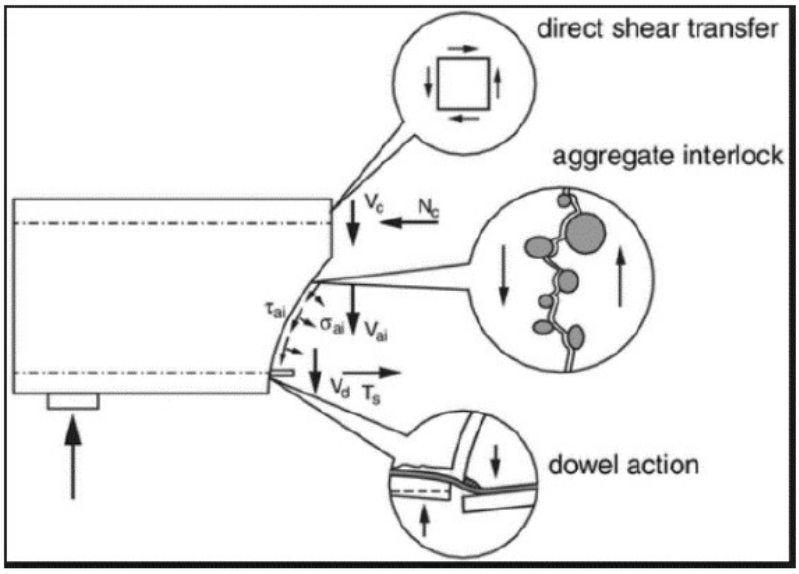

Figure 2.5: Shear stress transfer mechanisms [11]

3

Finite Element Modelling Strategies

The study of model uncertainty of finite element analysis is associated with a selected set of modelling choices. A set of modelling choices which is necessary for the idealization, discretization and analysis of a physical problem is referred in this report as a modelling strategy. The term solution strategy is commonly used in literature, however to avoid any misinterpretation with the term solution procedure, the name modelling strategy is used for this thesis work.

3.1. Definition of Finite Element Modelling Strategy

A non-linear finite element modelling strategy includes four main aspects:

a. Idealization of the physical problem

This includes the reasonable idealization of the geometry of the structure, the boundary conditions, applied loads and the interaction with surrounding structures.

b. Discretization of the idealized problem

This involves the type and size of finite element. Choosing the finite element that divides the geometry of the structure implies the selection of the displacement field. Once the displacement field is established the strains can be drawn from it. Discretization involves how and where these strains are calculated within an element. Among the choices in this aspect of the modelling strategy are analytical versus numerical integration, Gaussian versus Newton-Cotes numerical integration and even regular versus high integration scheme.

c. Constitutive model

At the heart of a structural finite element computation lies the relation that links the strains computed by the finite element to the stresses the structure is experiencing - this is the constitutive relation. Since the constitutive relation is material dependent, most finite element software provide material models that capture the linear and non-linear behaviour by taking user inputs. Choosing the appropriate material model along with a realistic input is a crucial part of modelling strategy.

d. Solution procedure

A non-linear analysis takes into account the varying stiffness of the structure as the loading progresses. In order to successfully calculate the stiffness of the structure at a given load step, an iterative process of solving the system of equations to obtain equilibrium between internal and external forces in the discretized system is necessary. Thus setting the appropriate method of applying the load, step size of the load, type of iterative solution

procedure, norm and tolerance of the chosen norm to accurately follow the equilibrium path are mandatory for a non-linear finite element modelling strategy.

A finite element modelling strategy should be specific for the problem at hand. Each of the four aspects of the modelling strategy should be selected carefully; failure to do so can lead to issues from solving an entirely different problem due to inaccurate idealization to misleading results due to inappropriate material models. The guideline for non-linear finite element analysis of concrete structures [6] serves as a starting point for engineers to perform NLFEA of concrete structures with a certain degree of accuracy.

3.2. Approach to Model Cracking in Concrete

To include the presence and effect of cracks in materials such as concrete, two types of crack modelling methods are available. These are the discrete and smeared crack concepts.

Discrete crack concept works by assigning non-linear interface elements where cracking is expected. The advantage of this method is that the simulation of cracking is done by a selected few interface elements that form a discontinuity in the continuum elements. The computation of crack strains and stresses need only be done for these interface elements and not the continuum elements. This method requires an earlier knowledge of the location and orientation of the crack in order to assign the interface elements simulating crack while the rest of the geometry is assigned linear elastic material properties.

The second method involves the smearing out of cracks throughout the continuum elements. This method allows a more realistic simulation of cracks. The exact location and orientation of cracks especially in a matrix-aggregate composite material such as concrete is difficult to pre-determine. In addition, a discrete crack with a distinct direction of propagation throughout the loading history does not mimic reality. Such is the case in reinforced concrete structures with distributed fracture. Due to the unpredictable behaviour of shear cracks especially in the absence of stirrups and distributed flexural cracks, smeared crack approach is the most realistic alternative for reinforced concrete beams.

The smeared crack concept, first introduced by Rashid [7], is based on having a stress-strain relation of the continuum element that can describe the process of crack formation. As described in the thesis dissertation by Rots [8], this approach also allows the switch from an initial isotropic stress-strain law to an orthotropic relation once crack initiates with the crack plane serving as the axis of orthotropy.

In Diana, different material models based on the smeared crack approach are available. One of them is the total strain based crack model. This crack model uses stress-strain relation based on total strain. In the total strain based crack model different approaches to model cracking are available. A common approach uses coaxial stress-strain concept which applies the constitutive relation in the principal strain direction. This is known as rotating crack model since the axis of application of the stress-strain relation shifts together with the direction of the principal strain vector. The rotating crack model has proved to give acceptable results for reinforced concrete structures over a long period of time. Another approach is the use of a fixed coordinate system for the constitutive model known as fixed crack concept. This approach has a fixed direction of the stress-strain relation upon the formation of cracks and the crack plane is used as the axis for a constitutive coordinate system. The second approach imitates more of the physical nature of cracks and thus becomes interesting.

For both the crack concepts the stress is calculated in the direction of crack. The crack

coordinate system is shown in figure 3.1.

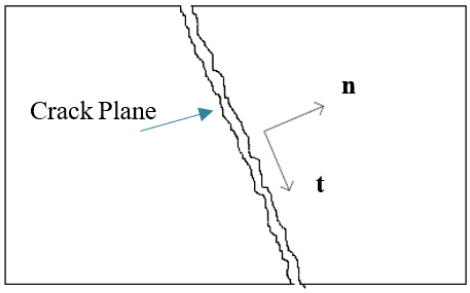

Figure 3.1: Crack coordinate system

The strain is computed in the local element axis and transformed into the direction of the crack plane using a transformation matrix given as equation (3.1). The difference between the rotating and fixed crack concepts is that the transformation matrix is fixed upon crack initiation for the fixed crack concept while it is continually calculated for the rotating crack concept based on the direction of the principal strain vector as that is the assumed crack plane.

$$\Delta\epsilon_{\mathrm{nt}} = \mathbf{T}\epsilon_{\mathrm{xy}} \tag{3.1}$$

For this thesis project both of these crack concepts will be investigated by applying them in different modelling strategies.

A particular aspect of the fixed crack concept is the issue of the shear stiffness of cracked surface. Fixing the crack orientation implies that the crack plane and the principal strain as well as the principal stress directions are not aligned. This raises the need to consider the presence of shear stresses on the fixed crack plane. The shear stiffness of a cracked section is governed by different factors and is believed to deteriorate based on the crack opening width. Thus the shear stiffness behaviour of the cracked surface needs to be incorporated in the fixed crack model.

Different shear behaviour models are available in Diana, however the damage based shear retention and the aggregate size based shear retention models will be studied for this thesis. It is crucial to verify the shear retention behaviour since the benchmark experiments do not possess shear reinforcement. The guideline for non-linear finite element modelling of concrete structure [6] recommends that explicit verification of shear retention model is necessary when using fixed crack model for reinforced concrete beams without shear reinforcement. A description of the two shear retention models implemented will be discussed.

A. Fixed Crack Model-Damage Based Shear Retention

This shear retention model reduces the shear stiffness with the same rate as the normal stiffness of the crack plane. The updated shear stiffness after cracking will then be:

$$G_{\mathrm{cr}} = \frac{\mu E}{2(1+\nu)} \tag{3.2}$$

Where, G_{cr} is the shear stiffness of the cracked surface, μ is the reduction factor for Young's Modulus on the cracked plane, E is the Young's Modulus and ν is the Poisson's ratio.

B. Fixed Crack Model-Aggregate Size Based Shear Retention

As mentioned in section 2.4, shear stresses in a cracked concrete are transferred through aggregate-matrix interlock mechanism. Along with factors such as the roughness and shape of the crack as well as concrete strength [9], aggregate interlock plays a fundamental role in the transfer of shear stresses on a cracked surface. The fractured surface in concrete experiences both the crack opening and shearing drift or displacement. As the shear displacement occurs, the contact area between the aggregate and matrix keeps changing predominantly due to local crushing of the matrix.

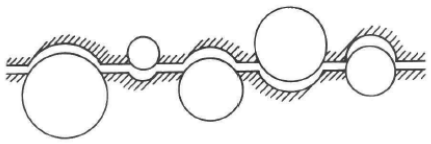

Figure 3.2: Aggregate-matrix interlock on a cracked surface [9]

This local crushing of the cement matrix by itself contributes to the initial increase of the shear stress on a crack. However after a certain shear strain value the shear stress drops to a constant value. Figure 3.3a shows this relation by Gambarova [5].

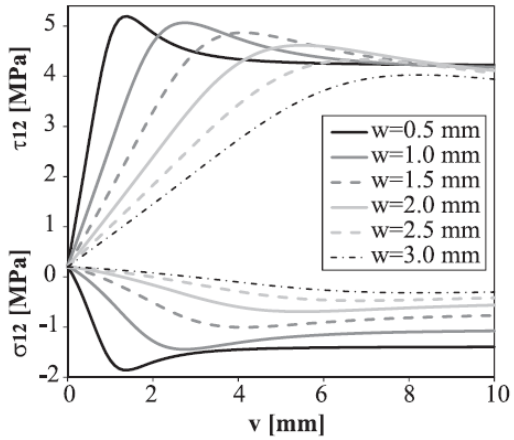

(a) Normal and shear stress versus vertical displacement of crack for differenet crack width

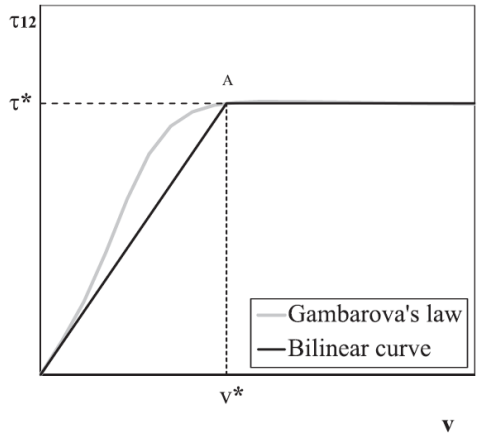

(b) Gambarova's relation and bi-linear representation of shear stress versus shear displacement

Figure 3.3: Relation between shear stress and vertical displacement [1]

A bi-linear representation of this relation shown in figure 3.3b is presented by Belletti et al. [1] which simplifies the relation shown in figure 3.3a and defines a shear stiffness reduction factor (β) based on the bi-linear assumption. Belletti et al. [1] also neglects the aggregate interlock effect for crack width higher than maximum aggregate size.

On the other hand, Diana provides an even more simplified linear expression for the shear reduction factor (β) that guarantees zero shear stiffness when the crack width reaches half the maximum aggregate size given by equation (3.3).

$$\beta = 1 - \frac{2\epsilon_{\mathrm{n}} h}{d_{\mathrm{agg}}} \tag{3.3}$$

Where ϵ_n is the crack strain normal to the crack surface, h is the element size and d_{agg} is the maximum aggregate size. Considering these series of simplifications of the aggregate-matrix interlock effect, the performance of the fixed crack model using the aggregate size based shear retention model was decided to be examined in this thesis.

3.3. Approach to Model Bond in Reinforced Concrete

The interaction between concrete and reinforcement dictates the structural response of reinforced concrete. The approach in computational mechanics to model the bond between concrete and reinforcement is an area of interest in NLFEA of reinforced concrete.

In Diana finite element software, the simulation of bond between concrete and reinforcement can be done in three ways. These are embedded reinforcement, bond-slip interface reinforcement and concept of tension-stiffening.

Embedded Reinforcement

This reinforcement model in Diana was formulated in a way to simulate perfect bond between concrete and reinforcement. To realize this the embedded reinforcement does not have its own degrees of freedom. It acquires the displacement and strains of the so-called 'Mother' element that it is embedded in. The mother element in this case is the concrete continuum element. This ensures perfect bond between concrete and reinforcement.

Bond-Slip Reinforcement

Bond-slip reinforcement on the other hand incorporates the deterioration of bond stress between concrete and reinforcement with relative slip. To model this behaviour, interface elements are used between the reinforcement and the surrounding concrete elements. The reinforcement element type can either be a truss or beam element. Diana does not output integration point results since the integration scheme of the reinforcement element and the interface element are not the same. As a result, the bond traction stress and relative slip between the reinforcement and concrete can only be extracted at the nodes.

Thus, the important aspect of using this reinforcement model is the type of bond stress-slip relation specified for the interface elements between concrete and reinforcement. Several bond-slip relations are provided in Diana, however for this thesis the one recommended by fib model code 2010 [4] is considered.

Fib Model Code 2010 puts forth a local bond-slip relation defined by the following piecewise function for the bond stress.

$$\tau_{bo} = \tau_{bmax}\left(\frac{S}{S_1}\right)^{\alpha} \qquad for 0 \leqslant S \leqslant S_1 \tag{3.4a}$$

$$\tau_{bo} = \tau_{bmax} \qquad for S_1 \leqslant S \leqslant S_2 \tag{3.4b}$$

$$\tau_{bo} = \tau_{bmax} - (\tau_{bmax} - \tau_f)\left(\frac{S - S_2}{S - S_3}\right) \qquad for S_2 \leqslant S \leqslant S_3 \tag{3.4c}$$

$$\tau_{bo} = \tau_{bf} \qquad for S \geqslant S_3 \tag{3.4d}$$

Where τ_{bo} is the bond stress value for a given slip whereas τ_{bmax} and τ_{bf} are the maximum bond-stress for a given concrete compressive strength and minimum friction traction stress respectively. S1, S2, S3 and S are the slip respective to the bond stress level. Figure 3.4a illustrates a typical bond stress-slip relation. These formulae are used to quantify the bond stress- slip relation depending on the mean concrete compressive strength.

	1	2	3	4	5	6
	Pull-Out (PO)		**Splitting (SP)**			
	$\varepsilon_s < \varepsilon_{s,y}$		$\varepsilon_s < \varepsilon_{s,y}$			
	Good bond cond.	**All other bond cond.**	**Good bond cond.**		**All other bond cond.**	
			unconfined	**stirrups**	**unconfined**	**stirrups**
τ_{bmax}	$2.5\sqrt{f_{cm}}$	$1.25\sqrt{f_{cm}}$	$7.0\cdot\left(\frac{f_{cm}}{25}\right)^{0.25}$	$8.0\cdot\left(\frac{f_{cm}}{25}\right)^{0.25}$	$5.0\cdot\left(\frac{f_{cm}}{25}\right)^{0.25}$	$5.5\cdot\left(\frac{f_{cm}}{25}\right)^{0.25}$
s_1	1.0 mm	1.8 mm	$s(\tau_{bmax})$	$s(\tau_{bmax})$	$s(\tau_{bmax})$	$s(\tau_{bmax})$
s_2	2.0 mm	3.6 mm	s_1	s_1	s_1	s_1
s_3	c_{clear} [1)]	c_{clear} [1)]	$1.2s_1$	$0.5c_{clear}$ [1)]	$1.2s_1$	$0.5c_{clear}$ [1)]
α	0.4	0.4	0.4	0.4	0.4	0.4
τ_{bf}	$0.40\,\tau_{bmax}$	$0.40\,\tau_{bmax}$	0	$0.4\,\tau_{bmax}$	0	$0.4\,\tau_{bmax}$

(a) Parameters defining the mean bond stress-slip relation according to equation (3.4)

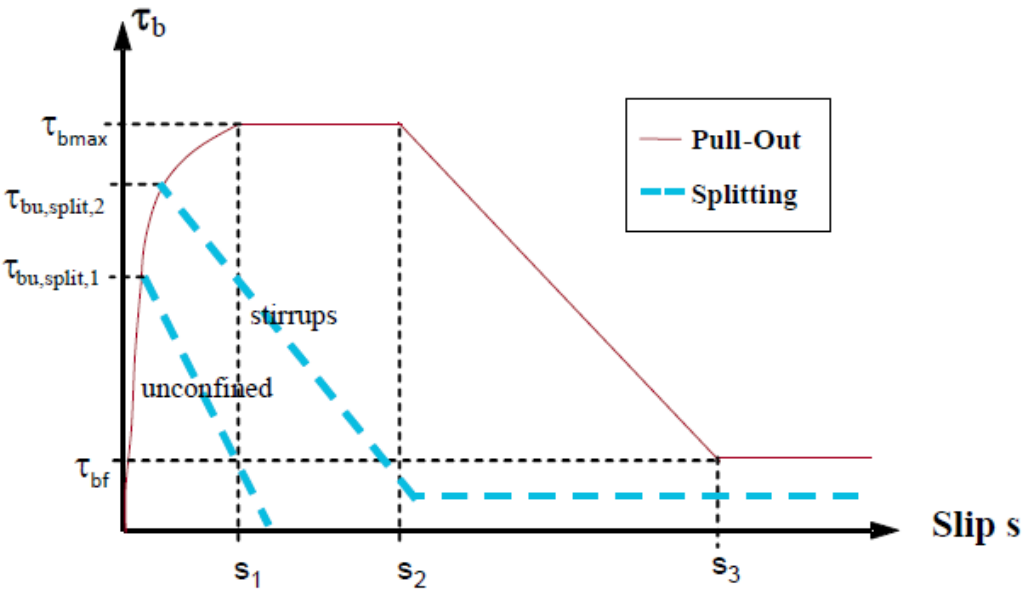

(b) A typical bond stress-slip graph of equation (3.4) for a pull-out and splitting failure tests

Figure 3.4: Local bond stress versus relative slip relation [4]

The concrete-reinforcement interaction in the case of the benchmark experiments is classified under the group specified in column 3 of figure 3.4a. This is based on the concrete cover and bond-conditions of the benchmark experiments. The concrete cover is not large enough to be categorized as a pull-out test. The longitudinal reinforcement used are deformed bars and the beam is unconfined by stirrups.

The Fib model code 2010 [4] suggests that the bond stress should be reduced if yielding of reinforcement occurs along the embedment length. It gives a reduction factor Ω that takes the steel strain after yielding into account to adjust the bond stress. This reduction factor is given by equation (3.5)a and equation (3.5)b.

$$\Omega = 1 \qquad \epsilon_s \leqslant \epsilon_y \tag{3.5a}$$

$$\Omega = 1 - 0.85(1 - e^{-5a^b}) \qquad \epsilon_y \leqslant \epsilon_s \leqslant \epsilon_u \tag{3.5b}$$

with

$$a = \frac{\epsilon_s - \epsilon_y}{\epsilon_u - \epsilon_y} \qquad and \quad b = [1 - \frac{f_{tm}}{f_{ym}}] \tag{3.6}$$

Where ϵ_y and ϵ_u are the steel yield and ultimate strains respectively. f_{ym} and f_{tm} are the yield and tensile strength of reinforcement respectively.

3.4. Description of Generic Finite Element Model

In section 1.5, it is mentioned that eight modelling strategies are investigated for this thesis project. These modelling strategies have some common modelling parameters. A description of the general characteristics of the finite element modelling strategies is outlined in this section.

The variables in each experiments such as the load position, material property and depth are controlled by utilizing a python script, attached in Annex B and Annex C, to easily modify these variables and build the numerical models.

3.4.1. Geometry of the Model

Figure 3.5: Geometry of finite element model

A 2D finite element model is used to numerically simulate the reinforced concrete beams of the benchmark experiments. A typical geometry of the beams is shown in figure 3.5. In section 2.2, it is mentioned that both ends of the beam were utilized to perform the experiments. However on the numerical model only the left end is used since all the analysis of the 67 experiments are performed independently without the inclusion of load history and the beams are symmetric. Thus, the use of different ends of the model is not relevant.

The model has a length of 8m and a clear span of 5m. The width of the beam is 300mm and the height depends on the selected experiment.

3.4.2. Material Properties

In this subsection, the material models of concrete and reinforcement as well as the model for concrete-reinforcement interaction is described.

A. Concrete Material Model

The tensile behaviour of concrete beyond the linear elastic phase is given by Hordijk's exponential softening curve. This is based on tensile fracture energy of concrete as well as

the finite element size(h_{eq}). This was done with the aim to prevent the effect of mesh size on the crack behaviour.

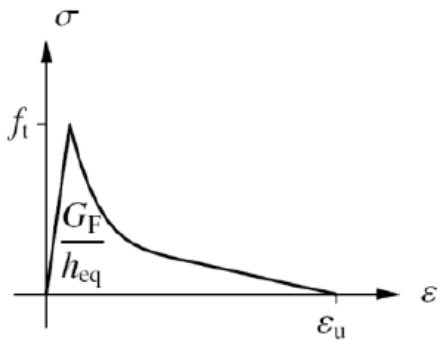

Figure 3.6: Hordijk tension softening model

$$\sigma = \begin{cases} f_t(1+(c_1\frac{\epsilon^{cr}}{\epsilon_u})\exp(-c_2\frac{\epsilon^{cr}}{\epsilon_u}) - \frac{\epsilon^{cr}}{\epsilon_u}(1+c_1^3)\exp(-c_2)) & 0 \le \epsilon^{cr} \le \epsilon_u \\ 0 & \epsilon^{cr} > \epsilon_u \end{cases} \tag{3.7}$$

Where, f_t is concrete tensile strength, ε^{cr} is the crack strain, ε_u is the ultimate strain, c_1 is a parameter given as 3 and c_2 as 6.93 [6].

The parabolic compression model is used to model compression softening behaviour. This is formulated using the compressive fracture energy which is taken as 250 times the tensile fracture energy. The formula implemented in Diana is described in equation (3.8) where G_c is the compressive fracture energy, α_c is the crushing compressive strain, α_u is the ultimate compressive strain and f_c is the compressive strength.

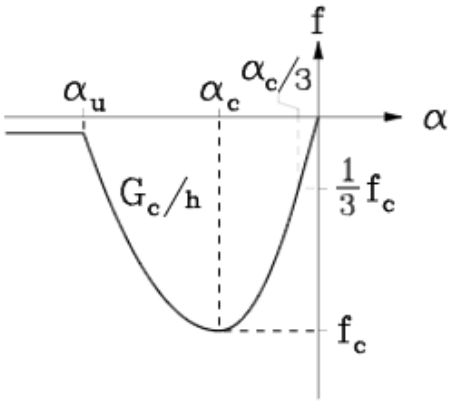

Figure 3.7: Parabolic compression model

$$f = \begin{cases} -f_c\frac{1}{3}\frac{\alpha_j}{\alpha_{c/3}} & \alpha_{c/3} < \alpha_j \le 0 \\ -f_c\frac{1}{3}(1+4(\frac{\alpha_j-\alpha_{c/3}}{\alpha_c-\alpha_{c/3}}) - 2(\frac{\alpha_j-\alpha_{c/3}}{\alpha_c-\alpha_{c/3}})^2) & \alpha_c < \alpha_j \le \alpha_{c/3} \\ -f_c(1-(\frac{\alpha_j-\alpha_c}{\alpha_u-\alpha_c})^2) & \alpha_u < \alpha_j \le \alpha_c \\ 0 & \alpha_j \le \alpha_u \end{cases} \tag{3.8}$$

$$\alpha_{c/3} = -\frac{1}{3}\frac{f_c}{E} \tag{3.9}$$

$$\alpha_c = -\frac{5}{3}\frac{f_c}{E} = 5\alpha_{c/3} \tag{3.10}$$

$$\alpha_u = \min(\alpha_c - \frac{3}{2}\frac{G_c}{hf_c}, 2.5\alpha_c) \tag{3.11}$$

Where, f_c is concrete compressive strength, $\alpha_{c/3}$ is the strain at which one-third of f_c is reached, α_c is the strain at which f_c is reached, α_u is the strain at which material is completely softened, G_c is compressive fracture energy and h is the finite element size.

B. Reinforcement Material Model

A linear strain hardening plastic constitutive relation is used to model the reinforcement. Once the reinforcement yields the stiffness of the steel is reduced to 0.02% of E_s.

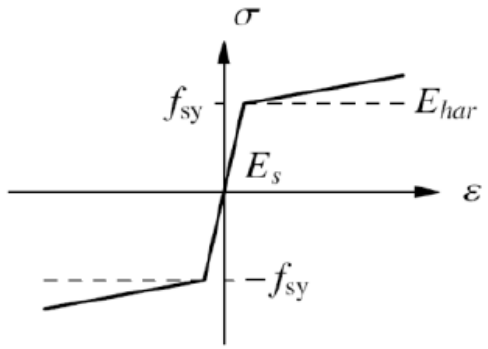

Figure 3.8: Linear hardening material model for steel

C. Bond-slip Interface Material Model

The normal (B_n) and tangential (B_t) stiffness of the bond-slip are given as:

$$B_{\mathrm{n}} = 100 * \frac{E_{\mathrm{c}}}{h} \tag{3.12}$$

$$B_{\mathrm{t}} = \frac{B_{\mathrm{n}}}{10} \tag{3.13}$$

Where, Ec is the Young's modulus of concrete and h is the element size. The 67 benchmark experiments have different material properties thus the formulas to calculate the values of the material properties are given in table 3.1.

Table 3.1: Input material properties for NLFEA

Concrete Material Properties	
Mean cubic compressive strength(f_c)(MPa)	$f_{c,cubic}$
Mean cylinder compressive strength(f_{cm})(MPa)	f_c*0.8
Mean tensile strength(f_{tm})(MPa)	2.12*ln(1+0.1*(f_{cm}))
Characteristic Compressive strength (f_k)(MPa)	f_{cm} - 8
Young's Modulus(E_c)(MPa)	$21500 * (f_{cm} * 0.1)^{0.33}$)
Fracture Energy(G_f)($N\backslash mm$)	$0.073 * (f_{cm}{}^{0.18})$
Compressive Fracture energy(G_c)($N\backslash mm$)	250*G_f
Poisson's Ratio(ν)	0.2
Reinforcement Material Properties	
Young's Modulus (Es)(MPa)	210000
Poisson's Ratio(ν)	0.3

3.4.3. Support Conditions

The support condition is modelled to represent the physical conditions. In the experiments steel plates were placed between the reinforced concrete beams and both the supports as well as the loading jack. In figure 3.9, the elements coloured blue represent the steel plates modelled to support the beam. They have a width of 300 mm, length of 100 mm and depth of 20 mm and linear elastic material properties with stiffness of steel taken as E_s.

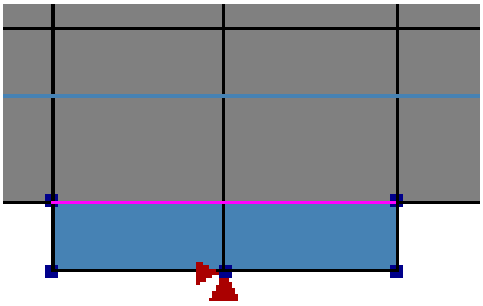

Figure 3.9: Hinge on left support with steel plate and interface elements

2D line quadratic interface elements are modelled between the beams and the plates to avoid the contribution from the stiffness of the steel plates to the stiffness of the beams. The interface elements are shown in pink in figure 3.9. The normal and tangential stiffness of these elements are given as K_n and K_t respectively:

$$K_n = \frac{E_s}{h} \tag{3.14}$$

$$K_t = \frac{K_n}{100} \tag{3.15}$$

Where, Es is the Young's modulus of steel and h is the element size.

3.4.4. Loading Conditions

To include the self-weight of the beam, phased analysis is utilized. Two phases are used. In the first phase the self-weight is applied at once with the assumption that cracking of concrete will not occur. This is later checked and proved to hold true thus all the analysis of the benchmark experiments are modelled this way. In the second phase, the point load is applied using displacement control. Imposed deformation of 1mm is used with load step size of 0.05 mm for all the analysis.

To avoid localization of stresses and to ensure even distribution of the load, steel plates are again used between the applied load and the beam. Interface elements are again used between the steel plate and the beam with properties given in equation (3.14) and equation (3.15).

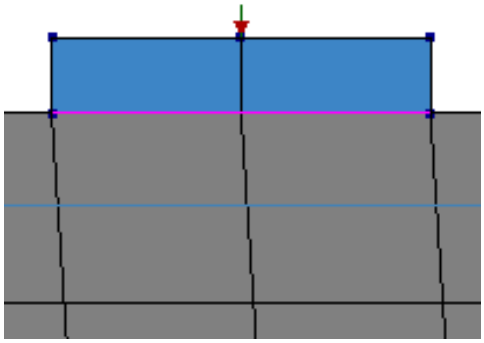

Figure 3.10: Loading condition in finite element models

3.4.5. Mesh

Regular plane stress elements are used to create the mesh of the geometry of the beam. Specifically the element known as CQ16M in Diana is used for the concrete and truss elements are used for the reinforcement. The CQ16M is a quadrilateral element with quadratic interpolation scheme and a Gaussian or 3X3 integration scheme is implemented to calculate the strains and stresses in the elements.

Three different types of meshing are used by varying the element size which are shown in figures 3.11, 3.12 and 3.13. The first two types of mesh are built using 25 mm and 50 mm element size for the entire beam while the third mesh type has 25 mm mesh in the middle section of the beam covering twice the area of the shear span and 50 mm mesh for the rest of the beam as shown in figure 3.13.

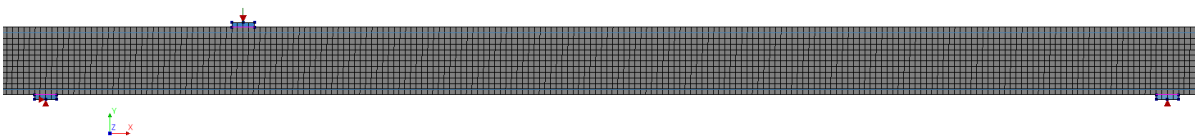

Figure 3.11: Meshing type 1 with 25mm element size

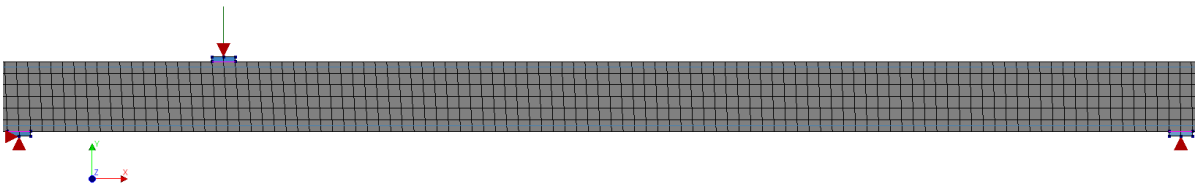

Figure 3.12: Meshing type 2 with 50mm element size

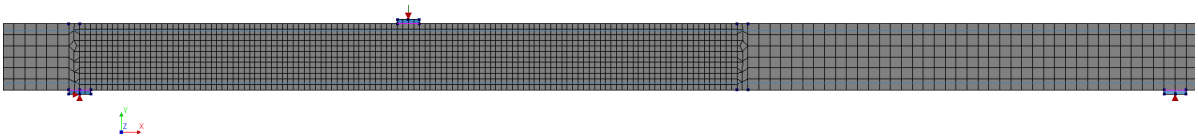

Figure 3.13: Meshing type 3 with 25mm element size only in twice the shear span area

3.4.6. Analysis Procedures

The analysis procedure or the iterative solution procedure and convergence norms used to solve equilibrium equations for all the non-linear finite element analyses was kept constant.

The Secant(Quasi-Netwon Raphson) iterative solution procedure is selected. This is done by referring to another research work [3] on reinforced concrete beams without shear reinforcement that showed the secant iterative solution procedure was preferable due to its ability to surpass the effect of local deformations in the equilibrium path. The computational effort required is also relatively lower then the Full or Regular Newton-Raphson solution procedure.

For the Quasi-Newton iterations the stiffness matrix is not computed for each iteration. Instead of that the stiffness matrix is computed once for the first iteration of a load step increment and then modified for the rest of the iterations for the given load step. The modification of the stiffness matrix is based on the out-of-balance force vector g_1 and the current iterative displacement increment δu_i. However it requires more iterations than the Full or Regular Newton-Raphson.

A maximum of 100 iterations was assigned with energy convergence norm having a tolerance of 0.001 as recommended in the Guideline for NLFEA of concrete structures [6].

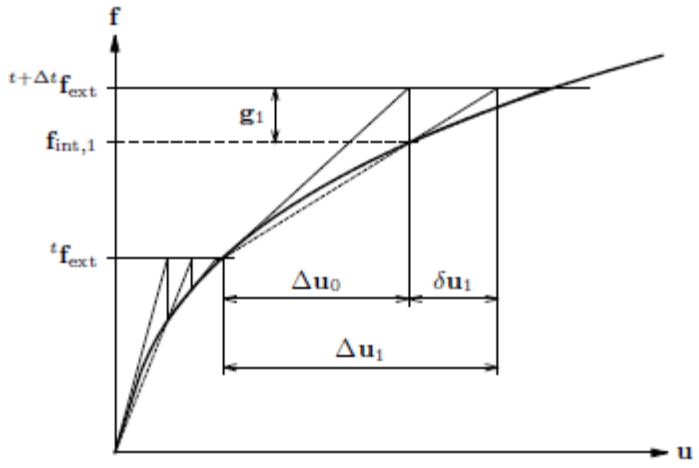

Figure 3.14: Iterative solution procedure for Quasi-Newton iterations

3.4.7. Summary of Finite Element Modelling Choices

Table 3.2: Summary of finite element modelling choices

Geometry of the Model	
Geometry	2-dimensional
Support Condition	
Load/Support plate	Steel Plate with interface elements
Left end	Restrained in X & Y axis
Right end	Restrained in Y axis
Load Condition	
Load application	Displacement control
Imposed deformation	1mm
Load step size	0.05mm
Material Models	
Concrete Material Model	
Concrete crack model	Smeared-Total Strain Based
Crack orientation	Fixed or Rotating
Shear retention	Damage or Aggregate size based
Tensile behaviour	Hordijk
Crack bandwidth	Rots
Compression behaviour	Parabolic
Tension-Compression (Effect of lateral crack)	Vecchio & Collins (Max reduction factor =0.4)
Compression-Compression (Effect of confinement)	Vecchio & Selby
Poisson effect	Damage based reduction
Reinforcement Material Model	
Von Mises plasticity	Linear Strain hardening
Type	Embedded or Bond-slip interface reinforcement
Mesh	
Continuum element type	Regular plane stress
Continuum element name	CQ16M
Reinforcement element type	Truss
Interface element type	2D line quadratic
Element size(h)	25 mm or 50mm
Interpolation scheme	Quadratic
Integration scheme	Gaussian (3X3)
Analysis Procedure	
Iterative solution procedure	Quasi-Newton Raphson (Secant)
Iterations per load step	100
Convergence norm	Energy
Convergence tolerance	0.001

3.5. Overview of Three Groups of Modelling Strategies applied for this Thesis

To quantify and understand the effect of modelling choices on model uncertainty eight different modelling strategies are develop for this thesis project. These eight modelling strategies are grouped into three depending on the purpose of study and the number of benchmark experiments that were analysed using each group.

The first group of the modelling strategies is formulated with the aim to study the simulation of shear behaviour using two of the shear retention models discussed in section 3.2

for the fixed crack models. In addition, the modelling strategies in this group are used to investigate the difference between fixed and rotating crack models by keeping the reinforcement the same in both cases. There are four modelling strategies in this group.

The main aim of formulating the modelling strategies in this group is to get a general understanding of the behaviour of reinforced concrete beams without shear reinforcement in numerical modelling and rule-out the less robust finite element models. Thus only nine of the benchmark experiments are analysed using these modelling strategies. The analyses results of the first group of modelling strategies with regards to model uncertainty are further discussed in chapter 4.

The second group of modelling strategies is developed after studying the results of the first group of modelling strategies. There are two modelling strategies in this group. All of the benchmark experiments are analysed using this group of modelling strategies and the results of these analyses are described and discussed in detail in chapter 5.

The third and last group has two modelling strategies. These two modelling strategies were developed to study mesh refinement on improving model uncertainty. Only 16 of the benchmark experiments were analysed using these two modelling strategies. These 16 experiments are referred to as 'original' or 'first' experiments. The reason for selecting the original experiments is to avoid the contribution of load history on model uncertainty.

All the eight modelling strategies are given names based on the applied variants of crack model, reinforcement bond model, mesh type (figures 3.11, 3.12 and 3.13) and shear retention behaviour. The names of each modelling strategy is listed below with the description of the variants given in table 3.3.

1st group

1. **F-EB-1-D**: **F**ixed crack-**E**m**b**edded reinforcement-Mesh type **1**- **D**amage based shear retention
2. **F-EB-1-A**: **F**ixed crack-**E**m**b**edded reinforcement-Mesh type **1**- **A**ggregate size based shear retention
3. **R-EB-1**: **R**otating crack-**E**m**b**edded reinforcement-Mesh type **1**
4. **R-BS-1**: **R**otating crack-**B**ond-**S**lip reinforcement-Mesh type **1**

2nd group

1. **F-EB-2-D**: **F**ixed crack-**E**m**b**edded reinforcement-Mesh type **2**- **D**amage based shear retention
2. **R-BS-2**: **R**otating crack-**B**ond-**S**lip reinforcement-Mesh type **2**

3 rd group

1. **F-EB-3-D**: **F**ixed crack-**E**m**b**edded reinforcement-Mesh type **3**- **D**amage based shear retention
2. **R-BS-3**: **R**otating crack-**B**ond-**S**lip reinforcement-Mesh type **3**

Table 3.3: Summary of the variants of the eight modelling strategies

1st group				
Name	**F-EB-1-D**	**F-EB-1-A**	**R-EB-1**	**R-BS-1**
Crack orientation	Fixed	Fixed	Rotating	Rotating
Reinforcement type	Embedded	Embedded	Embedded	Bond-slip
Mesh type	1	1	1	1
Shear retention	Damage Based	Aggregate based	NA	NA
No. of experimental samples	9	9	9	1
2nd group				
Name	**F-EB-2-D**		**R-BS-2**	
Crack orientation	Fixed		Rotating	
Reinforcement type	Embedded		Bond-slip	
Mesh type	2		2	
Shear retention	Damage Based		NA	
No. of experimental samples	67		67	
3rd group				
Name	**F-EB-3-D**		**R-BS-3**	
Crack orientation	Fixed		Rotating	
Reinforcement type	Embedded		Bond-slip	
Mesh type	3		3	
Shear retention	Damage Based		NA	
No. of experiments	16		16	

4

Analysis Results of the 1st Group of Modelling Strategies

In this chapter, the results of NLFEA conducted using four modelling strategies on nine benchmark experiments are discussed. The general layout of this chapter is such that detailed description of analyses results for three out of the nine experiments per modelling strategy is presented followed by an overview of model uncertainty for all nine experiments. These three experiments are named A902B2, A752A3 and C451A2. To showcase the numerical simulation capacity of the modelling strategies, the selected three experiments have flexural, shear and mixed failure modes which can help assess the ability of the modelling strategies to accurately predict different failure modes. The Diana crack strain shown for each experiment corresponds to the load step just after the peak load.

The aim of NLFEA using this first group of modelling strategies is to verify shear retention models to be used for fixed crack concept and to study the behaviour of both fixed and rotating crack models when used in combination with embedded reinforcement. For this thesis project, only two shear retention models, namely the damage based and aggregate size based shear retention models, are investigated.

The properties and observed experimental results of the nine experiments are shown in table 4.1, where P_u is the ultimate load and a is the shear span of the beam.

Table 4.1: Characteristics of the nine experiments

Name	$f_{c,cubic}$(MPa)	As(mm^2)	d(mm)	a(mm)	P_u(KN)	Failure mode
A 902B2	78.5	1Ø12+2Ø20	276	1000	124.2	Shear
A752A3	78.5	3Ø16	273	850	120	F+S
A601A2	78.5	1Ø10+2Ø16	275.5	750	102.1	F+S
B701B2	81.1	3Ø20	471.5	1500	202.4	Shear
B502A3	81.9	1Ø16+2Ø20	472.5	1700	173.6	Shear
B701B1	81.1	3Ø20	471.5	1700	193.6	Flexural
C901A3	23.7	1Ø12+2Ø20	271.5	1000	84 .1	Shear
C751A2	23.7	3Ø16	270	1000	84.5	Shear
C451A2	23.7	3Ø12	272.5	1000	52.9	Flexural

4.1. F-EB-1-D : Fixed Crack-Embedded-Mesh 1-Damage Based

The first modelling strategy in this group is **F-EB-1-D**. To showcase the degree of accuracy of this modelling strategy, results of three out of the nine experiments are shown in this section.

A. A902B2- Experiment with shear failure

Table 4.2: Description of benchmark experiment A902B2

Name	R_{exp}(KN)	R_{num}(KN)	θ	Exp. Failure	Num. failure
A 902B2	124.2	123.05	1.01	Shear	Shear

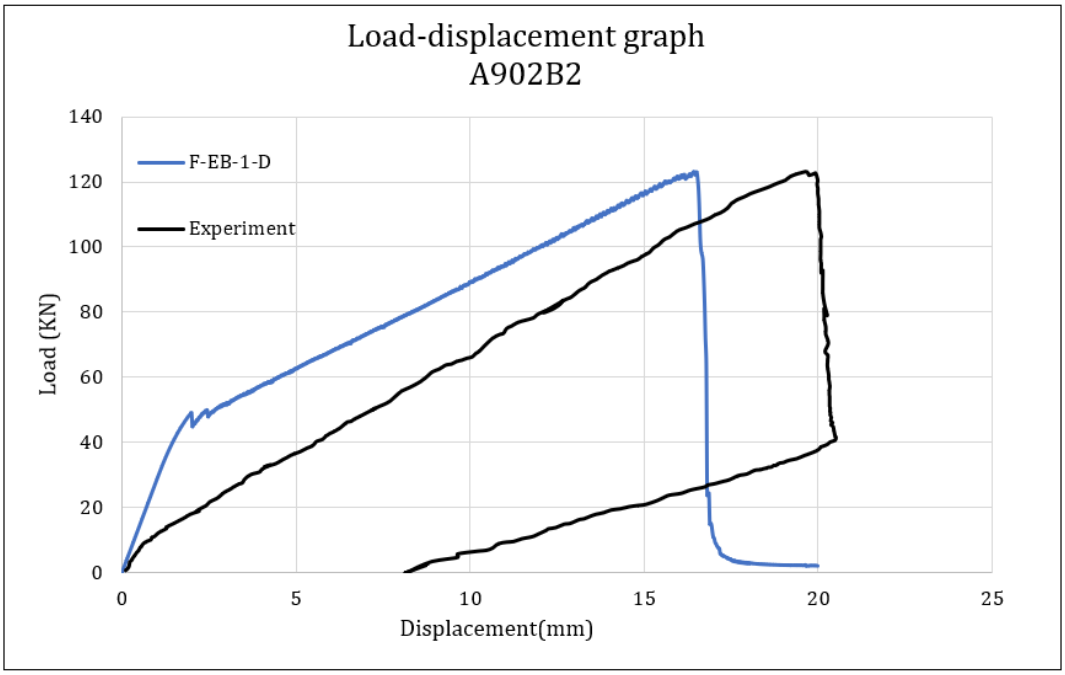

Figure 4.1: Load-displacement graph of experiment-**A902B2** using F-EB-1-D

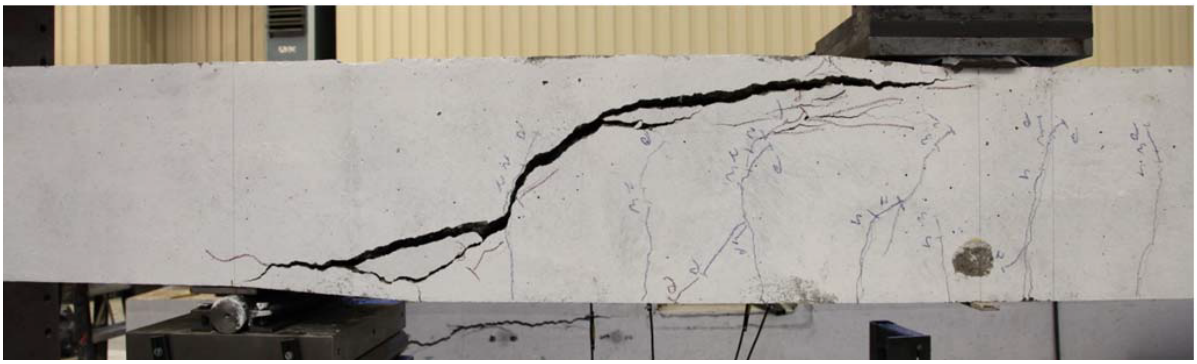

Figure 4.2: Observed experimental crack pattern after failure of A902B2

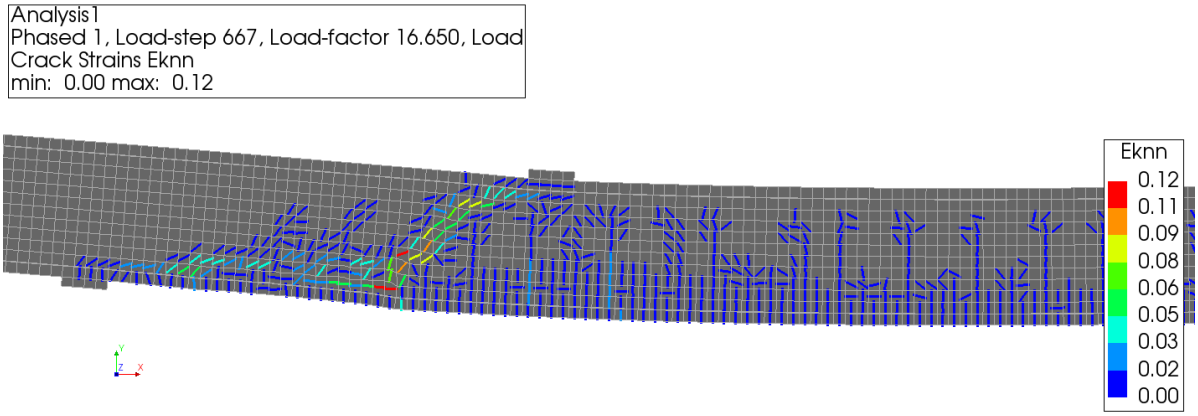

Figure 4.3: Failure crack strain of A902B2 at a load factor of 16.65 mm

The global behaviour of the experiment A902B2 is shown by the load-displacement graph in figure 4.1. This graph shows a difference in initial stiffness of the beam between the numerical prediction using **F-EB-1-D**, and the experimental outcome. This is because A902B2 is not the first experiment conducted on the reinforced concrete beam specimen and the numerical models do not take into account the load history of the experiments. Upon cracking of concrete, the numerical model shows a reduction of the global stiffness of the beam which leads to a similar behaviour as that of the experiment, however, due to the initial high stiffness present in the numerical model, the vertical displacement at the position of the load is lower than that of the experiment. In addition we can also see that the peak load is comparable with that of the experiment with only 1.01 model uncertainty ratio and the numerical model also shows shear failure mode which was also observed in the experiment. The numerical shear failure behaviour of A902B2 is shown in figure 4.3.

B. A752A3- Experiment with flexure and shear failure

Table 4.3: Description of benchmark experiment A752A3

Name	R_{exp}	R_{num}	θ	Exp. Failure	Num. failure
A752A3	120	134.67	0.89	F+S	F+S

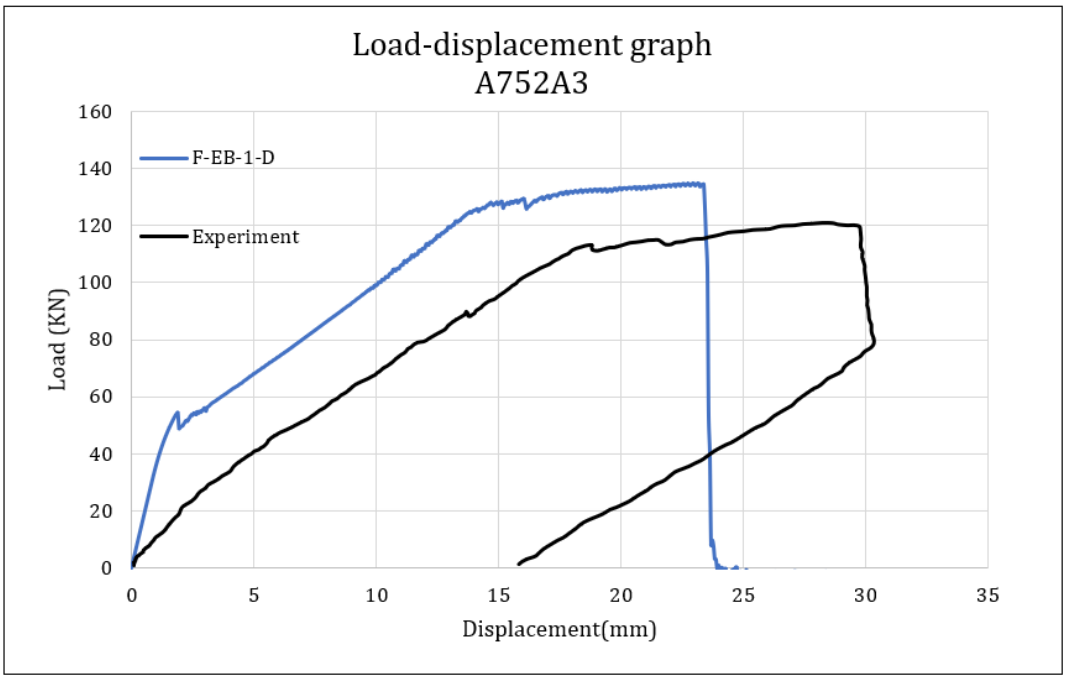

Figure 4.4: Load-displacement graph of experiment A752A3 using F-EB-1-D

Prior to reaching the ultimate state, the numerical model shows a global stiffness which is similar to what is observed in the experiment. The lack of inclusion of load history is still apparent in the stiffer load-displacement relation exhibited by **F-EB-1-D** in figure 4.4. Due to the initial higher stiffness witnessed in the numerical model, the ultimate load is also predicted to be higher resulting in a non-conservative value of the model uncertainty ratio of 0.89. The behaviour of A752A3 from the numerical simulation using the modelling strategy **F-EB-1-D** shows failure with a combination of flexure and shear, which is also referred in the experimental report [10] as mixed mode failure. This failure type is similar to what was observed during the experiment with even the numerical shear failure crack pattern in figure 4.7 showing similarity to that of the experiment as shown in figure 4.5. Figure 4.6 shows the flexural crack strains at the moment of yielding of the bottom reinforcement at a load level of 13.8 mm, these flexural cracks are later morphed or inclined to give the flexural shear cracks that will cause ultimate failure of the beam.

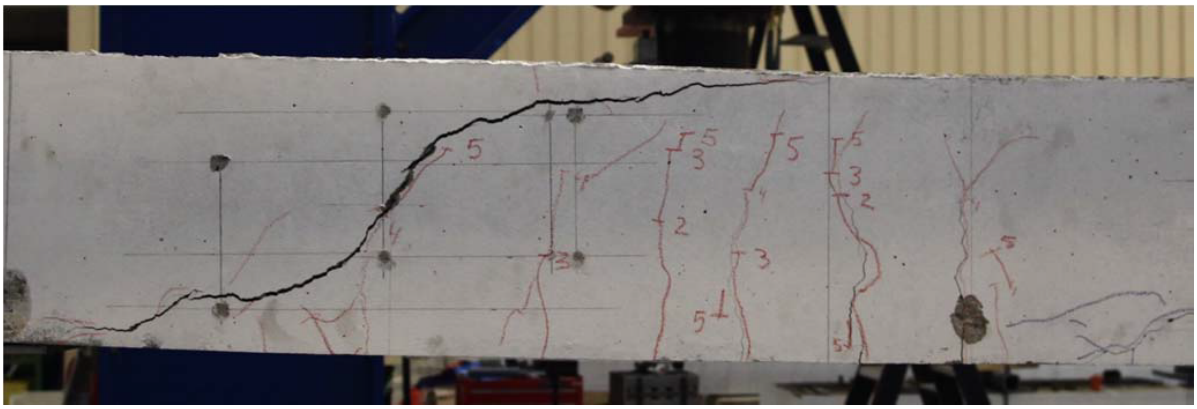

Figure 4.5: Observed experimental failure crack pattern in experiment A752A3

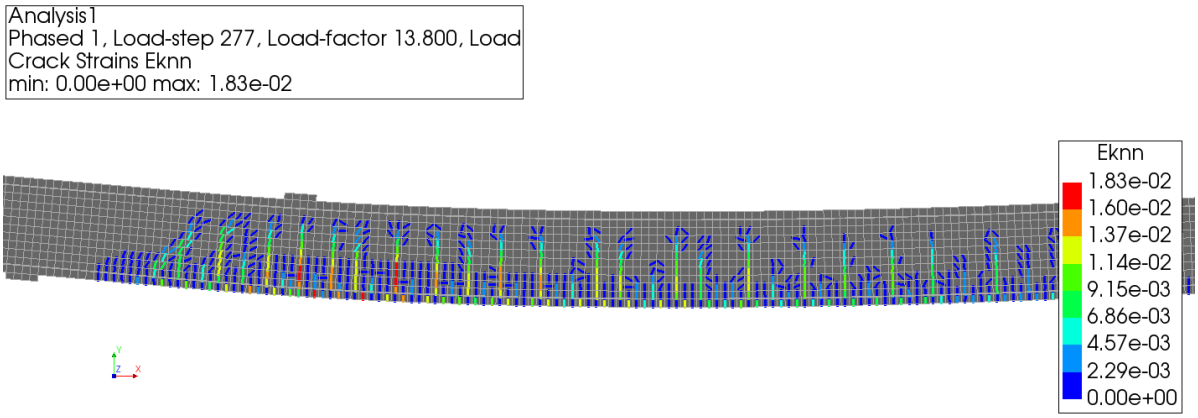

Figure 4.6: Crack strain of A752A3 at load factor of 13.8 mm- bottom reinforcement yields

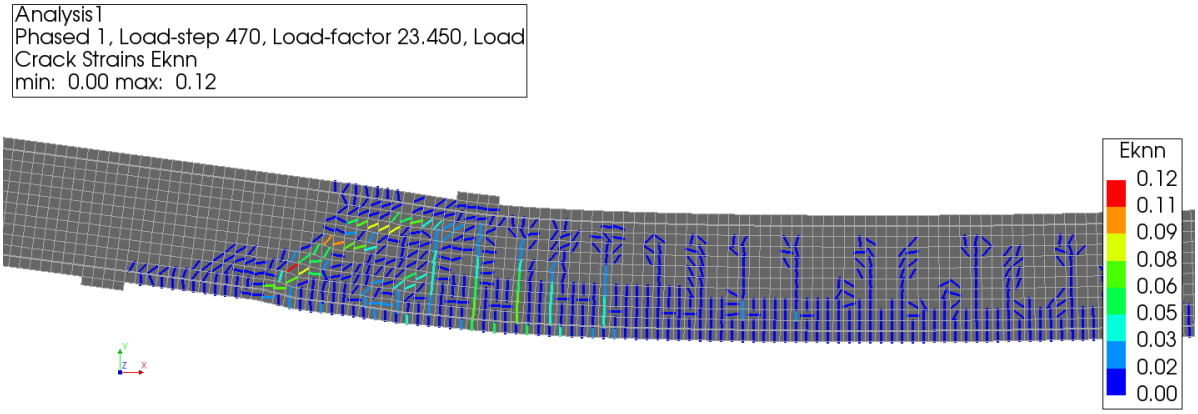

Figure 4.7: Crack strain of A752A3 at load factor of 23.45 mm -brittle shear failure occurs

CA75-1Y, CA75-1S, CC45-1

C. C451A2- Experiment with flexural failure

Table 4.4: Description of the benchmark experiment C451A2

Name	R_{exp}(KN)	R_{num}(KN)	θ	Exp. Failure	Num. failure
C451A2	52.9	65.65	0.81	Flexure	Flexure

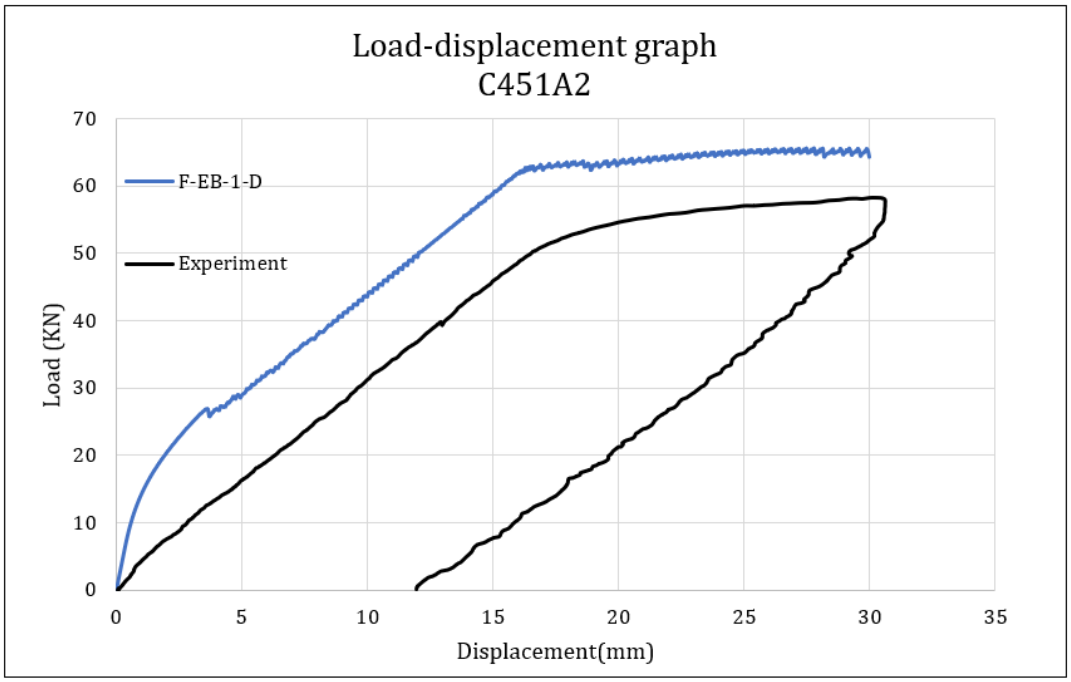

Figure 4.8: Load-displacement graph of experiment-**C451A2** using F-EB-1-D

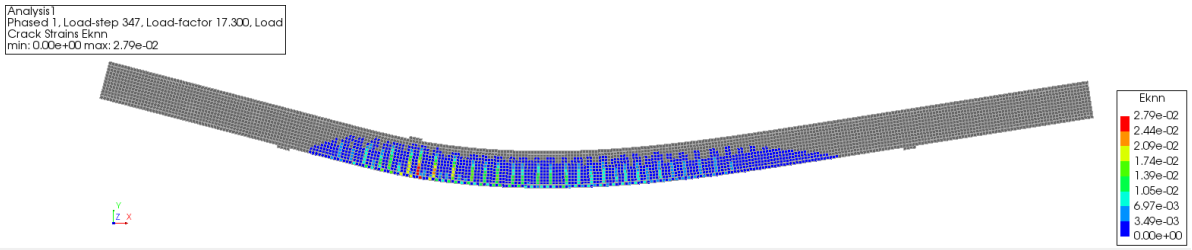

Figure 4.9: Failure crack strain of C451A2 at a load factor 17.3 mm

Figure 4.10: Observed experimental failure crack pattern in C451A2

Looking into the numerically predicted behaviour of C451A2 using the modelling strategy **F-EB-1-D** in figure 4.8, a similarity in the global behaviour is visible with the experimental result. The effect of exclusion of load history is again visible since it creates a shift in the load-displacement relation. The failure mode is accurately predicted as flexural failure which is shown in the crack strain diagram in figure 4.9 with an extended ductile plateau

also visible in figure 4.8. The ultimate load or capacity for flexural failure mode is defined as the yielding of the reinforcement and for this experiment **F-EB-1-D** results in a model uncertainty ratio of 0.81. Although this modelling strategy gives a good prediction of the failure mode the model uncertainty value is relatively high.

4.2. F-EB-1-A : Fixed Crack-Embedded-Mesh 1-Aggregate Size Based

The second modelling strategy in this group is **F-EB-1-A**. The analysis results of the three experiments using this modelling strategy are presented in this section. These experiments are the same as discussed for **F-EB-1-D** in section 4.1.

A. A902B2- Experiment with shear failure

Table 4.5: Description of the experiment-A902B2

Name	R_{exp}(KN)	R_{num}(KN)	θ	Exp. Failure	Num. failure
A 902B2	124.2	132.47	0.94	Shear	Flexure

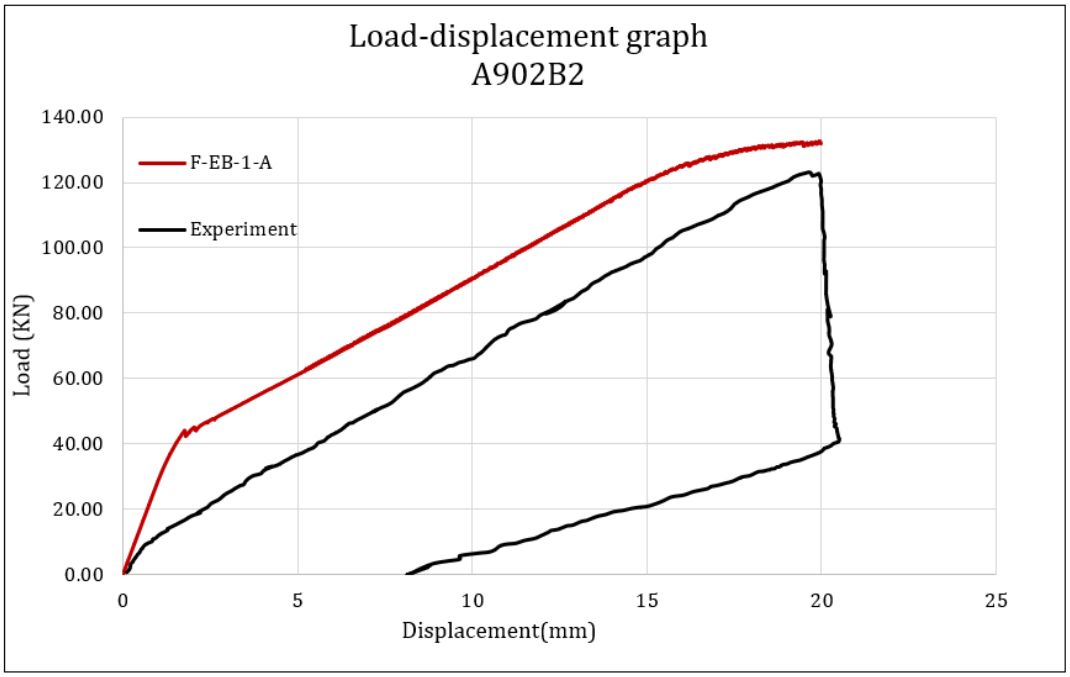

Figure 4.11: Load-displacement graph of experiment-**A902B2** using F-EB-1-A

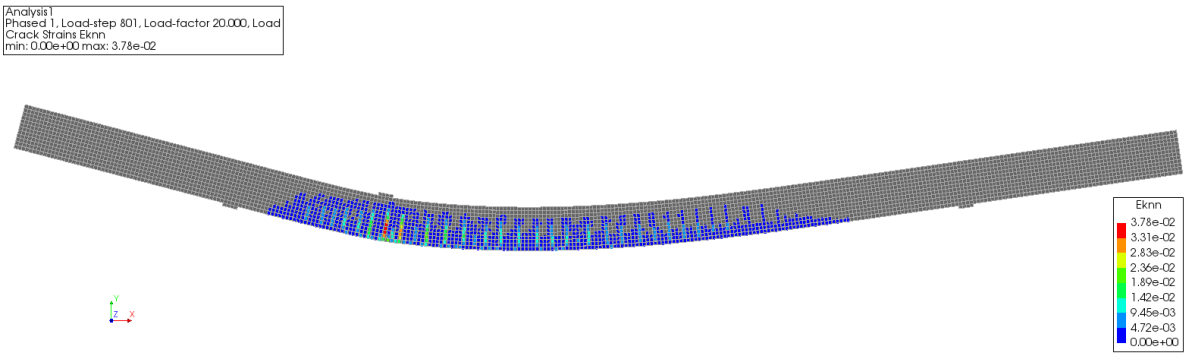

Figure 4.12: Failure crack strain of A902B2 at a load factor of 20 mm

The load-displacement graph of A902B2 using **F-EB-1-A** is shown in figure 4.11 and a comparable load-deformation response with the experiment upon cracking of concrete is visible. However the graph also shows that a higher peak load is attained when using **F-EB-1-A** resulting in a non-conservative model uncertainty of 0.94. The displacement controlled analysis for experiment A902B2 using both modelling strategies **F-EB-1-D** and **F-EB-1-A** is conducted up to the same load level, however **F-EB-1-A** is not able to show the brittle shear failure that was observed in the experiment as well as in the analysis of **F-EB-1-D** as can be seen from figure 4.12.

B. A752A3- Experiment with flexure and shear failure

Table 4.6: Description of the experiment-A752A3

Name	R_{exp}	R_{num}	θ	Exp. Failure	Num. failure
A752A3	120	147.5	0.81	F+S	Flexure

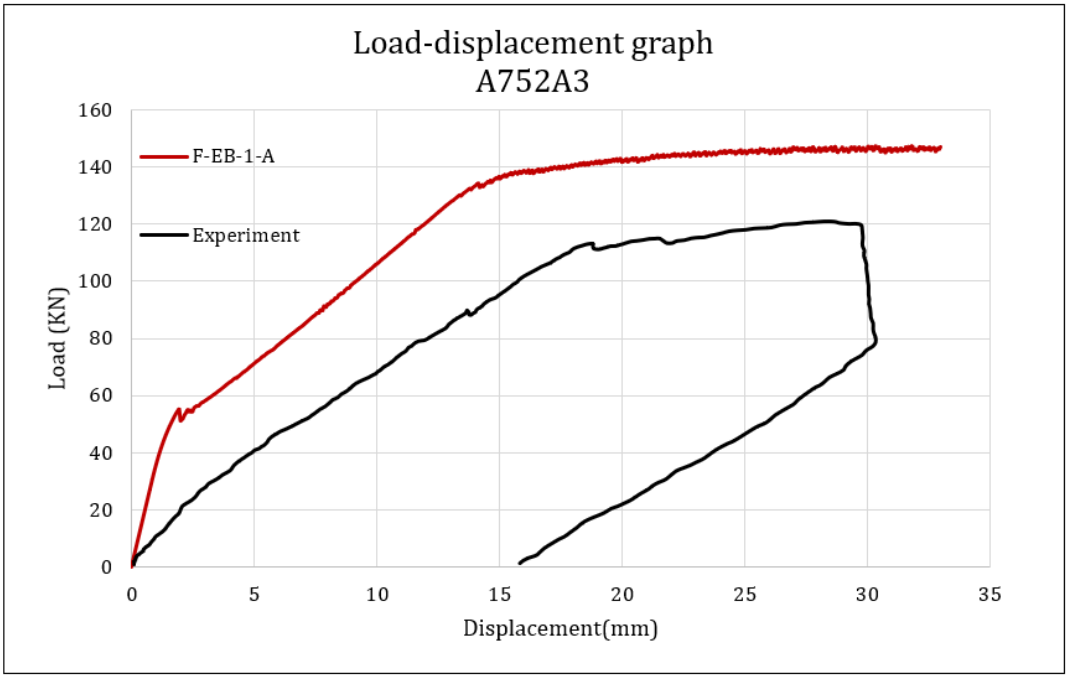

Figure 4.13: Load-displacement graph of experiment A752A3 using F-EB-1-A

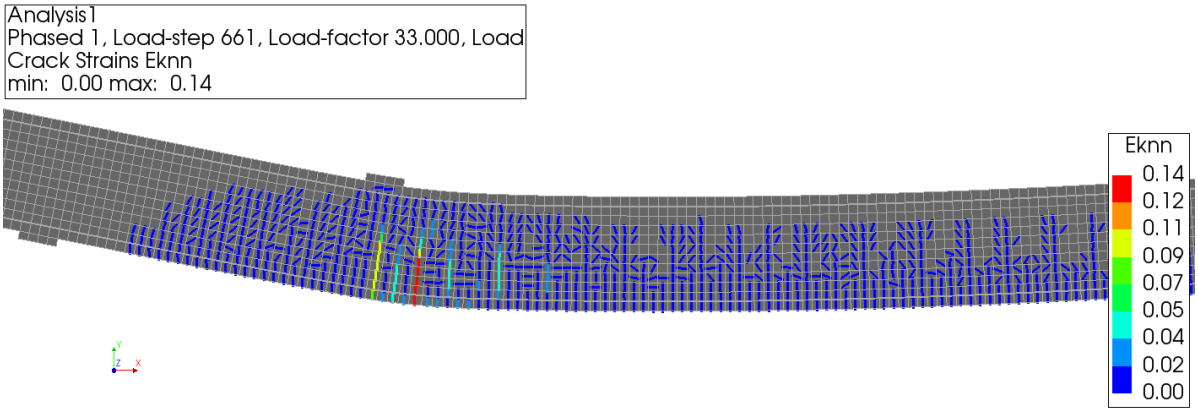

Figure 4.14: Failure crack strain of A752A3 at a load factor mm

The behaviour of A752A3 from the numerical simulation using **F-EB-1-A**, as can be seen in figure 4.13, gives a higher capacity for the same vertical displacement as that of the experiment. This results in a model uncertainty of 0.81 which is a non-conservative or unsafe prediction. In addition the failure mode is flexure with the reinforcement even reaching its ultimate or tensile strength. Figure 4.14 shows the last load step with a large concentrated crack right below the position of the load having a crack width of 3.52 mm. This does not match the experimental observed mixed failure mode unlike what is seen while using **F-EB-1-D**.

C. C451A2- Experiment with flexural failure

Table 4.7: Description of the experiment-C451A2

Name	R_{exp}	R_{num}	θ	Exp. Failure	Num. failure
C451A2	52.9	70.55	0.75	Flexure	Flexure

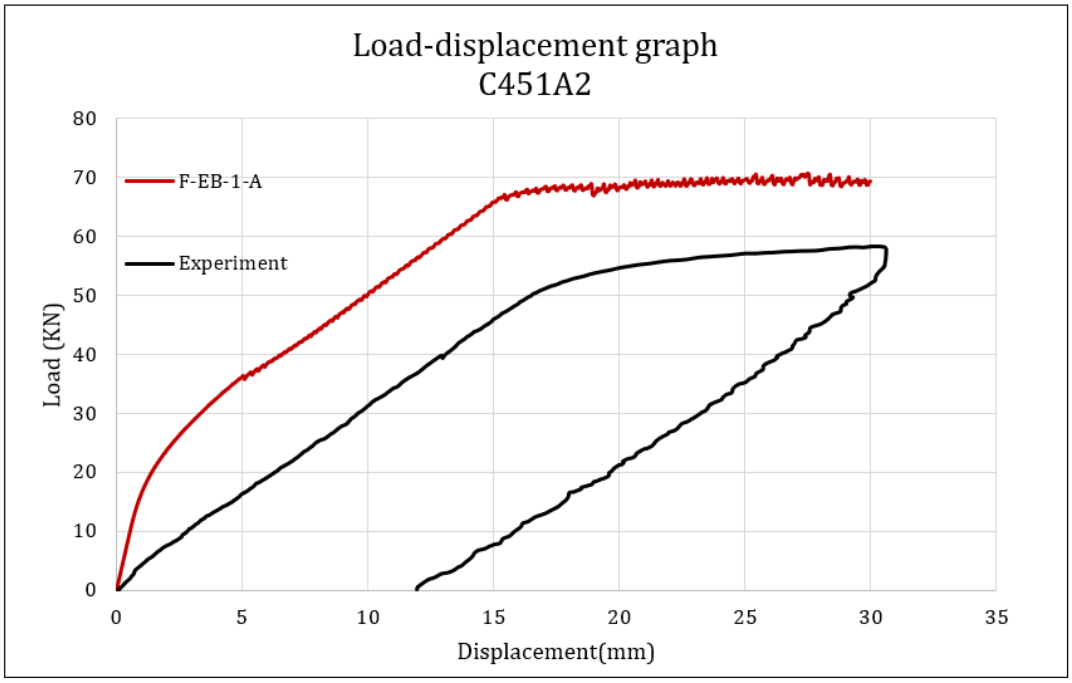

Figure 4.15: Load-displacement graph of experiment-**C451A2** using F-EB-1-A

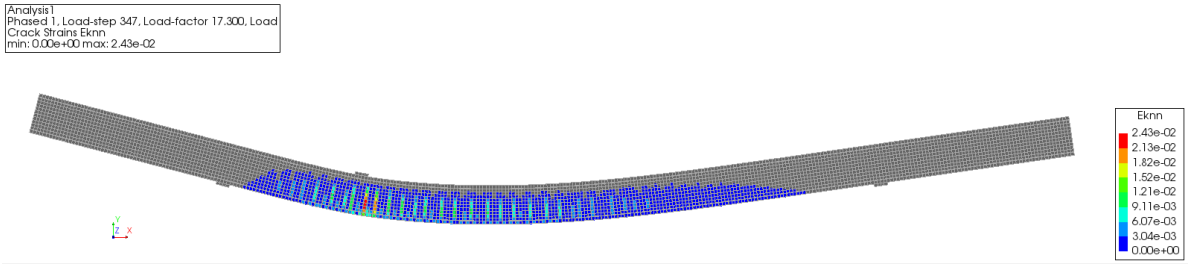

Figure 4.16: Failure crack strain of C451A2 at a load factor of 17.3 mm

As can be seen in figure 4.15, the load-displacement response of C451A2 obtained using **F-EB-1-A** shows a stiff global response when compared to the experiment. Due to this reason, the model uncertainty ratio is 0.75, which indicates a high contrast between the experimental and the NLFEA peak load or ultimate capacity. On the other hand, the failure mode is accurately predicted as flexural failure which can be seen from the crack pattern in figure 4.16 as well as from the ductile plateau of the load-displacement graph in figure 4.15.

4.3. R-EB-1 : Rotating Crack-Embedded-Mesh 1

The third modelling strategy in the first group is **R-EB-1** and in this section analysis results of the same three experiments A902B2, A752A3 and C451A2 using this modelling strategy are presented in this section.

A. A902B2- Experiment with shear failure

Table 4.8: Overview of experimental and numerical results of A902B2 using **R-EB-1**

Name	R_{exp}(KN)	R_{num}(KN)	θ	Exp. Failure	Num. failure
A 902B2	124.2	112.76	1.10	Shear	Delamination

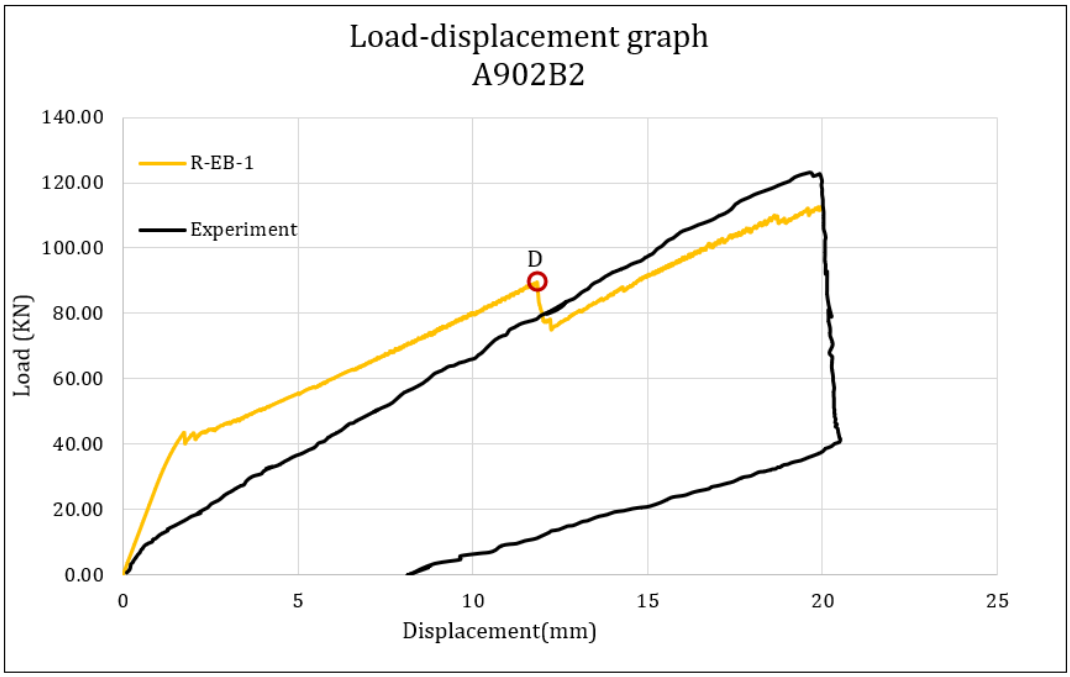

Figure 4.17: Load-displacement graph of experiment-**A902B2** using R-EB-1

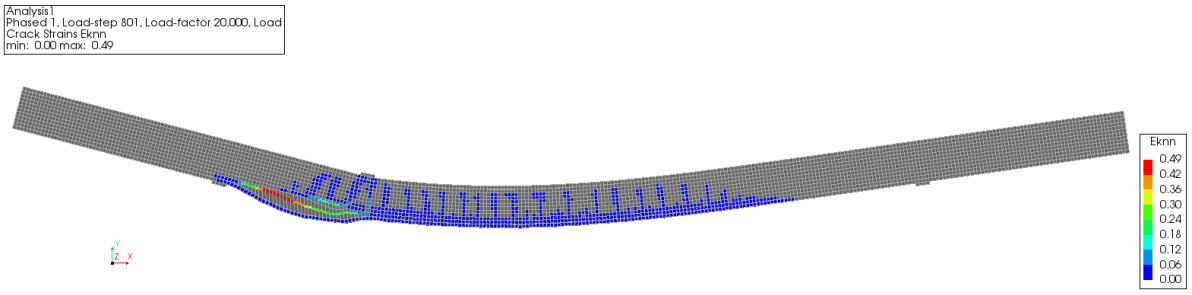

Figure 4.18: Failure crack strain of A902B2 at a load factor of 20 mm

The experiment A902B2 is again analysed using the modelling strategy **R-EB-1** and the load-displacement graph in figure 4.17 is plotted. The global response observed from the analysis does not resemble the experimental output as can be seen from figure 4.17. A loss of strength due to delamination of the bottom concrete cover is observed which is marked in red on the graph shown in figure 4.17. The capacity of the beam does increase even after this point, however the observed failure mode is dominated by the continued delamination of the concrete cover in the shear span of the beam as can be seen from figure 4.18.

B. A752A3- Experiment with flexure and shear failure

Table 4.9: Description of the experiment-A752A3

Name	R_{exp}	R_{num}	θ	Exp. Failure	Num. failure
A752A3	120	132.84	0.90	F+S	Flexure

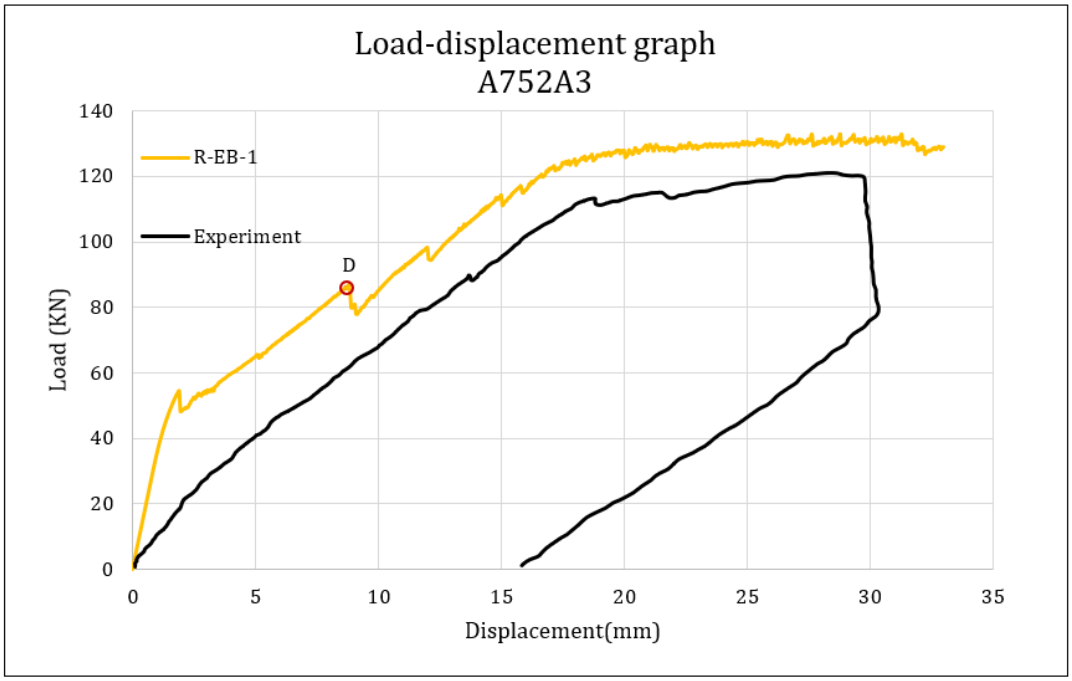

Figure 4.19: Load-displacement graph of experiment A752A3 using R-EB-1

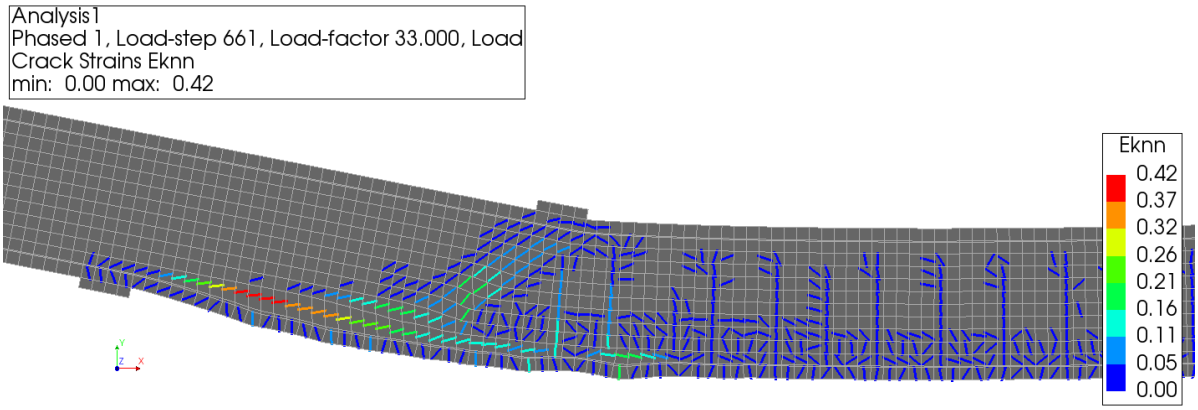

Figure 4.20: Failure crack strain of A752A3 at a load factor mm

The global behaviour of A752A3 as seen from the numerical model using **R-EB-1** in the figure 4.19, shows a comparable stiffness with the experimental global response, however a drop in the capacity of the beam initiated at the point marked in red indicates the formation of longitudinal cracks along the reinforcement. A vertical crack opening of 3.24 mm is registered along the reinforcement at this load factor of 8.9 mm with the crack width reaching up to 10 mm at the last load step. This indicates the delamination of the bottom concrete cover in the loaded shear span of the beam. This failure type does not resemble what is observed in the experiment. A diagonal shear crack appears to develop in figure **??**, however

the large crack strain of 0.42 shows the concrete cover has been spalled off. Nonetheless, a non-conservative model uncertainty of 0.9 is recorded due to the redistribution of stresses to the reinforcement.

C. C451A2- Experiment with flexural failure

Table 4.10: Description of the experiment-C451A2

Name	R_{exp}	R_{num}	θ	Exp. Failure	Num. failure
C451A2	52.9	62.06	0.85	Flexure	Delamination

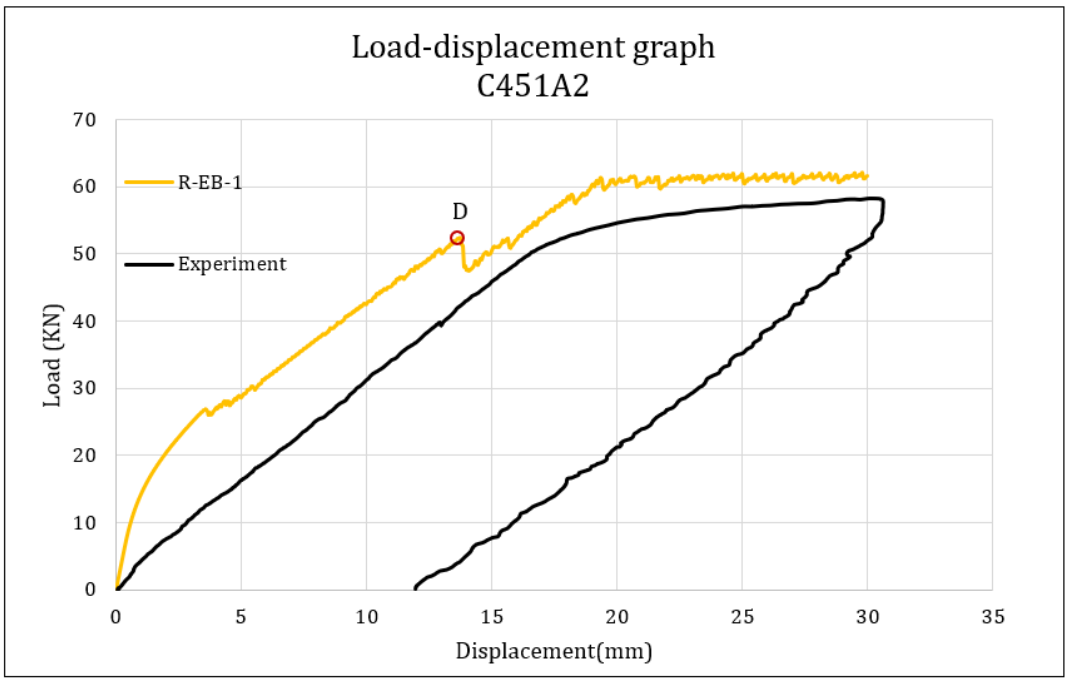

Figure 4.21: Load-displacement graph of experiment-**C451A2** using R-EB-1

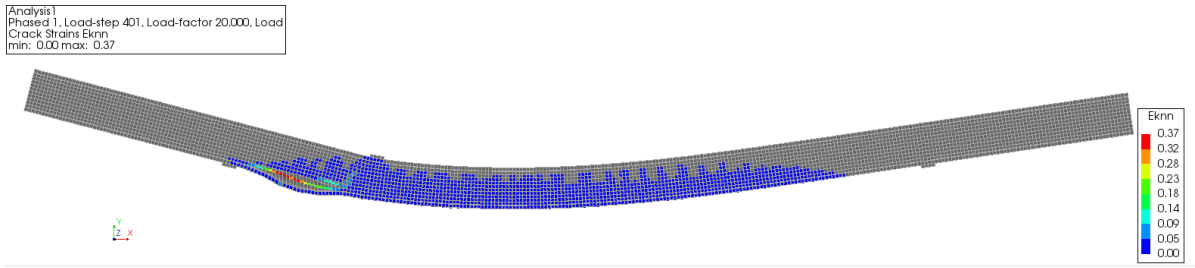

Figure 4.22: Failure crack strain of C451A2 at a load factor of 20 mm

Figure 4.21 shows the load-displacement graph of C451A2 from the experiment and the NLFEA performed using the modelling strategy **R-EB-1**. From this figure, it is apparent that the graph of **R-EB-1**, shows a stiffer but comparable response with the experiment up to the point marked in red, which signifies the drop in strength of the beam due to the delamination of the bottom concrete cover in the shear span of the beam. Upon the formation of this secondary longitudinal crack seen in figure 4.22, the reinforcement takes

over and a rise in the capacity is again visible in figure 4.21 followed by the yielding of the reinforcement.

4.4. R-BS-1 : Rotating Crack-Bond Slip-Mesh 1

The fourth modelling strategy in this group is **R-BS-1**. This modelling strategy is developed as an improvement of the **R-EB-1**. The delamination of concrete below the reinforcement is observed for all nine experiments in the case of **R-EB-1** which leads to the wrong failure mode. The cause of this is the large longitudinal crack strain along the reinforcement which is believed to be an effect of the assumption of perfect bond when using embedded reinforcement. The relative displacement or slip between concrete and reinforcement results in longitudinal principal strain along the reinforcement when perfect bond is assumed. The embedded reinforcement coupled with rotating crack model thus results in the consideration of the principal strain along the reinforcement as crack strain and the delamination of concrete cover becomes the dominating failure mode. Thus the embedded reinforcement is replaced with bond-slip interface reinforcement. This modified modelling strategy is used to analyse only A902B2 out of the nine experiments to observe the expected improvement of results.

A. A902B2- Experiment with shear failure

Table 4.11: Description of the experiment-A902B2

Name	R_{exp}(KN)	R_{num}(KN)	θ	Exp. Failure	Num. failure
A 902B2	124.2	137.09	0.91	Shear	Shear

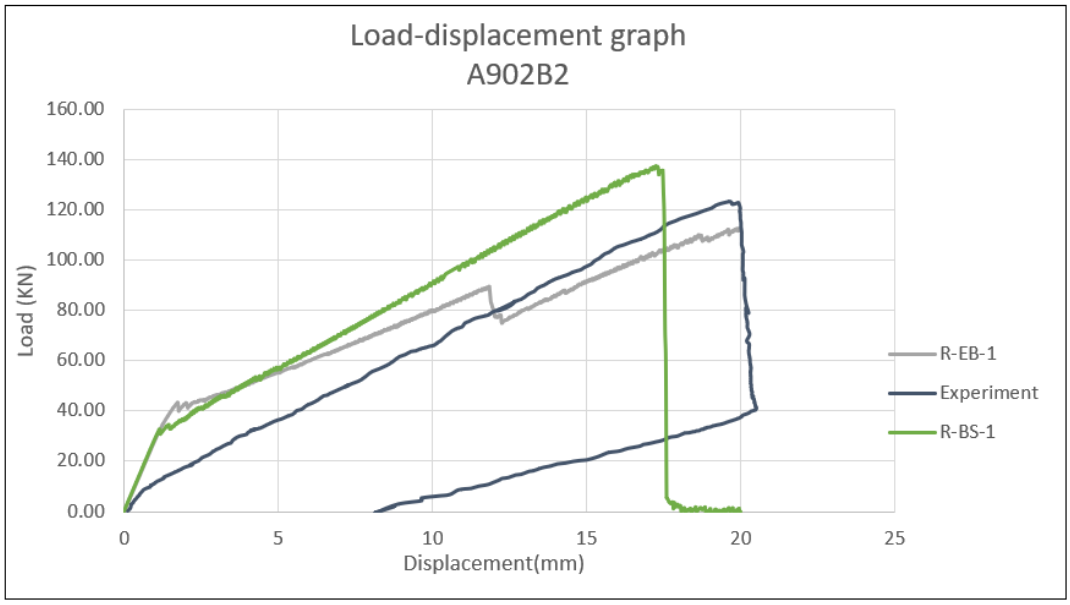

Figure 4.23: Load-displacement graph of A902B2 using R-EB-1 and R-BS-1

The numerical load-displacement response of A902B2 using the modelling strategy **R-BS-1** which is shown in green in figure 4.23 exhibits a similar post-cracking (secondary) stiffness as that of the experiment. It also does not show an earlier drop in the capacity

of the beam due to the formation of longitudinal cracks along the reinforcement unlike **R-EB-1**. Shear failure mechanism governs the ultimate limit state which matches the experimental result. Figure 4.24 shows the diagonal shear cracks formed at failure with an approximate crack width of 6.25 mm. The model uncertainty of the modelling strategy **R-BS-1** is 0.91 which implies a higher numerical prediction than the experiment. The global stiffness obtained using **R-EB-1** is expected to be higher than that obtained using **R-BS-1** since perfect bond is assumed in **R-EB-1**, however due to the effect of the governing longitudinal crack this is not exhibited.

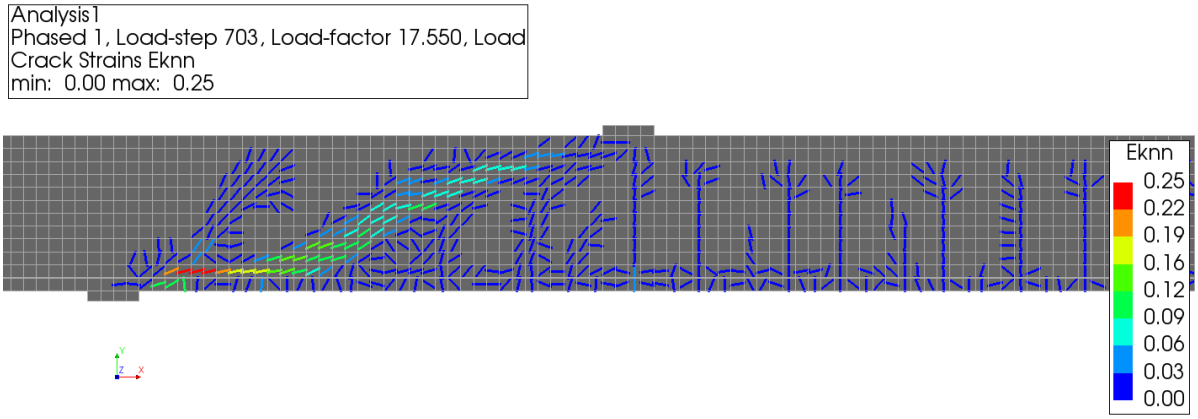

Figure 4.24: Failure crack strain of A902B2 at a load factor of 17.55 mm

4.5. Discussion

In this section, the analyses results of nine benchmark experiments using the first group of modelling strategies are discussed and the performance of the modelling strategies with respect to failure load and failure mechanism predictions are evaluated. Following this, certain conclusions are drawn from the observed trends.

The evaluation of each modelling strategy in this group consists of the assessment of the predicted failure load and failure mechanism with respect to experimentally observed results. As a result, the two criteria of performance evaluation are the accuracy of the predicted failure load and the accuracy of the predicted failure mechanism. Although the term 'accuracy' is used when comparing numerical results with experimental outcomes, it is important to remember that the experimental results can also be erroneous. However, for this study, the experimental results are set as benchmark and the numerical predictions are measured against these results. The assumption that mean material properties are realized in the experiment is made and the numerical simulation adheres to this assumption. It is important to note that the actual realized material properties determine the ultimate capacity and failure mechanism.

Criteria 1 : Accuracy of failure Load predictions

The accuracy of the failure load predictions are measured using the definition of model uncertainty given by the ratio in equation (1.1). The nine experiments are analysed using three of the modelling strategies of the first group and the respective model uncertainty ratios of these experiments are shown in figure 4.25. The last modelling strategy in this group, referred to as **R-BS-1**, is used to analyse only the experiment named A902B2, as mentioned in section 4.4, and its results are also discussed here.

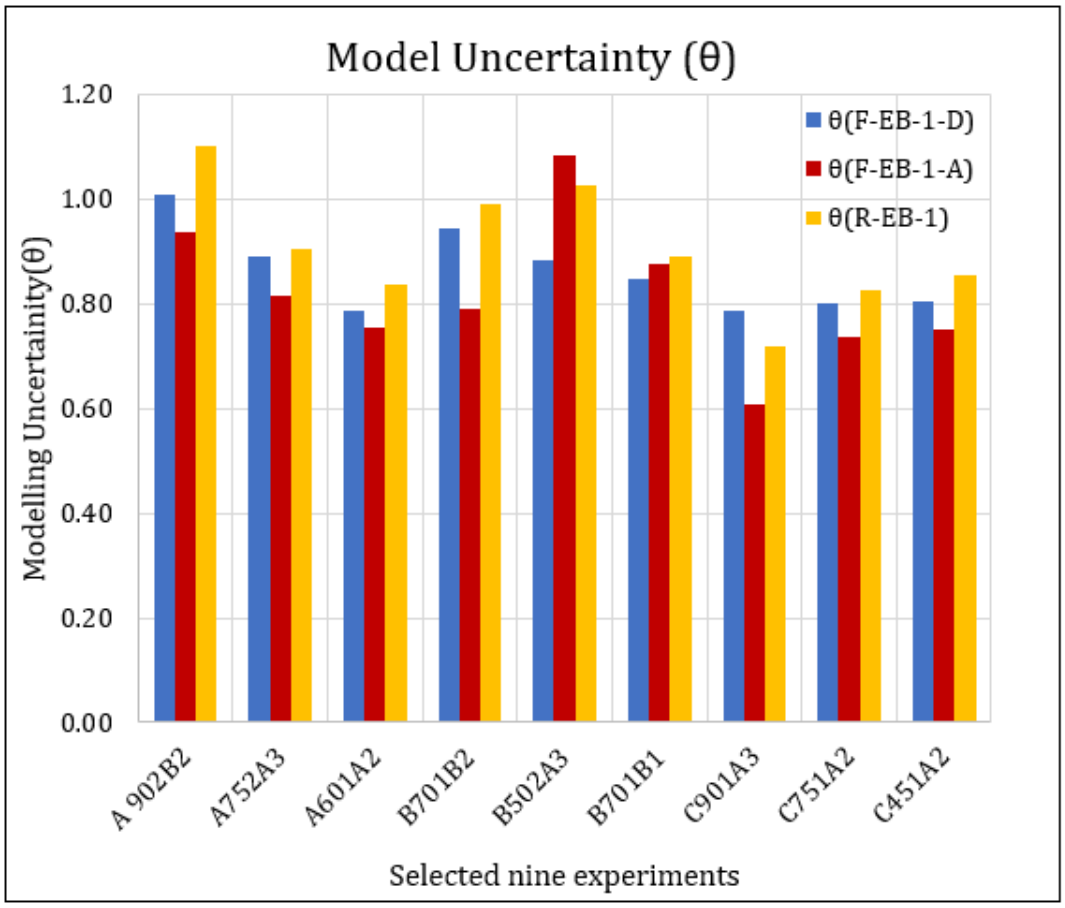

Figure 4.25: Model uncertainty of the first group of modelling strategies

Table 4.12: Mean and coefficient of variation of the model uncertainty of the first group of modelling strategies

Name	**F-BS-1-D**	**F-EB-1-A**	**R-EB-1**
Mean (θ)	0.861	0.817	0.905
COV (θ)	8.50%	15.70%	12.20%

- Based on table 4.12 it is possible to see that **F-EB-1-D** resulted in a mean model uncertainty ratio of 0.861 and a coefficient of variation of 8.5%. This indicates that the average prediction using **F-EB-1-D** is non-conservative which is also seen in the load-displacement graphs in figures 4.26, 4.27 and 4.28. Although, the effect of prior loading is not included in the numerical models which is believed to contribute to the model uncertainty, it is possible to say that on average **F-EB-1-D** results in relatively higher prediction of the failure load.

- On the other hand, **F-EB-1-A** has a mean model uncertainty of 0.817 and a coefficient of variation (COV) of 15.7%. The mean as well as the COV of the model uncertainty indicate that it has performed less accurately when compared to both **F-EB-1-D** and **R-EB-1**. Furthermore **F-EB-1-A** results in the stiffest predictions for eight out of the nine experiments which is illustrated in Figures 4.26, 4.27 and 4.28. This explains

the mean model uncertainty ratio of 0.817 which shows the highest deviation from 1 when compared to mean model uncertainty ratios of **F-EB-1-D** and **R-EB-1** as stated in table 4.12.

- **R-EB-1** has a mean and COV of model uncertainty ratio of 0.905 and 12.25% which is the lowest deviation of the ratio from 1. This indicates that **R-EB-1** predicted on average the most accurate failure loads for the nine experiments listed in table 4.1. However **R-EB-1** failed to give good predictions of the associated failure mechanisms in all of the nine experiments. As mentioned in section 4.3, **R-EB-1** results a failure mode characterized by delamination of the concrete cover which governs the behaviour of all nine experiments.

- Due to the delamination failure type observed when using **R-EB-1**, the modelling strategy **R-BS-1** is developed which has bond-slip reinforcement instead of embedded reinforcement. This change in the approach to model concrete-reinforcement interaction proved to eliminate the delamination failure type. This is possibly due to the large principal strain that occurs along the reinforcement when using **R-EB-1** is now accounted as the relative slip between concrete and reinforcement when using **R-BS-1**. However analysis of A902B2 using **R-BS-1** shows a higher failure load prediction than in the case of **R-EB-1** as illustrated in figure 4.26. This can be explained due to the fact the premature delamination failure has been avoided when using **R-BS-1**.

- Concluding from the observed trends from analyses of the nine experiments, it is possible to say that both F-EB-1-A and F-EB-1-A gave stiffer predictions than **R-EB-1**. This is due to the fact that fixed crack models suffer from stress-locking which also explains the popularity of the rotating crack models for reinforced concrete structures in NLFEA practices.

To compare the difference in numerical predictions among **F-EB-1-D**, **F-EB-1-A** and **R-EB-1**, the load-displacement graphs for the three experiments A902B2, A752A3 and C451A2 are presented in figures 4.26, 4.27 and 4.28.

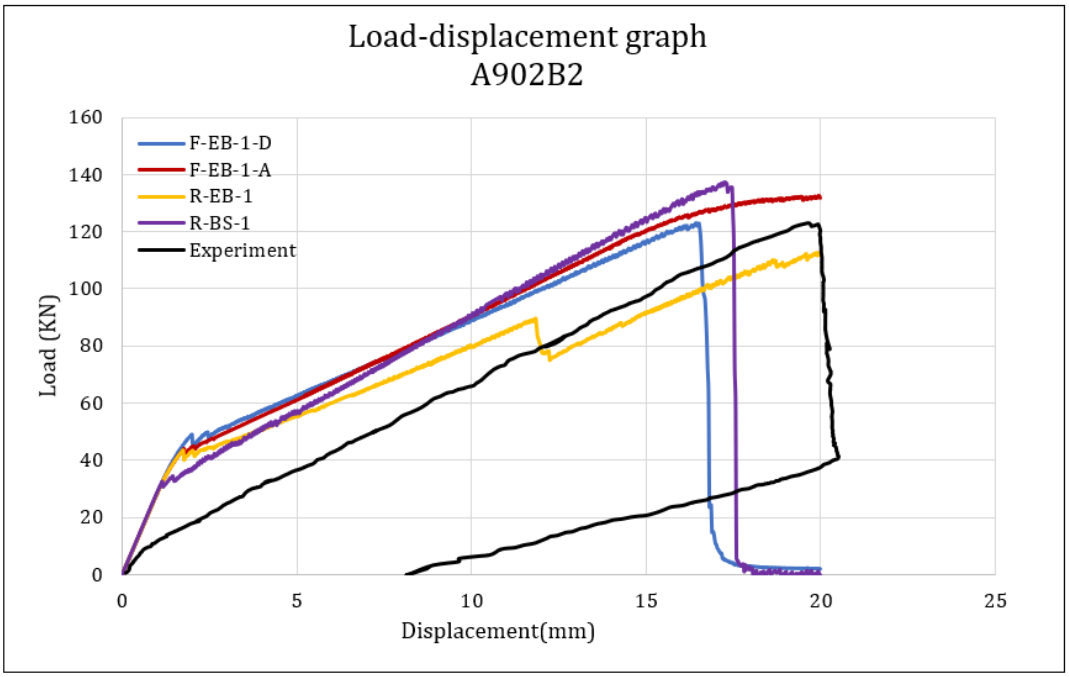

Figure 4.26: Load-displacement graph of A902B2 using the first group of modelling strategies

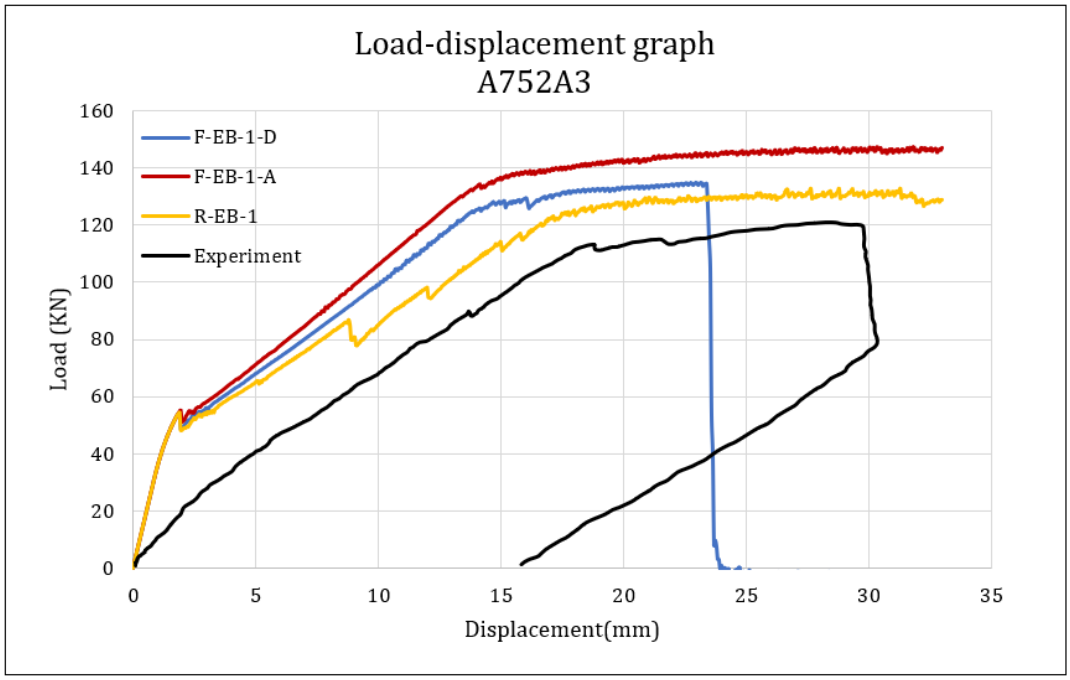

Figure 4.27: Load-displacement graph of A752A3 using the first group of modelling strategies

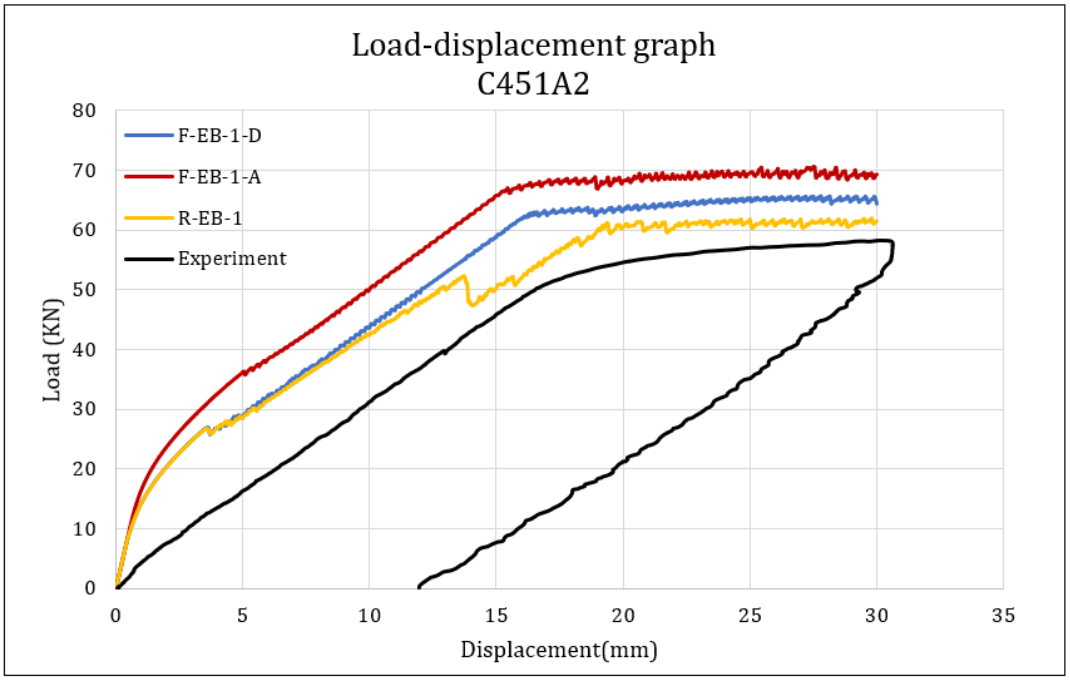

Figure 4.28: Load-displacement graph of C451A2 using the first group of modelling strategies

Criteria 2 : Accuracy of failure mechanism predictions

In table 4.13 the experimentally observed failure modes of the nine experiments along with the failure modes predicted using **F-EB-1-D**, **F-EB-1-A** and **R-EB-1** are presented to help compare how accurately the modelling strategies can predict failure modes.

Table 4.13: Failure mode predictions using the first group of modelling strategies

Name	Exp. Failure	**F-EB-1-D**	**F-EB-1-A**	**R-EB-1**
A 902B2	Shear	Shear	Shear	Delamination
A752A3	F+S	F+S	Flexural	Delamination
A601A2	F+S	Flexural	Flexural	Delamination
B701B2	Shear	Shear	Flexural	Delamination
B502A3	Shear	Shear	Flexural	Delamination
B701B1	Flexural	Shear	Shear	Delamination
C901A3	Shear	Shear	Flexural	Delamination
C751A2	Shear	Shear	Flexural	Delamination
C451A2	Flexural	Flexural	Flexural	Delamination

- From table 4.13, it is possible to see that **F-EB-1-D** is able to accurately predict the failure mechanism of eight of the nine benchmark experiments. From the load-displacement graphs in figures 4.26, 4.27 and 4.28 it is possible to see that **F-EB-1-D** is able to predict shear, mixed mode and flexural failure types accurately. For figure 4.27, **F-EB-1-D** is the only modelling strategy that is able to predict the mixed mode failure type. The failure crack strain diagrams in figures 4.3, 4.6, 4.7 and 4.9 also show close similarity to the experimentally observed crack patterns and behaviour of the beams at failure. This can be explained by the fact that the fixed crack model mimics the true

nature of cracking which is that once concrete cracks the fracture is fixed at the same location and orientation and does not vanish and rotate based on the direction of the principal plane. This helps the modelling strategies with fixed crack concept to accurately capture the crack patterns which help in accurately predicting the failure mode.

- **F-EB-1-A** appears to result in mostly flexural failure modes with seven out of the nine experiments predicted to failure in flexure. This indicates that the aggregate size based shear retention model overestimates the shear stiffness of the cracked plane which avoids or prolongs the formation of flexural shear cracks. Due to this, **F-EB-1-A** is neither able to predict the brittle behaviour nor the shear crack formation for beams failing in shear.

- A significant crack strain along the longitudinal reinforcement occurs when using **R-EB-1** which is seen in figures 4.18, 4.20 and 4.22. A phenomenon which looks like delamination of the concrete below the longitudinal reinforcement takes over the analysis leading to failure of the beams. This is due to the use of embedded reinforcement which assumes perfect bond between concrete and reinforcement. The downside of this assumption is that the slip between concrete and reinforcement is mistaken as a large strain causing the orientation of the principal strain to align along the reinforcement and since the rotating crack concept changes the crack orientation based on the direction of the principal strain, cracking of concrete occurs along the reinforcement leading to the delamination of the concrete cover.

Based on the evaluation of the modelling strategies, **F-EB-1-D** and **R-BS-1** showed relatively good performance with regards to failure load and failure mode predictions. As a result, these two modelling strategies are selected for further study of model uncertainty by utilizing the entire benchmark experiments and the results of this study are presented in chapter 5. However the mesh type used in **F-EB-1-D** and **R-BS-1** is the one shown in figure 3.11 which has element size of 25 mm for the entire geometry. This is found to be computationally expensive and element size is changed to 50 mm as shown in figure 3.12 for the analyses performed on all the benchmark experiments. The effects of using a coarser mesh is also discussed in chapter 5.

5

Analysis Results of the 2nd Group of Modelling Strategies

The second group of modelling strategies is discussed in this chapter. All the 67 benchmark experiments are analysed using two modelling strategies in this group. These two modelling strategies are formulated based on the robustness of the modelling strategies of the first group that are used to analyse nine of the benchmark experiments. In this chapter, the trends that are observed in the model uncertainty ratio are presented using probabilistic distributions and a single experiment is chosen to showcase the simulation of failure behaviour.

The analyses using the first group of modelling strategies showed that the modelling strategies F-EB-1-D and R-BS-1 gave good predictions with respect to failure load and failure mechanism of the nine experiments. As a result these two modelling strategies are chosen to perform NLFEA on all the benchmark experiments. However an important modification is made to F-EB-1-D and R-BS-1 by changing the meshing from type 1 to type 2 as shown in figure 3.11 and figure 3.12 respectively. The 25mm element size of mesh type 1 requires relatively high computational time and effort thus is considered too fine to perform analysis of 67 experiments. Thus an element size of 50mm was decided to be used. The 50mm element size is in line with the six elements along the height recommendation given in [6] for both 300 mm and 500 mm beam height.

Changing the mesh type by definition changes the discretization of the finite element model and as a result creates new modelling strategies. The modelling strategies F-EB-1-D and R-BS-1 are now modified to become F-EB-2-D and R-BS-2 respectively. In this chapter the model uncertainty of F-EB-2-D and R-BS-2 will be presented and discussed. In addition, the accuracy of prediction of failure mechanism is investigated as part of understanding the model uncertainty.

5.1. F-EB-2-D : Fixed Crack-Embedded-Mesh 2-Damage Based

In this section, model uncertainty of **F-EB-2-D** for all benchmark experiments will be discussed. As shown in table 3.2, The geometry, support condition, load condition and analysis procedure are constant for all the eight modelling strategies and the difference between the modelling strategies is due to the material models and mesh type used. Thus, Table 5.1 lists the specific material models for concrete and reinforcement and the discretization of the geometry that characterize **F-EB-2-D**.

Table 5.1: Applied material models and discretization in **F-EB-2-D**

F-EB-2-D	
Concrete Material Model	
Concrete crack model	Smeared-Total Strain Based
Crack orientation	Fixed
Shear retention	Damage based
Tensile behaviour	Hordijk
Crack bandwidth	Rots
Compression behaviour	Parabolic
Tension-Compression	Vecchio & Collins (Max reduction factor =0.4)
Compression-Compression	Vecchio & Selby
Poisson effect	Damage based reduction
Reinforcement Material Model	
Von Mises plasticity	Linear Strain hardening
Type	Embedded reinforcement
Mesh	
Continuum element type	Regular plane stress
Continuum element name	CQ16M
Reinforcement element type	Truss
Interface element type	2D line quadratic
Element size(h)	50mm
Interpolation scheme	Quadratic
Integration scheme	Gaussian (3X3)

By using the definition presented in table 5.1 the modelling strategy **F-EB-2-D** is set up. Subsequently NLFEA using this modelling strategy is performed for all benchmark experiment and the numerical failure load and failure mechanism for each analysis is recorded. These results along with the model uncertainty defined by θ are given in Annex A. Using these results, the goodness of this modelling strategy to simulate the behaviour of reinforced concrete beams is studied. The influence of lack of shear reinforcement in the specimens used for the benchmark experiments on numerical failure behaviour is also investigated.

Firstly the accuracy of prediction of failure load is studied. Numerical failure is defined as the drop of 10% of the load in the load-displacement response. Figure 5.1 illustrates the match between experimentally obtained failure loads and numerically predicted failure loads. In this figure the line represents exact match between experimental and numerical failure loads. As seen from Figure 5.1, the majority of the predicted failure loads fall below

the line which implies that failure load predictions for most benchmark experiments are underestimated which accounts for 80.5% of the experiments.

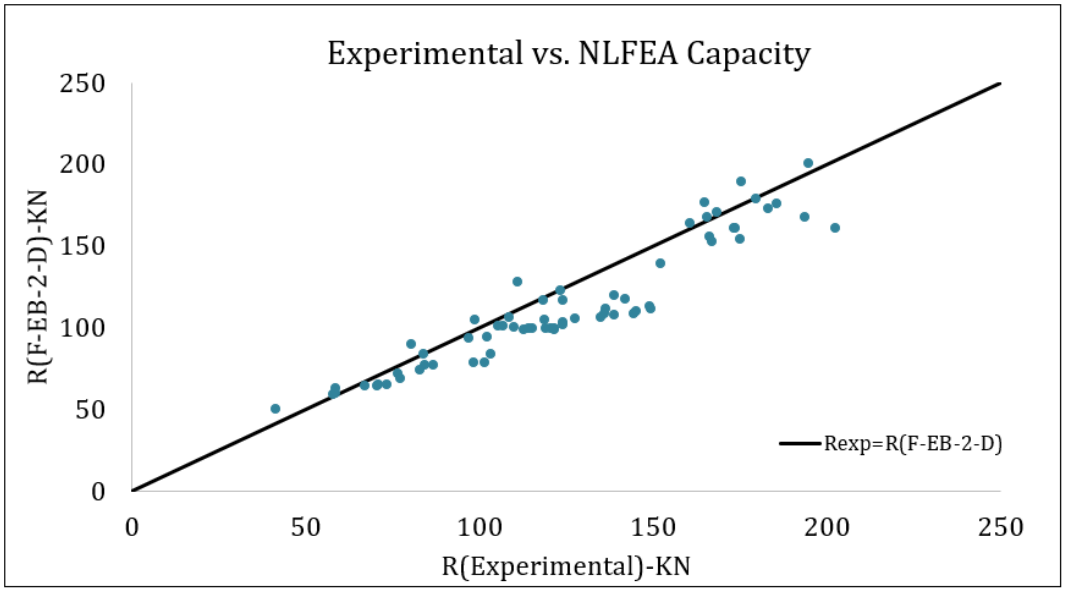

Figure 5.1: Graphical representation of experimental vs. predicted NLFEA failure load using **F-EB-2-D**

The model uncertainty of all the benchmark experiments using this modelling strategy was computed as per equation (1.1) and a mean value of 1.108 and coefficient of variation of 10.877% is obtained. The model uncertainty data is fitted to a normal, log-normal and a non-parametric (kernel) probabilistic distribution using MATLAB and shown in figure 5.2. The log-likelihood of the normal probability distribution function is equal to 47.15 and that of the log-normal probability distribution function is equal to 46.71. The goodness of fit of the model uncertainty data to a normal probabilistic distribution and log-normal probabilistic distribution is shown in figure 5.3 and figure 5.4 respectively.

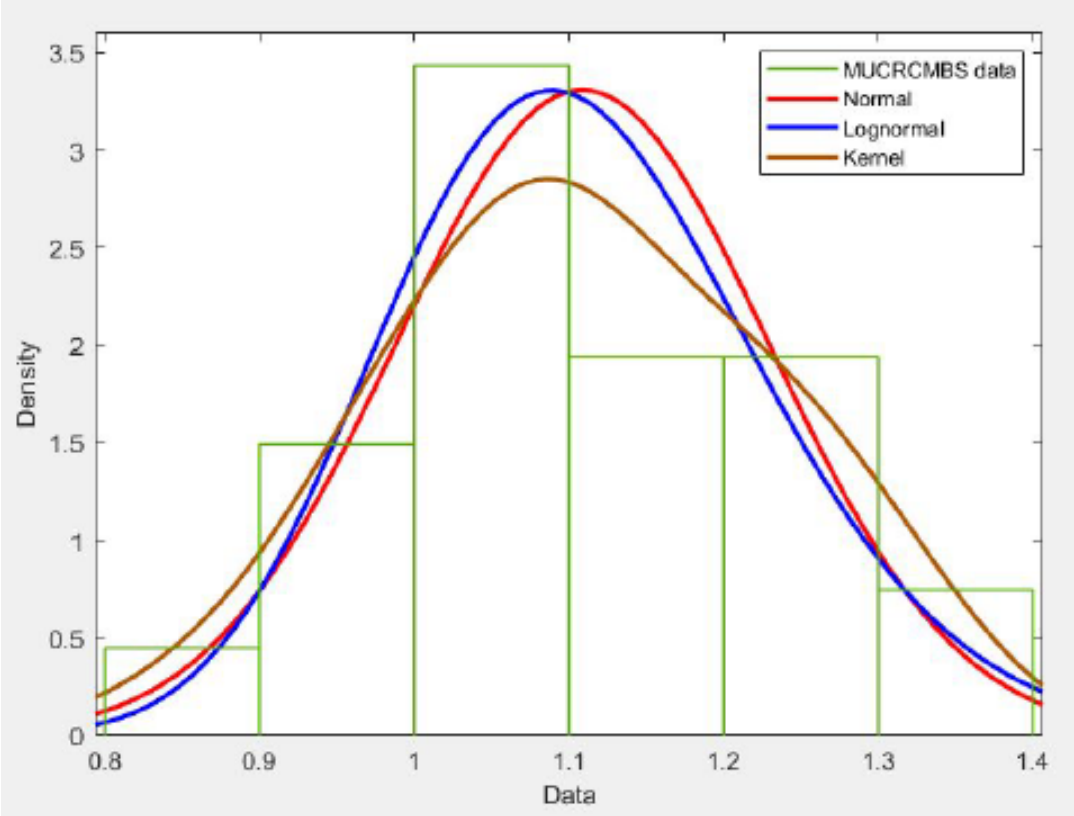

Figure 5.2: MATLAB probabilistic fitting of modelling uncertainty θ of **F-EB-2-D**

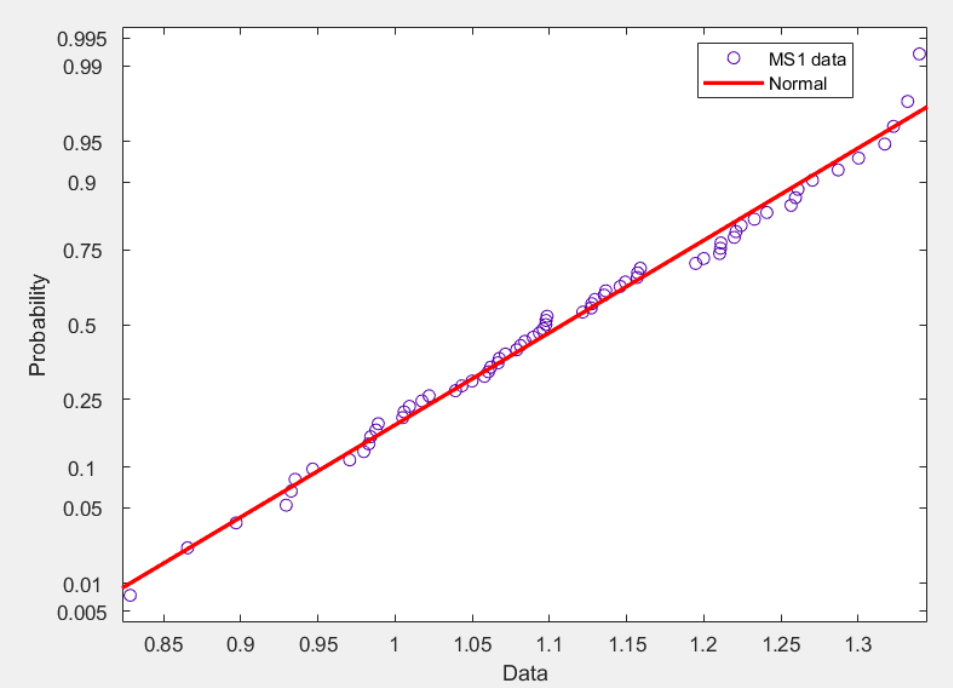

Figure 5.3: Goodness of fit of model uncertainty data of **F-EB-2-D** to normal distribution

The failure load model uncertainty ratios show a general good fit to both normal and log-normal probabilistic distributions as can be seen from figures 5.3 and 5.4. However the

value of the data at the tail of the distribution seems to fit both distributions the least. Thus, the two values at the right end tail that show high deviation from the lines in figures 5.3 and 5.4 are selected to investigate the reason for the high model uncertainty. These two experiments are A902A3 and A121A3 with model uncertainty ratios of 1.339 and 1.332 respectively. Both of these experiments have experimental shear failure. However it is found that the experiment A121A3 was repeated and named A121B1 which has an experimental mixed mode failure type. The model uncertainty ratio for A121B1 is 0.983 which indicates a large difference in the experimental failure load. This signifies the contribution of variability of the experimental results to the model uncertainty ratio.

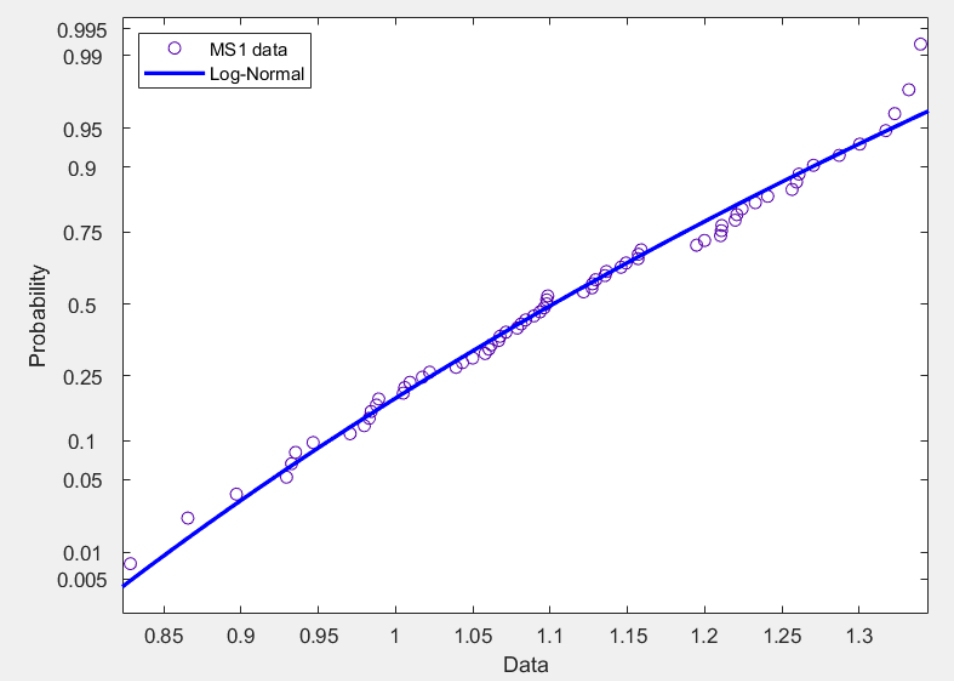

Figure 5.4: Goodness of fit of model uncertainty data of **F-EB-2-D** to log-normal distribution

Following the study of model uncertainty of **F-EB-2-D** with respect to prediction of failure load, the model uncertainty with respect to failure mechanism prediction is analysed. The predicted failure mechanism using the modelling strategy **F-EB-2-D** for majority of the benchmark experiments is a shear failure followed by regain of load resistance due to redistribution of stresses to longitudinal reinforcement up to yielding point. This type of failure is referred in this report as 'shear then yielding'. In the 'shear then yielding' failure type the formation of a compressive strut between the point load and the nearby support leads to a brittle shear crack which results in more than 10% drop of load in the load-displacement response. The point in the analysis just before this drop is considered as the peak load or capacity of the beams.

29 of the 67 benchmark experiments showed shear then yielding failure type. The experiments that showed this type of failure have a shear slenderness ratio (a/d) of less than 4. These 29 experiments have either of the three types of experimental failure modes. To showcase the accuracy of predicted failure behaviour using **F-EB-2-D**, A121A1 is discussed in detail which has an experimental flexural failure and is the first experiment on the beam specimen. The analysis of A121A1 using the modelling strategy **F-EB-2-D** resulted in a

shear failure with regain of resistance. The formation of compressive strut appears to cause large shear displacement of already existing cracks which leads to a brittle shear failure. Once the compressive strut fully forms as shown in figure 5.6, the part of the beam to the left of the position of the load (part with compressive strut) and the part to the right the load experience a relative displacement between each other resulting in considerable shear displacement in the cracked section. The shear displacement is visible in figure 5.7 from the distorted finite elements where the shear crack occurs.

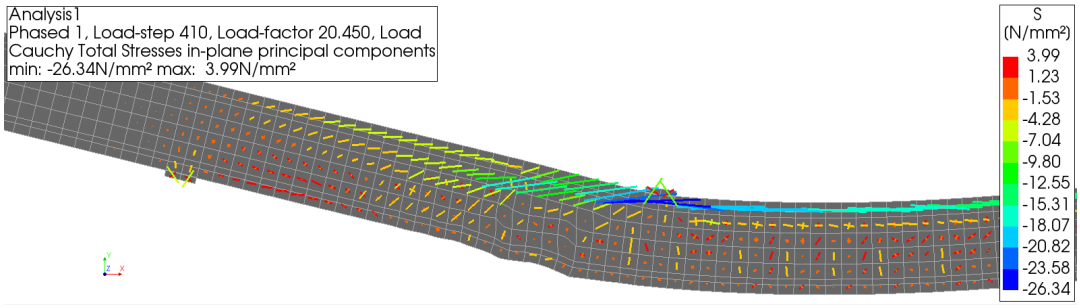

Figure 5.5: Principal stress plot of load step just before full compressive strut formation- RC beam A121A1

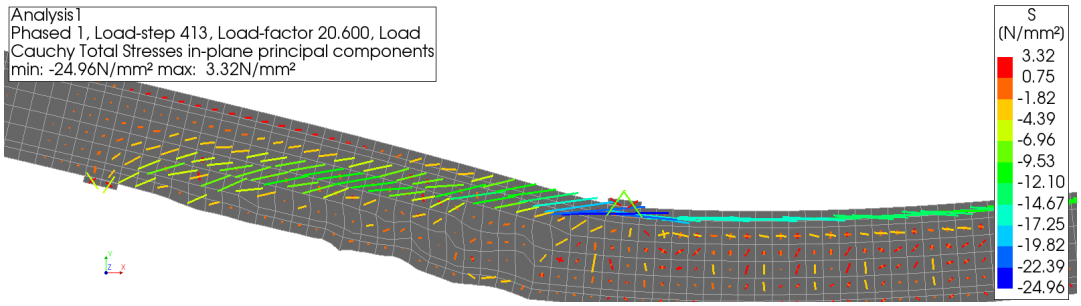

Figure 5.6: Principal stress plot of load step at full compressive strut formation- RC beam A121A1

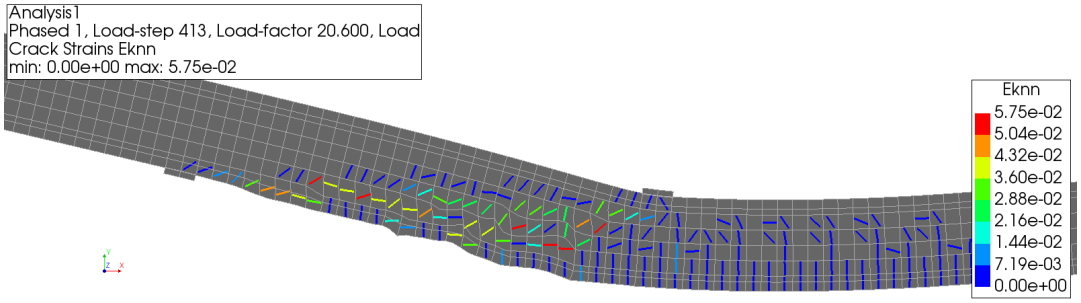

Figure 5.7: Crack strain plot of load step at full compressive strut formation - RC beam A121A1

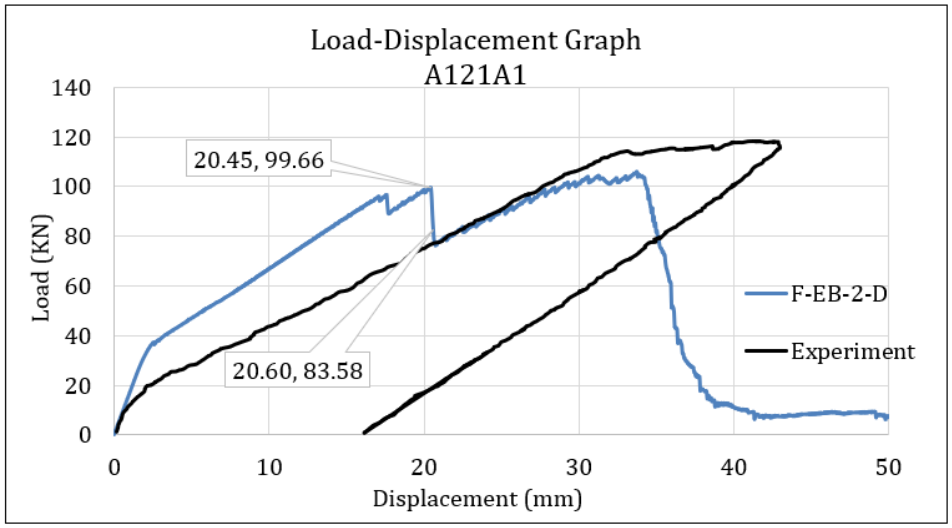

Figure 5.8: Load-displacement graph of A121A1 using **F-EB-2-D**

The load-displacement graph of A121A1 in figure 5.8 also shows the drop of the resistance at a displacement of 20.45 mm which is the load factor before the formation of compressive strut and formation of the shear failure. It is also interesting to see the stress in the reinforcement for such type of failure and as can be seen from the graph in figure 5.9, the stress at a node of the reinforcement located in the loaded shear span of the beam mimics the load-displacement response shown in figure 5.8. The drop in the reinforcement stress occurs at the same load factor of 20.45 mm and the behaviour of the beam after the 20.45 mm appears to be mainly dictated by the reinforcement.

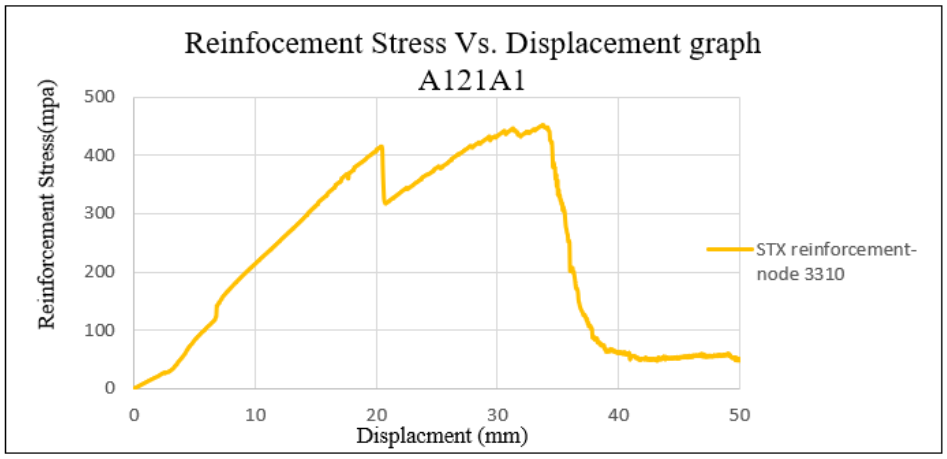

Figure 5.9: Reinforcement stress versus displacement graph of A121A1

Looking into table 5.2 and the general trend of the analyses results of **F-EB-2-D**, it is possible to see that all of the 27 experimental shear failures are predicted accurately while 77.8% of the experiments having flexural failure are predicted to have shear failure and 84.6% of the experiments with mixed mode failure are predicted to fail in shear as well. 59 out of the 67 experiments are predicted to fail in shear. Thus, shear failure is the dominating failure mechanism when using **F-EB-2-D** with 47.7% of the benchmark experiments

predicted to have matching failure mechanism with their respective experimental failure behaviour.

Table 5.2: Match between experimental and numerical failure mechanisms of the 67 benchmark experiments

F-EB-2-D / Experiment	Flexure	Shear	Flexure+Shear
Flexure	3	21	3
Shear	0	27	0
Flexure+Shear	0	11	2

To analyse the effect of failure mode on the model uncertainty ratio, probabilistic distribution of the model uncertainty ratio of the tests that exhibited flexural and shear failure during the experiments are plotted separately in figure 5.10. Among 67 benchmark experiments, 27 fail in flexure and 27 fail in shear. The normal and log-normal distributions of the model uncertainty ratio for flexural failure have a mean of 1.08 and a COV of 11.4%. On the other hand, the normal and log-normal distributions of the model uncertainty ratio for shear failure resulted in a mean of 1.15 and COV of 9.6%. This shows that shear failure results in higher failure load model uncertainty ratio when using **F-EB-2-D**. The fact that equal number of experiments failed in flexure and shear helps in making this comparison.

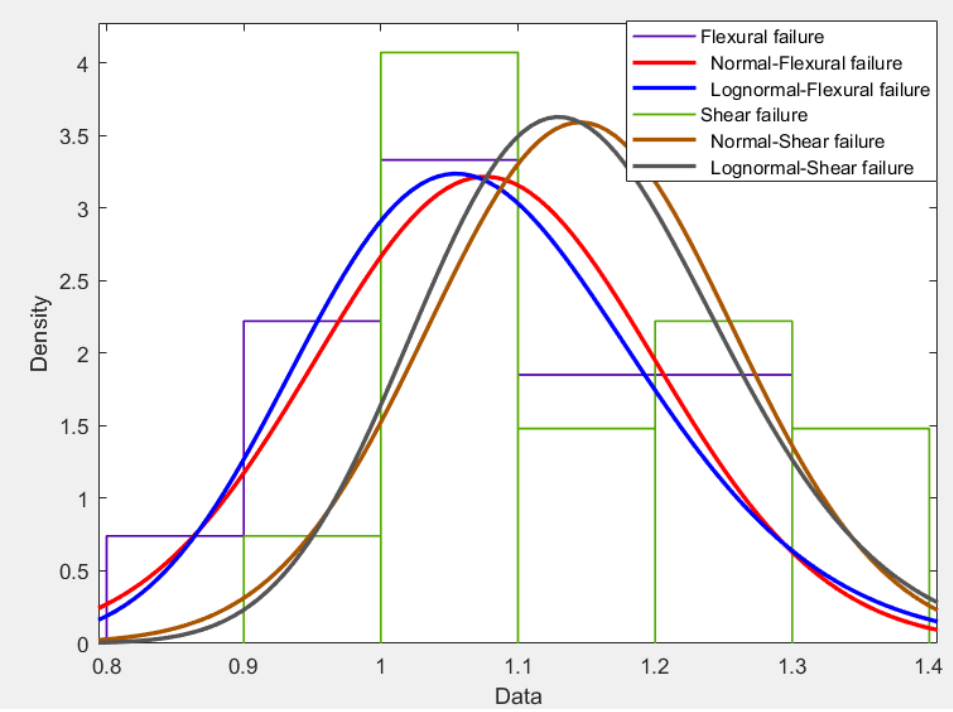

Figure 5.10: MATLAB probabilistic fitting of modelling uncertainty of **F-EB-2-D** based on failure mode

5.2. R-BS-2 : Rotating Crack-Bond Slip-Mesh 2

This section describes the analyses results of the modelling strategy **R-BS-2**. The model uncertainty (θ) of **R-BS-2** in predicting the capacity of the benchmark experiments is given in Annex B. The fundamental characteristics of the modelling strategy **R-BS-2** are presented in table 5.3.

Table 5.3: Applied material models and discretization in **R-BS-2**

R-BS-2	
Concrete Material Model	
Concrete crack model	Smeared-Total Strain Based
Crack orientation	Rotating
Shear retention	Not applicable
Tensile behaviour	Hordijk
Crack bandwidth	Rots
Compression behaviour	Parabolic
Tension-Compression	Vecchio & Collins (Max reduction factor =0.4)
Compression-Compression	Vecchio & Selby
Poisson effect	Damage based reduction
Reinforcement Material Model	
Von Mises plasticity	Linear Strain hardening
Type	Bond-slip reinforcement
Mesh	
Continuum element type	Regular plane stress
Continuum element name	CQ16M
Reinforcement element type	Truss
Interface element type	2D line quadratic
Element size(h)	50mm
Interpolation scheme	Quadratic
Integration scheme	Gaussian (3X3)

The model uncertainty as defined in equation (1.1) is quantified for all benchmark experiments and the trend in the predicted failure mechanisms are discussed in this section. Figure 5.11 shows the match between experimental and numerical capacity predicted using **R-BS-2** with the line defining a perfect match. It can be seen from figure 5.11 that approximately equal number of experiments lie above and below the line. However, more than half of the analyses of the benchmark experiments resulted in underestimated predictions of failure load.

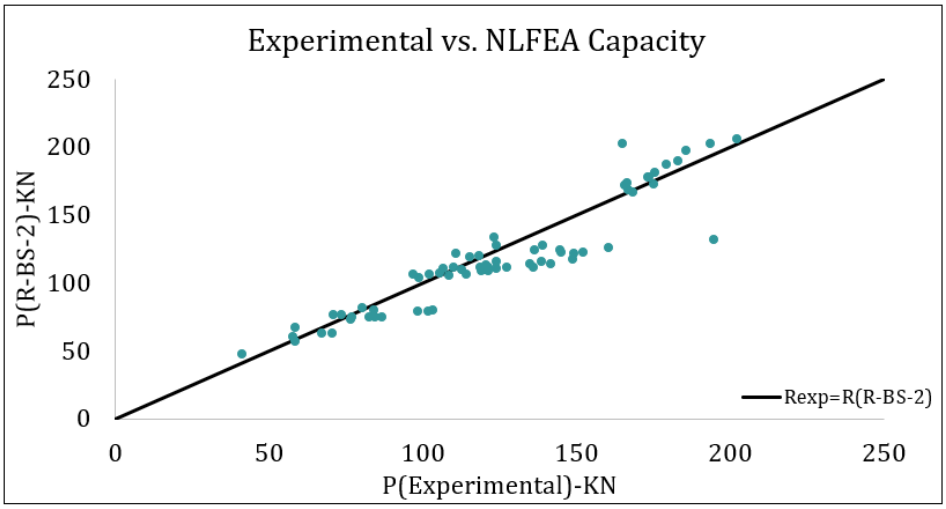

Figure 5.11: Graphical representation of experimental vs. predicted NLFEA failure load using **R-BS-2**

The probabilistic distributions for this modelling strategy show a concentration of values around 1 as shown in figure 5.12 which causes the distribution to be a bit skewed. A mean value of 1.06 and coefficient of variation (COV) of 11.7% are calculated for the model uncertainty using this modelling strategy. The goodness of fit of the model uncertainty ratio to both normal and log-normal probabilistic distributions are shown in figures 5.13 and 5.14 with a log-likelihood of 44.65 and 47.02 respectively.

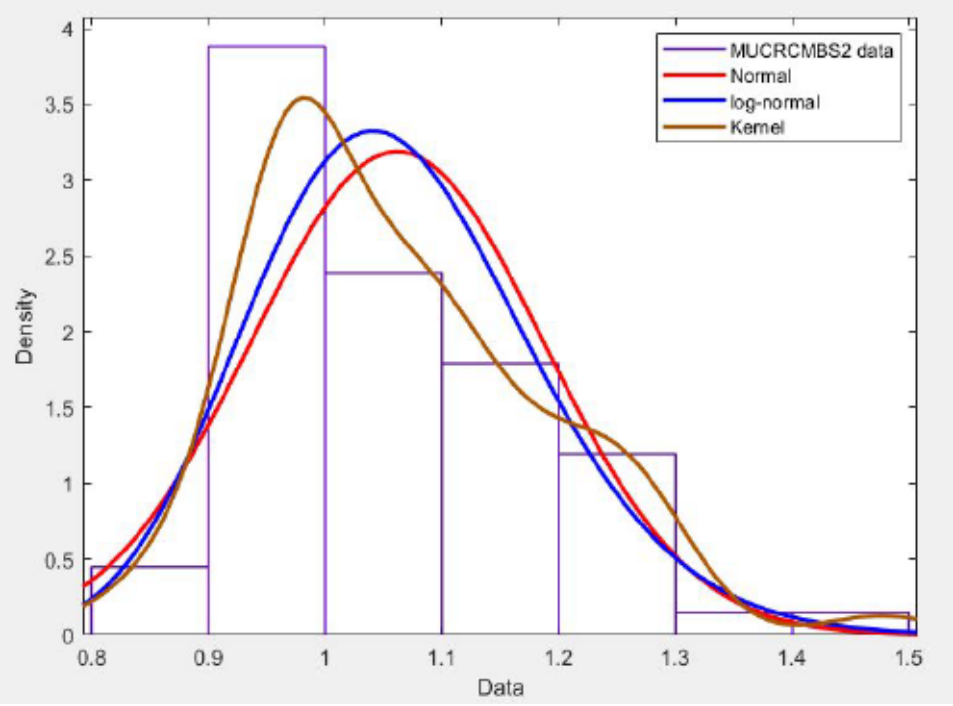

Figure 5.12: MATLAB probabilistic fitting of modelling uncertainty θ of **R-BS-2**

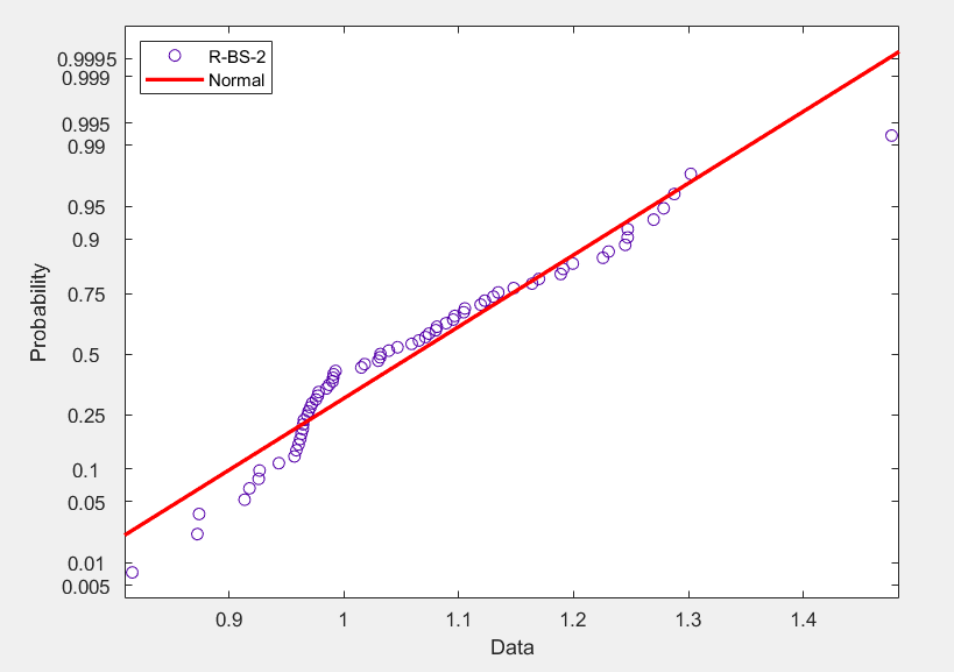

Figure 5.13: Goodness of fit of model uncertainty data of **R-BS-2** to normal distribution

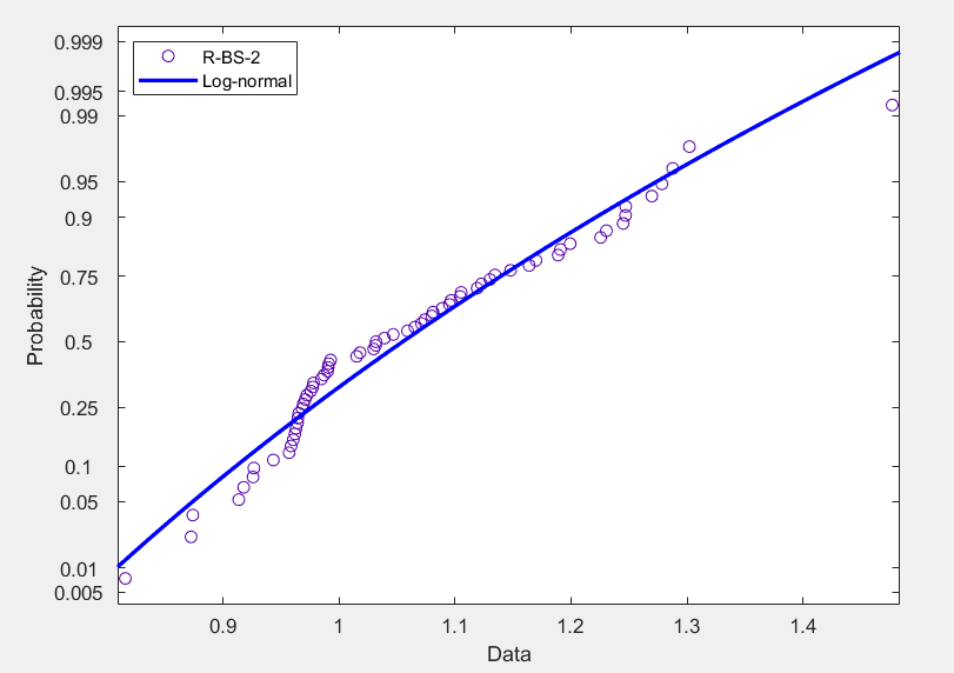

Figure 5.14: Goodness of fit of model uncertainty data of **R-BS-2** to normal distribution

The experiment A121A1 is again used to showcase the accuracy of the failure behaviour predictions using **R-BS-2**. The load-displacement response of A121A1 using **R-BS-2** is illustrated in figure 5.15 and shows a brittle failure at 23.1 mm displacement. This figure combined with the principal strain plot in figure 5.16 and the failure crack strain plot in figure 5.17 shows a predicted shear failure. When compared to the result of the modelling strategy **F-EB-2-D**, the shear failure caused by **R-BS-2** does not show any regain of its resistance. This shows that both modelling strategies, **F-EB-2-D** and **R-BS-2**, are not able to exhibit the flexural failure of A121A1.

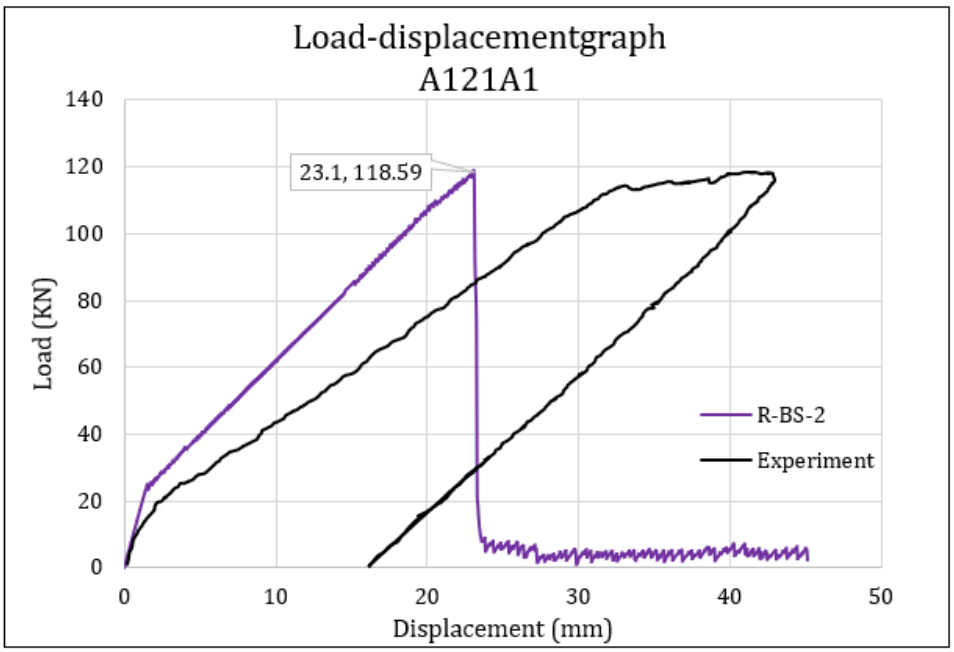

Figure 5.15: Load-displacement graph of A121A1

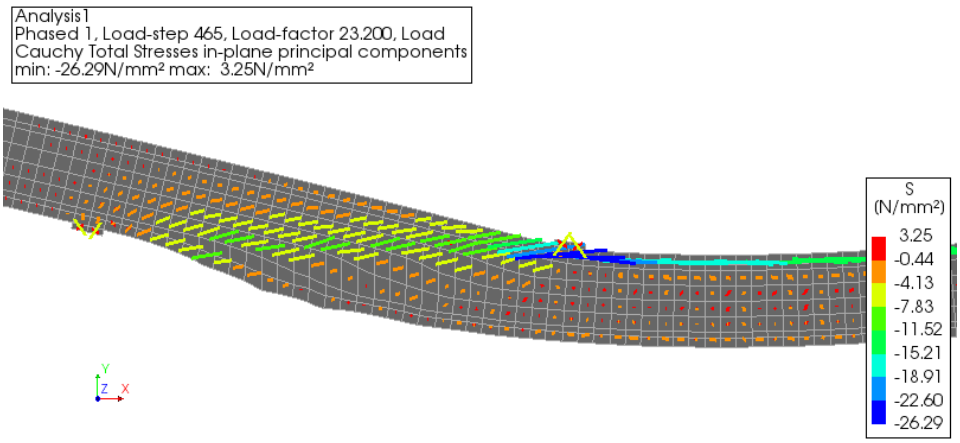

Figure 5.16: Principal stress plot at failure of A121A1 using **R-BS-2**

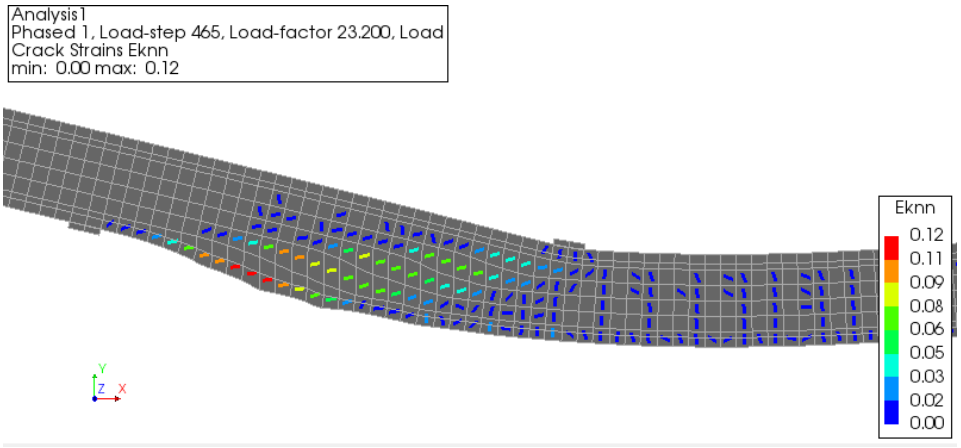

Figure 5.17: Crack strain at failure of A121A1 using **R-BS-2**

Subsequently, to understand the correlation between the failure load model uncertainty ratio and the type of failure mechanism, the probabilistic distributions are plotted separately in figure 5.18 for flexural and shear failure types. From this figure, the experiments with flexural failure show a mean of 1.02 and COV of 9.75% while the experiments with shear failure resulted in a mean model uncertainty ratio of 1.07 and COV of 11.17%. The mean model uncertainty ratio corresponding to shear failure shows more deviation from 1 with a larger spread when compared to flexural failure.

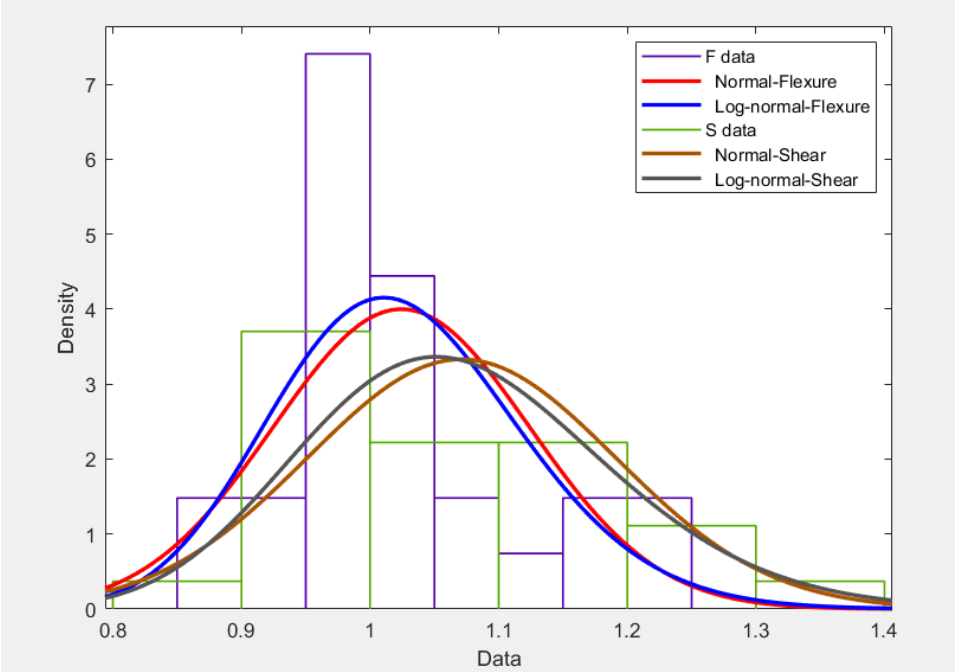

Figure 5.18: MATLAB probabilistic fitting of modelling uncertainty θ of **R-BS-2**

In addition to the model uncertainty ratio, the accuracy of failure mode predictions is another measure of the performance of **R-BS-2**. To do this, table 5.4 is used to show the number of experiments with their respective experimental and numerically predicted failure modes using **R-BS-2**. The values in the diagonal of table 5.4 show matching experimental and numerical predictions which accounts for 50.7% of the experiments. 22 out of 27 of

the experimental shear failures are predicted accurately and only 8 out of 27 of the experimental flexural failure are predicted accurately. This indicates that the modelling strategy **R-BS-2** is not well suited to predict flexural failure which appears to be due to the formation of shear cracks before or just after yielding of the reinforcement. This shows that shear cracks occur before the reinforcement reaches large plastic strain which causes 10 out of 27 flexural failures to be predicted as mixed mode failure types.

Table 5.4: Match between experimental and numerical failure mechanisms

Experiment \ R-BS-2	Flexure	Shear	Flexure+Shear
Flexure	8	9	10
Shear	4	22	1
Flexure+Shear	0	9	4

5.3. Discussion

The failure load model uncertainty ratios of 67 benchmark experiments using both **F-EB-2-D** and **R-BS-2** are computed to make comparison of the two modelling strategies. From the mean model uncertainty values of 1.12 and 1.08 of **F-EB-2-D** and **R-BS-2** respectively, it can be deduced that **R-BS-2** shows better prediction of failure load. In addition, the evaluation of the two modelling strategies based on the accuracy of failure mode predictions shows that **R-BS-2** performed better by accurately predicting the failure mode of 51% of the experiments while **F-EB-2-D** gave accurate predictions for 48% of the experiments.

Both these modelling strategies suffered heavily from the change of mesh type. The larger element size of 50mm proves to be incapable of capturing the accurate failure mode. The reason for this is the fact that the benchmark experiments are conducted on specimens of reinforced concrete beams without shear reinforcement. The formation and propagation of cracks is crucial in determining the behaviour of such beams. Increasing the element size decreases the number of degrees of freedom. This affects the displacement field of the finite element model as well as the strain and stress fields. In addition the number of integration points that calculate the stresses in the structure are also reduced. Thus, the use of larger element size appears to have caused wrong failure mode predictions. It is important to realize an element size of 50 mm is one-sixth of the beam height (H/6) for the beams having 300 mm height and one-tenth (H/10) for the beams having 500 mm height and still is not able to exhibit accurate failure modes for both beam heights. This raises the need for the verification of the finite element size before performing NLFEA based on the type of reinforced concrete structure.

In an effort to study the effect of mesh refinement, both modelling strategies **F-EB-2-D** and **R-BS-2** are modified to have the discretization of mesh type 3 shown in figure 3.13 and the modified modelling strategies are referred to as **F-EB-3-D** and **R-BS-3**. The experiment A121A1 is analysed using **F-EB-3-D** and **R-BS-3** and both resulted in an improvement of failure mode predictions as can be seen from figure 5.19. Both the modified modelling strategies **F-EB-3-D** and **R-BS-3** are able to predict flexural failure with **R-BS-3** resulting in an extended ductile plateau. However, the predicted failure load while using the modified modelling strategies **F-EB-3-D** and **R-BS-3** is higher the experimental results. As a result, further study on the effect of mesh refinement is performed using 16 of the first experi-

ments.

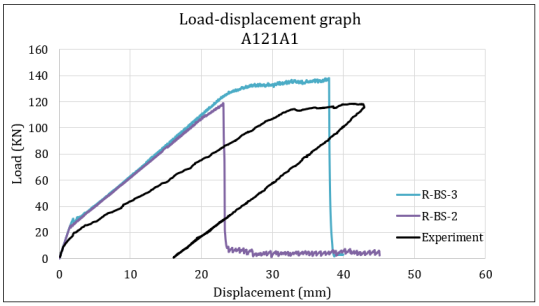

(a) Comparison of **F-EB-2-D** and **F-EB-3-D**

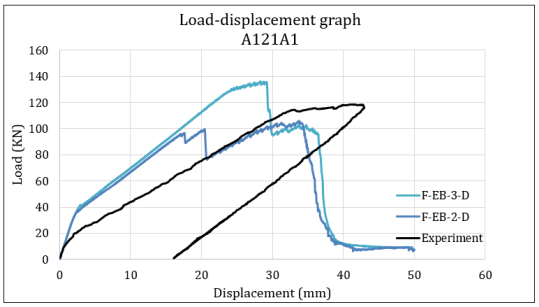

(b) Comparison of **R-BS-2** and **R-BS-3**

Figure 5.19: Mesh refinement study on A121A1

The study of the correlation between the failure load model uncertainty and the experimental failure modes shows that on average shear failure modes show higher model uncertainty with more spread in figures 5.10 and 5.18. In both cases the experiments with shear failure displayed relatively high model uncertainty. This can be associated with the fact that shear failure in beams without shear reinforcement is governed by the properties of the concrete than flexural failure which is influenced by the property of the reinforcement.

Furthermore, the trend of the model uncertainty ratios of both **F-EB-2-D** and **R-BS-2** indicate the influence of reinforcement ratio which can be seen from the figure 5.20. Experiments having reinforcement ratio lower than 0.6% show on average lower model uncertainty ratio in both modelling strategies. Keeping in mind the effect of coarse mesh mentioned above, this can also be due to the increased flexural capacity of the beams with higher reinforcement ratio which causes the numerical models to fail in shear due to the fact that the beams are not reinforced for shear.

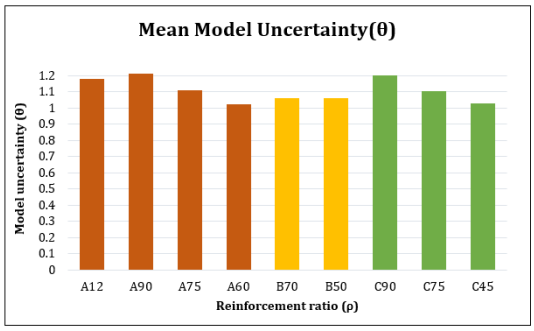

(a) Mean model uncertainty of **F-EB-2-D** based on ρ of A, B and C series of experiments

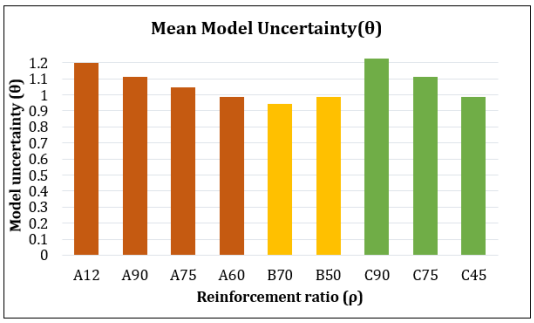

(b) Mean model uncertainty of **R-BS-2** based on ρ of A, B and C series of experiments

Figure 5.20: Influence of reinforcement ratio (ρ) of the benchmark experiments on model uncertainty ratio

In the following chapter, the analyses results from the two modified modelling strategies, **F-EB-3-D** and **R-BS-3** on 16 of the first or original experiments are presented.

6

Analysis Results of the 3rd Group of Modelling Strategies

The refinement of mesh in selected sections of the beam proves to predict better failure mechanism. This is expanded further to analyse 16 original or first experiments. The reason for selection of the original experiments is to avoid the effect of load history on model uncertainty and evaluate the modelling strategies on their merit of predicting failure behaviour.

6.1. F-EB-3-D : Fixed Crack-Embedded-Mesh 3-Damage Based

This modelling strategy is based on a modified version of the modelling strategy F-EB-2-D which was discussed in chapter 5. The modification is done by changing the mesh type. The mesh type is changed from type 2 in figure 3.12 to type 3 in figure 3.13. 16 original experiments, mostly having experimental flexural failure are analysed using the modelling strategy **F-EB-3-D**. Table 6.1 lists the fundamental characteristics of **F-EB-3-D**.

Table 6.1: Applied material models and discretization in **F-EB-3-D**

F-EB-3-D	
Concrete Material Model	
Concrete crack model	Smeared-Total Strain Based
Crack orientation	Fixed
Shear retention	Damage based
Tensile behaviour	Hordijk
Crack bandwidth	Rots
Compression behaviour	Parabolic
Tension-Compression	Vecchio & Collins (Max reduction factor =0.4)
Compression-Compression	Vecchio & Selby
Poisson effect	Damage based reduction
Reinforcement Material Model	
Von Mises plasticity	Linear Strain hardening
Type	Embedded reinforcement
Mesh	
Continuum element type	Regular plane stress
Continuum element name	CQ16M
Reinforcement element type	Truss
Interface element type	2D line quadratic
Element size(h)	25 & 50mm
Interpolation scheme	Quadratic
Integration scheme	Gaussian (3X3)

Following the analyses of the 16 original experiments using **F-EB-3-D**, the model uncertainties of each analysis is quantified using the definition of θ as described in equation (1.1). The statistical distribution of the model uncertainty values is also plotted using MATLAB and illustrated in figure 6.1. A mean value of 0.926 and a coefficient of variation (COV) of 8.25% is obtained. Both of this statistical parameter showed improvement when compared to those of **F-EB-2-D**. However, it is also important to note that the statistical uncertainty is higher in this case since the mean and COV values are based on a smaller set of data.

The predicted behaviour of the experiment A121A1 using **F-EB-3-D** will be further described. The load-displacement graph of A121A1 shows a stiffer numerically predicted behaviour. This graph also shows the presence of ductile plateau which indicates that the failure mechanism is flexure. Although the failure behaviour resembles that of the experiment, the displacement still shows a difference compared to that of the experiments.

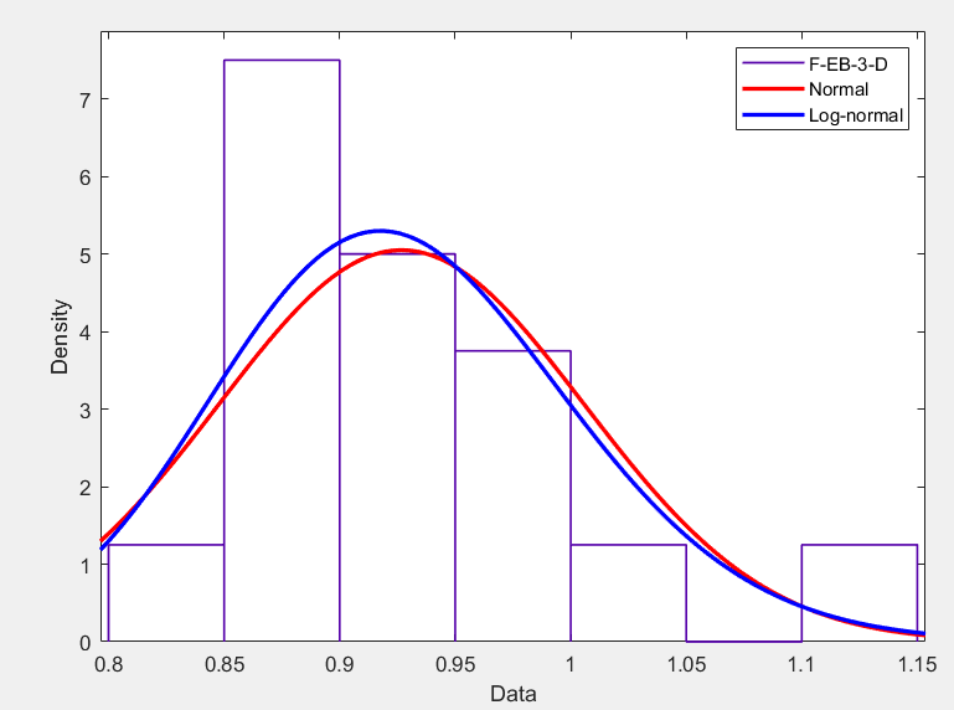

Figure 6.1: Statistical distribution of model uncertainty using **F-EB-3-D**

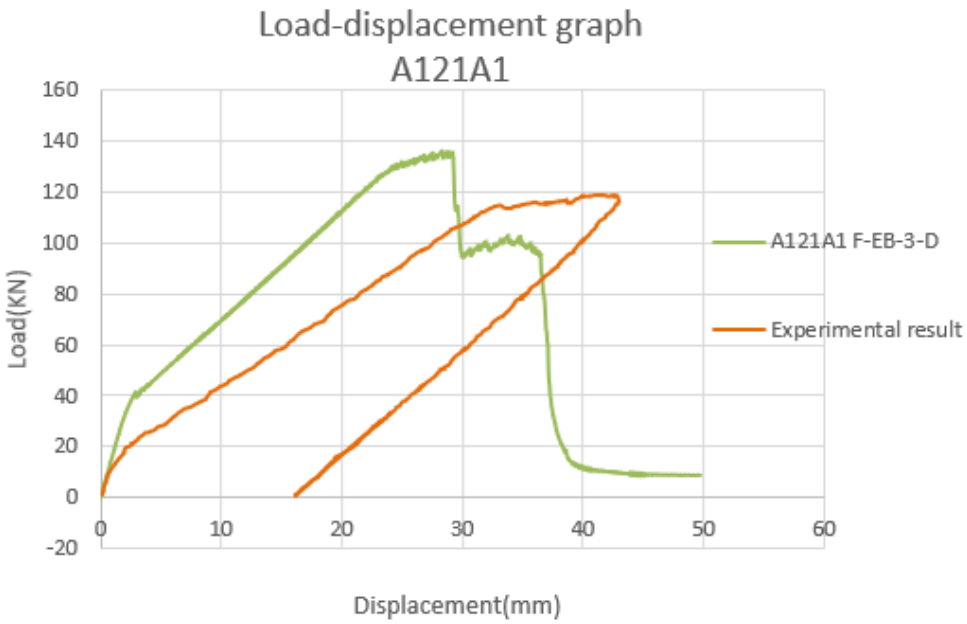

Figure 6.2: Load-displacement graph of A121A1 using **F-EB-3-D**

The failure mechanism of A121A1 at the peak resistance is shown in figure 6.3. This figure shows high flexural crack strain below the point load which leads to yielding of the reinforcement. The stress in the reinforcement before failure is also shown in figure 6.4.

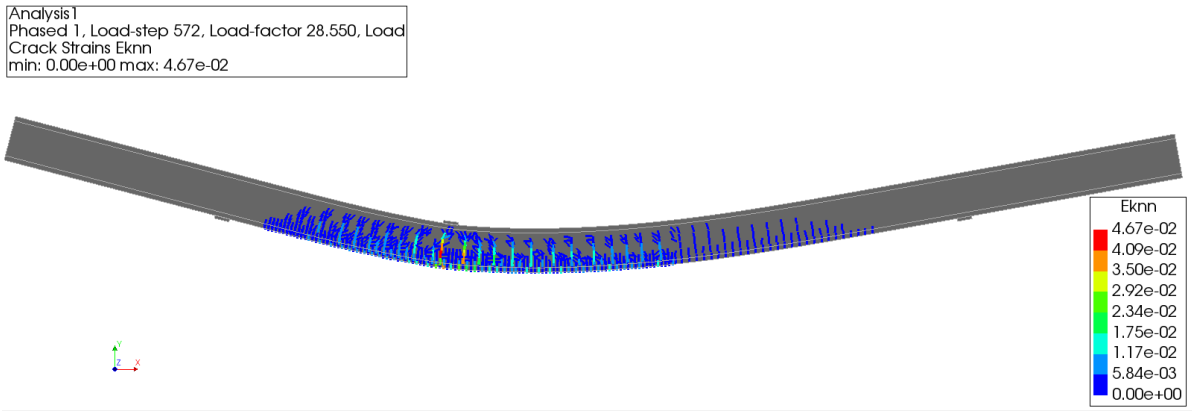

Figure 6.3: Crack strain at failure of A121A1 using **F-EB-3-D**

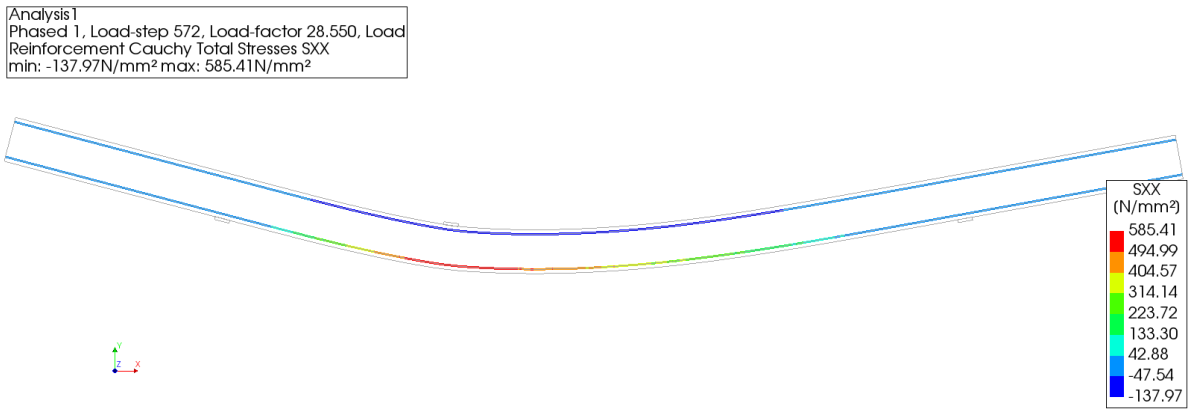

Figure 6.4: Stress in reinforcement at failure of A121A1 using **F-EB-3-D**

The match of experimental and predicted failure mode using **F-EB-3-D** is immensly improved when compared to the previous modelling strategies. 87.5% of the experiments have matching failure modes, this can be seen from table 6.4.

Table 6.2: Experimental and numerical failure mechanisms

Experiment \ R-BS-2	Flexure	Shear	Flexure+Shear
Flexure	10	1	1
Shear	0	3	0
Flexure+Shear	0	1	0

6.2. R-BS-3 : Rotating Crack-Bond Slip-Mesh 3

This modelling strategy, in similar fashion as **F-EB-3-D**, is a modified version of **R-BS-2**. The mesh type was modified from type 2 to type 3. 16 original experiments are again used to study the model uncertainty of this modelling strategy. Table 6.3 lists the fundamental characteristics of **R-BS-3**.

Table 6.3: Applied material models and discretization in **R-BS-3**

R-BS-2	
Concrete Material Model	
Concrete crack model	Smeared-Total Strain Based
Crack orientation	Rotating
Shear retention	Not applicable
Tensile behaviour	Hordijk
Crack bandwidth	Rots
Compression behaviour	Parabolic
Tension-Compression	Vecchio & Collins (Max reduction factor =0.4)
Compression-Compression	Vecchio & Selby
Poisson effect	Damage based reduction
Reinforcement Material Model	
Von Mises plasticity	Linear Strain hardening
Type	Bond-slip reinforcement
Mesh	
Continuum element type	Regular plane stress
Continuum element name	CQ16M
Reinforcement element type	Truss
Interface element type	2D line quadratic
Element size(h)	25 & 50mm
Interpolation scheme	Quadratic
Integration scheme	Gaussian (3X3)

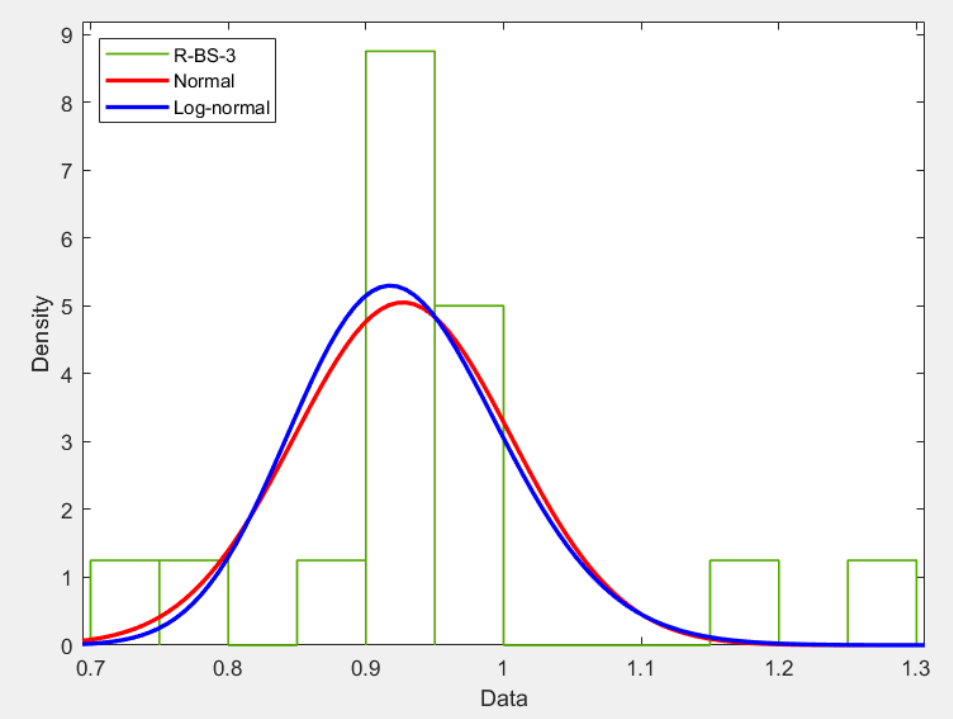

Figure 6.5: Statistical distribution of model uncertainty using **R-BS-2**

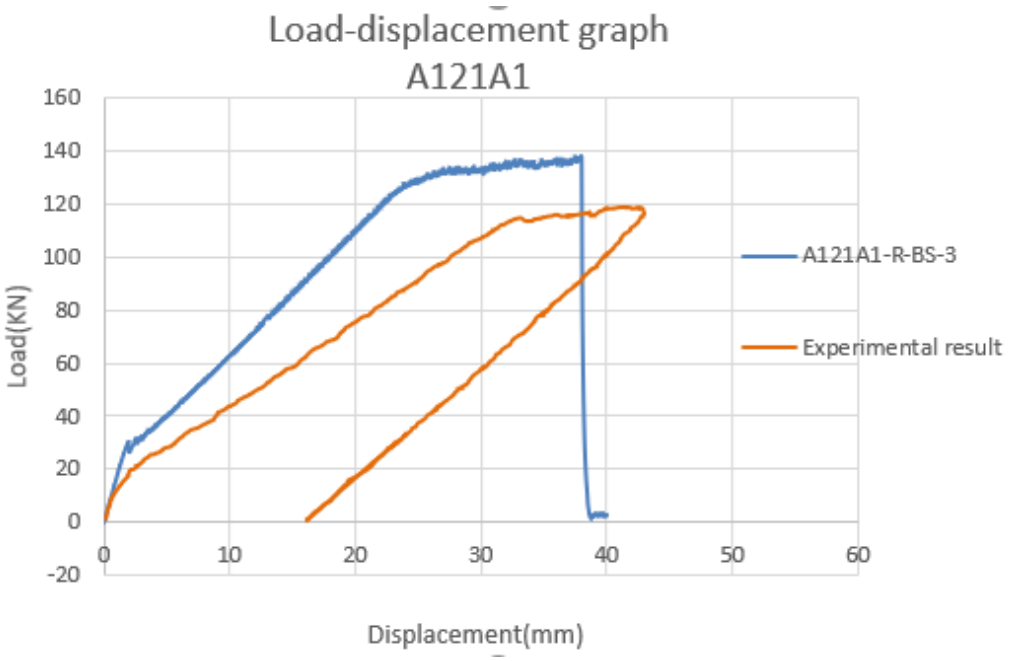

Figure 6.6: Load-displacement graph of A121A1 using **R-BS-3**

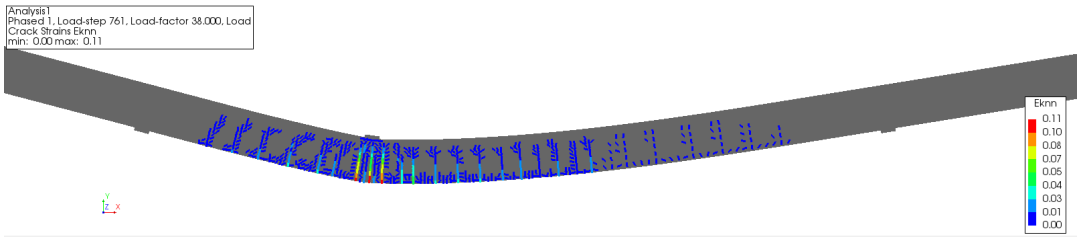

Figure 6.7: Crack strain plot of A121A1 at failure using **F-EB-3-D**

Table 6.4: Experimental and numerical failure mechanisms

Experiment \ R-BS-2	Flexure	Shear	Flexure+Shear
Flexure	11	1	0
Shear	0	2	1
Flexure+Shear	0	1	0

6.3. Discussion

The two modified modelling strategies gave better predictions of the failure mechanism. The mean and COV values of the model uncertainty also showed improvements.

This shows that for reinforced beams without shear reinforcement finer mesh in the critical region where flexural and shera cracks are expected results in more accurate predictions. Majority of the analyses showed match between experimental and numerical failure mechanisms. However the results appear to more stiffer than in previous cases.

7

Correlation of Numerically Predicted Failure Load and Failure Mechanism

The model uncertainty and the predicted failure mechanisms have a correlation as shown in [2]. To quantify this relation the degree of ductility of the numerical failure mechanism is related to the model uncertainty through the ratio known as ductility index. This ratio is defined as :

$$X = \frac{W_{\text{pl,st}}}{W_{\text{pl,sys}}} \tag{7.1}$$

Where W_{plst} and W_{plsys} are the plastic dissipated energy in the steel and the total plastic dissipated energy in the system or structure. This ratio indicates how much of the plastic dissipated energy in the system is taken up by the steel or reinforcement, allowing the measurement of the ductility of the failure mechanism. For this thesis project, ductility index is calculated for the 16 analyses performed using the modelling strategy **F-EB-3-D** as mentioned in section 6.1 and the results are used to study the relation between the ductility of the numerical failure mode and the model uncertainty.

7.1. Method of Calculation of Ductility Index

To calculate the ductility index, the plastic dissipated energy in the reinforcement and the system are computed separately.

7.1.1. Plastic dissipated energy in the reinforcement

The plastic dissipated energy in the reinforcement is calculated by implementing equation (7.2) to equation (7.4) using the stress and strain outputs at each integration point of the reinforcement for all load steps of the NLFEA. A tabular output format of Diana is used to obtain the stress and strain of each integration point in the local x-axis of the reinforcement and these outputs are then manipulated using a Python script to perform the numerical computation using the above mentioned equations. This Python script is attached in Annex D.

$$\Delta W_{\text{tot,st}_n} = \frac{1}{2}(\sigma_{n-1} + \sigma_n)(\varepsilon_n - \varepsilon_{n-1}) \tag{7.2}$$

$$W_{\text{tot,st}_n} = W_{\text{tot,st}_{n-1}} + \Delta W_{\text{tot,st}_n} \tag{7.3}$$

$$W_{\text{pl,st}_m} = W_{\text{tot,st}_m} - W_{\text{el,st}} \tag{7.4}$$

Equation (7.2) describes $\Delta\ W_{\text{tot,st}_n}$ which is the incremental dissipated energy in the reinforcement for a single load step, *n*, and equation (7.3) states the total dissipated energy, $W_{\text{tot,st}_n}$, up to the current load step *n*, which is the summation of $\Delta\ W_{\text{tot,st}_n}$ for all load steps up to *n*. These two equations are computed for each load step and finally equation (7.4) is used to calculate the plastic dissipated energy, $W_{\text{pl,st}_m}$, in the reinforcement for the last load step *m*. σ_n and σ_{n-1} are the stress in the reinforcement for the current (*n*) and previous (*n-1*) load steps while ε_n and ε_{n-1} are the strain in the reinforcement for the current and previous load steps respectively. $W_{\text{el,st}}$ is the elastic dissipated energy in the reinforcement which is given as:

$$W_{\text{el,st}} = \frac{1}{2} * (f_{\text{y}}) * (\varepsilon_y) \tag{7.5}$$

Equation (7.2) to equation (7.5) calculate the plastic dissipated energy at a single integration point of the reinforcement per unit volume, in order to compute the plastic dissipated energy in the entire reinforcement, the result of equation (7.4) is multiplied by the volume of a single integration point and summed for all integration points of the reinforcement.

$$W_{\text{pl,st}} = \sum_{i=1}^{r} W_{\text{pl,st}_m} * Vol_{intg} \tag{7.6}$$

where *r* is the number of integration points in the reinforcement.

7.1.2. Plastic dissipated energy in the system

The total plastic dissipated energy in the system is calculated by taking the area under the load-displacement graph after unloading. This is done by first running the analysis and registering the load step which results in the peak load and then unloading from this load step. For this study, the analyses of 16 experiments performed using the modelling strategy **F-EB-3-D**, are used and **F-EB-3-D** uses the total strain based crack model for concrete which only allows secant unloading. Due to this, unloading of all the 16 experiments results in a load-displacement graph as shown in figure 7.1. The shaded area in figure 7.1 represents the plastic dissipated energy in the system which is calculated by taking the difference of the area under the loading and unloading graphs. The area under these graphs are calculated in MATLAB using an approximation rule due to the irregular shape of the graphs.

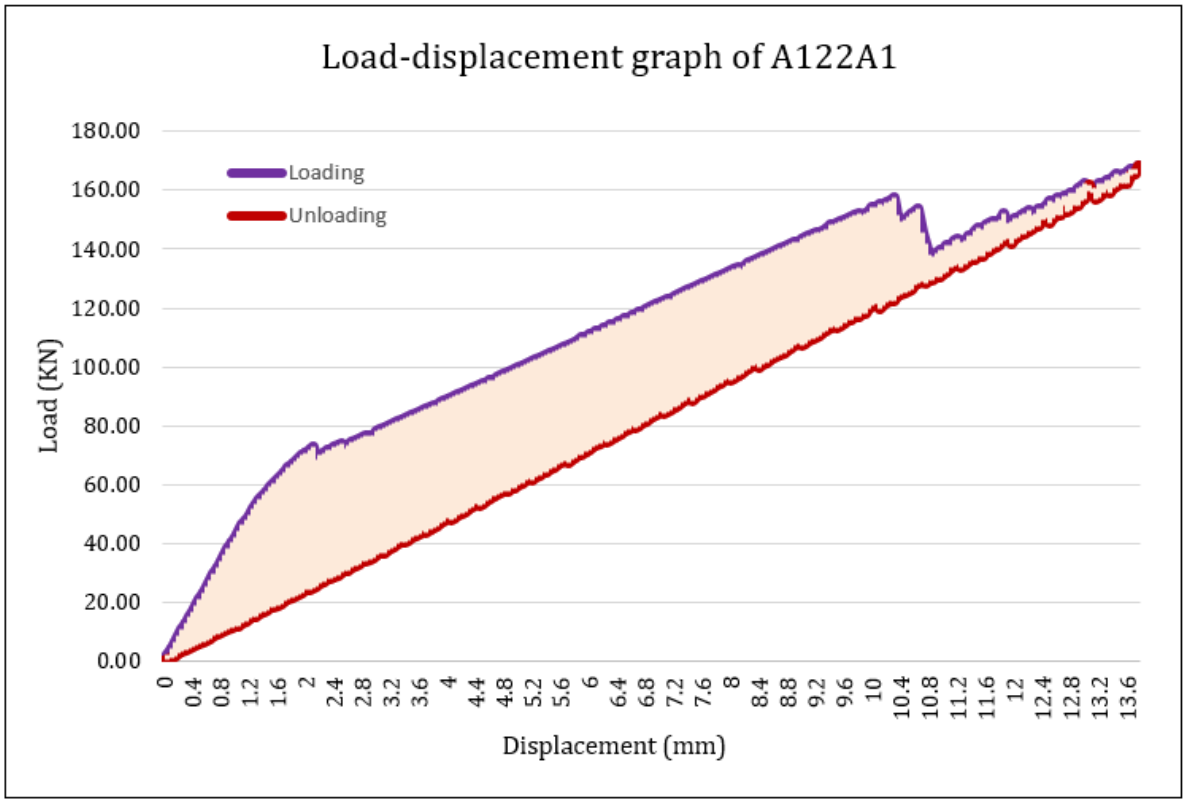

Figure 7.1: Load-displacement graph with unloading to calculate the plastic dissipated energy in the structure

7.2. Relation between Model Uncertainty and Ductility Index for F-EB-3-D Modelling Strategy

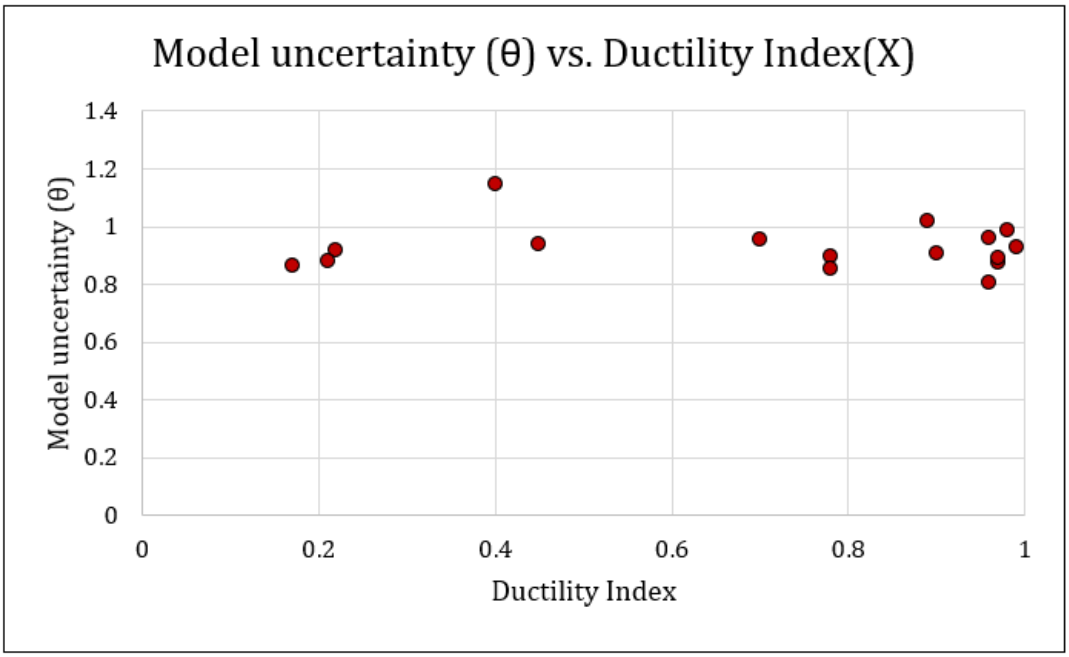

Figure 7.2: Correlation between numerical failure mode and model uncertainty using **F-EB-3-D**

Table 7.1: Model uncertainty and ductility index of **F-EB-3-D**

Name	θ	DI	Exp failure	Num failure
A121A1	0.957	0.700	F	F
A122A1	1.148	0.400	F/S	S
A123A1	0.917	0.220	S	S
A901A1	0.898	0.780	F	F+S
A902A1	0.880	0.210	S	S
A751A1	0.855	0.780	F	F
A752A1	0.941	0.450	F	S
A601A1	0.908	0.900	F	F
A602A1	0.874	0.970	F	F
B701A1	0.986	0.980	F	F
B702A1	0.864	0.170	S	S
B501A1	1.017	0.890	F	F
B502A1	0.957	0.960	F	F
C901A1	0.928	0.990	F	F
C751A1	0.893	0.970	F	F
C451A1	0.806	0.960	F	F

7.3. Discussion

High ductility index means the plastic dissipated energy is carried mostly by the reinforcement and this shows us that a ductile behaviour is observed from the numerical models. On the other hand lower values of the ductility index show brittle numerical failure. The analyses with lower ductility show relatively more spread of the model uncertainty ratio. However since the number of experiments are limited to 16 and the majority of the experiments show numerical flexural failure, the statistical uncertainty is higher.

The ductility index shows the brittle or ductile nature of the numerically predicted failure mode and relating this to the model uncertainty disregards the experimentally observed failure behaviour. Although it can be used as an objective tool to characterize the numerical failure mode, it is also dependent on the accuracy of the modelling strategy used which is affected by factors such as the discretization of the geometry, the iterative solution procedure, the applied material model or the idealization of the geometry.

For the above mentioned reasons, a correlation between ductility index and the model uncertainty ratio should not always be made since it associates the ability of a modelling strategy to predict the ultimate capacity with its ability to predict the failure mode which happen to be independent as can be seen from the results of the second and third group of modelling strategies. In some cases, a certain modelling strategy predicts the failure load with high accuracy but fails to predict the ductile or brittle nature of the failure mode.

However figure 7.2 shows that higher ductility index values are on average associated with model uncertainty ratio close to 1.

Conclusions

1. Based on the results of the study on the model uncertainty of NLFEA of reinforced concrete structures, it is possible to see that the implemented approach in NLFEA of reinforced concrete structures does indeed result in different model uncertainty, which leads to the conclusion that it is possible to use a NLFEA with a low model uncertainty if certain aspects of the numerical model are chosen carefully.

2. The results of this study show that the model uncertainty of a given NLFEA modelling strategy is indeed influenced by the type of failure mode of the structure. Brittle shear failure on average resulted in higher model uncertainty than ductile flexural failure. The properties of the structure such as cross-sectional height, reinforcement ratio and concrete compressive strength also affect the resulted model uncertainty for a given NLFEA modelling strategy. The effect of reinforcement ratio is even more pronounced with lower model uncertainty obtained for reinforcement ratio lower than 0.6%.

3.The use of rotating crack model with embedded reinforcement demonstrated failure due to delamination of the concrete cover. As a result, rotating crack models should be used in combination with bond-slip reinforcement for reinforced concrete beams without shear reinforcement. On the other hand, the fixed crack model with embedded reinforcement proved to be capable of predicting both flexural and shear failure modes while the behaviour of fixed crack model with bond-slip reinforcement is outside the scope of this thesis project and thus was not investigated.

4. From the study on different modelling strategies, it is possible to see that the rotating crack model in combination with bond-slip reinforcement is able to give on average a lower model uncertainty than the fixed crack model in combination with embedded reinforcement. However sufficiently small element size must be used in order to result in comparable numerical predictions in both cases. The use of element size of one-sixth and one-tenth of the cross-sectional height proved to be insufficient for the benchmark experiments performed on reinforced concrete beams without shear reinforcement.

5. Implementation of a fine mesh in the section of the beams where flexural or shear crack are expected, resulted in accurate prediction of failure mechanisms and reduced the model uncertainty ratio. Due to this, it can be concluded that verification of the required element size is important for NLFEA especially when considering concrete structures susceptible to brittle failure. Thus, the recommendation of element size of one-sixth of the height (H/6) in [6] is found to be insufficient and should be verified before application.

6. The correlation between the model uncertainty of the failure load and the numerical failure mode is made using the ductility index ratio however it is important to understand the effect of solving the correct set of equations accurately on the computed ductility index and an accurate correlation can be made if the numerically predicted failure mechanism resembles that observed in the experiment.

Recommendations

1. The model uncertainty of NLFEA is affected by how accurately the numerical model is developed and one important aspect is the consideration of the load history of the structure in the finite element model. Although majority of the time the existing loading condition is simulated, the effort to incorporate the effect of prior loading scenario should be made.

2. The investigation of the performance of fixed crack model with bond-slip reinforcement should be carried out to compare the resulting model uncertainty with the modelling strategies investigated in thesis project and give a more comprehensive recommendation of the preferred approach to numerically model reinforced concrete beams without shear reinforcement.

3. The different available material models to simulate the deterioration of bond stress and the relative slip between concrete and reinforcement should further be investigated besides the relation recommended in the fib model code 2010 [4] which is used to model the bond-slip reinforcement in this study.

4. For this thesis project, the accuracy of failure mode prediction is assessed using visual inspection, however it is recommended to investigate ways that can objectively measure the accuracy of the predicted failure mode and compare it with that of the experiment.

5. Model uncertainty of NLFEA with respect to the accuracy of the predicted deformation or displacement should also be investigated and incorporated with the model uncertainty of the ultimate capacity. Although for simply supported beams the accuracy of the predicted deformation has less importance, for structurally indeterminate members it can have a pronounced effect on the simulation of the failure behaviour.

A

Annex A

Table A.1: Predicted failure load and failure mechanism of 67 benchmark experiments using **F-EB-2-D**

No.	Experiment Name	Exp. Peak load(KN)	NLFEA Peak Load (KN)	MUC	NLFEA Failure mode	Exp. Failure mode	Exp. Yield load
1	A121A1	115.3	99.66	1.157	Shear	Flexure	
2	A121A2	138.8	107.84	1.287	Shear	Flexure	
3	A121A3	144.6	108.54	1.332	Shear	Shear	
4	A121B1	160.6	163.39	0.983	Shear	Flexure+ shear	
5	A122A1	194.7	200.61	0.971	Flexure+ shear	Flexure+ shear	
6	A122B1	152.3	138.96	1.096	Shear	Shear	
7	A123A1	136.5	111.5	1.224	Shear	Shear	
8	A123A2	139	119.94	1.159	Shear	Shear	
9	A123B1	134.9	106.18	1.27	Shear	Flexure	
10	A123B2	148.9	113.03	1.317	Shear	Flexure+ shear	
11	A901A1	105.6	100.59	1.05	Shear	Flexure	
12	A901A2	123.9	103.25	1.2	Shear	Flexure	
13	A901A3	145	109.59	1.323	Shear then Yielding	Shear	
14	A901B1	127.5	105.34	1.21	Shear then Yielding	Shear	
15	A901B2	124.2	116.43	1.067	Shear then Yielding	Shear	
16	A902A1	120.7	99.66	1.211	Shear then Yielding	Shear	
17	A902A2	136	108.23	1.257	Shear then Yielding	Flexure	
18	A902A3	149.4	111.51	1.34	Shear then Yielding	Shear	
19	A902B1	121.5	98.55	1.233	Shear then Yielding	Flexure	
20	A902B2	124.2	101.82	1.22	Shear then Yielding	Shear	
21	A751A1	97.1	93.45	1.039	Shear then Yielding	Flexure	
22	A751A2	118.4	116.38	1.017	Shear then Yielding	Shear	
23	A751B1	106.7	100.62	1.06	Shear then Yielding	Shear	
24	A751B2	110.1	100.29	1.098	Shear then Yielding	Flexure+ shear	
25	A752A1	108.7	106.36	1.022	Shear then Yielding	Flexure	
26	A752A2	119	99.6	1.195	Shear then Yielding	Shear	
27	A752A3	121.6	99.6	1.221	Shear then Yielding	Flexure+ shear	
28	A752B2	141.9	117.19	1.211	Shear then Yielding	Flexure+ shear	
29	A601A1	80.3	89.53	0.897	Flexure	Flexure	
30	A601A2	102.1	94.18	1.084	Shear then Yielding	Flexure	
31	A601B1	118.7	104.53	1.136	Shear then Yielding	Flexure+ shear	
32	A601B2	123.2	122.6	1.005	Flexure with shear cracks	F with flexural shear cracks	
33	A602A1	98.8	104.38	0.947	Shear then Yielding	Flexure	
34	A602A2	112.8	98.44	1.146	Shear then Yielding	Flexure	
35	A602A3	114.2	99.38	1.149	Shear then Yielding	Flexure+ shear	
36	A602B1	58	59.2	0.98	Flexure	Flexure	
37	A602B2	110.9	128.14	0.865	Shear then Yielding	Flexure+ shear	
38	B701A1	175.5	188.84	0.929	Flexure+ shear	Flexure	
39	B701A2	179.5	178.46	1.006	Shear	Flexure	
40	B701A3	185.7	175.53	1.058	Shear	Flexure	
41	B701B1	193.6	167.31	1.157	Shear	Flexure	
42	B701B2	202.4	160.5	1.261	Shear	Shear	
43	B702A1	183.2	172.52	1.062	Shear then Yielding	Shear	
44	B702B1	164.9	176.33	0.935	Shear	Shear	
45	B501A1	168.5	170.37	0.989	Flexure+ shear	Flexure	
46	B501A2	166.4	155.31	1.071	Shear	Shear	
47	B501B1	165.7	167.79	0.988	Shear	Shear	
48	B502A1	166.9	152.63	1.094	Shear	Flexure	
49	B502A2	175.1	154.07	1.136	Shear	Flexure	
50	B502A3	173.6	160.56	1.081	Shear	Shear	
51	B502B1	173.2	160.56	1.079	Shear	Shear	
52	C901A1	98.5	78.21	1.259	Shear	Flexure	
53	C901A2	103.4	83.33	1.241	Shear	Shear	
54	C901A3	84.1	83.33	1.009	Shear	Shear	
55	C901B1	101.7	78.21	1.3	Shear	Shear	
56	C751A1	76.5	71.66	1.068	Shear	Flexure	
57	C751A2	84.5	76.93	1.098	Shear	Shear	
58	C751A3	86.7	76.93	1.127	Shear	Shear	
59	C751B1	82.8	73.82	1.122	Shear	Flexure+ shear	
60	C451A1	41.4	49.99	0.828	Flexure	Flexure	
61	C451A2	58.6	59.54	0.984	Flexure+ shear	Flexure	
62	C451A3	73.5	65.07	1.129	Shear then Yielding	Flexure+ shear	
63	C451A4	70.9	65.07	1.09	Shear then Yielding	Shear	
64	C451B1	58.5	62.73	0.933	Shear then Yielding	Flexure	
65	C451B2	70.6	64.32	1.098	Shear then Yielding	Flexure+ shear	
66	C451B3	67.1	64.32	1.043	Shear then Yielding	Flexure	
67	C451B4	77.2	68.47	1.127	Shear then Yielding	Shear	

Table A.2: Predicted failure load and failure mechanism of 67 benchmark experiments using **R-BS-2**

No.	Experiment Name	Exp. Peak load(KN)	NLFEA Peak Load (KN)	MUC	NLFEA Failure mode	Exp. Failure mode
1	A121A1	115.3	99.66	1.157	Shear	Flexure
2	A121A2	138.8	107.84	1.287	Shear	Flexure
3	A121A3	144.6	108.54	1.332	Shear	Shear
4	A121B1	160.6	163.39	0.983	Shear	Flexure+ shear
5	A122A1	194.7	200.61	0.971	Flexure+ shear	Flexure+ shear
6	A122B1	152.3	138.96	1.096	Shear	Shear
7	A123A1	136.5	111.5	1.224	Shear	Shear
8	A123A2	139	119.94	1.159	Shear	Shear
9	A123B1	134.9	106.18	1.27	Shear	Flexure
10	A123B2	148.9	113.03	1.317	Shear	Flexure+ shear
11	A901A1	105.6	100.59	1.05	Shear	Flexure
12	A901A2	123.9	103.25	1.2	Shear	Flexure
13	A901A3	145	109.59	1.323	Shear then Yielding	Shear
14	A901B1	127.5	105.34	1.21	Shear then Yielding	Shear
15	A901B2	124.2	116.43	1.067	Shear then Yielding	Shear
16	A902A1	120.7	99.66	1.211	Shear then Yielding	Shear
17	A902A2	136	108.23	1.257	Shear then Yielding	Flexure
18	A902A3	149.4	111.51	1.34	Shear then Yielding	Shear
19	A902B1	121.5	98.55	1.233	Shear then Yielding	Flexure
20	A902B2	124.2	101.82	1.22	Shear then Yielding	Shear
21	A751A1	97.1	93.45	1.039	Shear then Yielding	Flexure
22	A751A2	118.4	116.38	1.017	Shear then Yielding	Shear
23	A751B1	106.7	100.62	1.06	Shear then Yielding	Shear
24	A751B2	110.1	100.29	1.098	Shear then Yielding	Flexure+ shear
25	A752A1	108.7	106.36	1.022	Shear then Yielding	Flexure
26	A752A2	119	99.6	1.195	Shear then Yielding	Shear
27	A752A3	121.6	99.6	1.221	Shear then Yielding	Flexure+ shear
28	A752B2	141.9	117.19	1.211	Shear then Yielding	Flexure+ shear
29	A601A1	80.3	89.53	0.897	Flexure	Flexure
30	A601A2	102.1	94.18	1.084	Shear then Yielding	Flexure
31	A601B1	118.7	104.53	1.136	Shear then Yielding	Flexure+ shear
32	A601B2	123.2	122.6	1.005	Flexure with shear cracks	F with flexural shear cracks
33	A602A1	98.8	104.38	0.947	Shear then Yielding	Flexure
34	A602A2	112.8	98.44	1.146	Shear then Yielding	Flexure
35	A602A3	114.2	99.38	1.149	Shear then Yielding	Flexure+ shear
36	A602B1	58	59.2	0.98	Flexure	Flexure
37	A602B2	110.9	128.14	0.865	Shear then Yielding	Flexure+ shear
38	B701A1	175.5	188.84	0.929	Flexure+ shear	Flexure
39	B701A2	179.5	178.46	1.006	Shear	Flexure
40	B701A3	185.7	175.53	1.058	Shear	Flexure
41	B701B1	193.6	167.31	1.157	Shear	Flexure
42	B701B2	202.4	160.5	1.261	Shear	Shear
43	B702A1	183.2	172.52	1.062	Shear then Yielding	Shear
44	B702B1	164.9	176.33	0.935	Shear	Shear
45	B501A1	168.5	170.37	0.989	Flexure+ shear	Flexure
46	B501A2	166.4	155.31	1.071	Shear	Shear
47	B501B1	165.7	167.79	0.988	Shear	Shear
48	B502A1	166.9	152.63	1.094	Shear	Flexure
49	B502A2	175.1	154.07	1.136	Shear	Flexure
50	B502A3	173.6	160.56	1.081	Shear	Shear
51	B502B1	173.2	160.56	1.079	Shear	Shear
52	C901A1	98.5	78.21	1.259	Shear	Flexure
53	C901A2	103.4	83.33	1.241	Shear	Shear
54	C901A3	84.1	83.33	1.009	Shear	Shear
55	C901B1	101.7	78.21	1.3	Shear	Shear
56	C751A1	76.5	71.66	1.068	Shear	Flexure
57	C751A2	84.5	76.93	1.098	Shear	Shear
58	C751A3	86.7	76.93	1.127	Shear	Shear
59	C751B1	82.8	73.82	1.122	Shear	Flexure+ shear
60	C451A1	41.4	49.99	0.828	Flexure	Flexure
61	C451A2	58.6	59.54	0.984	Flexure+ shear	Flexure
62	C451A3	73.5	65.07	1.129	Shear then Yielding	Flexure+ shear
63	C451A4	70.9	65.07	1.09	Shear then Yielding	Shear
64	C451B1	58.5	62.73	0.933	Shear then Yielding	Flexure
65	C451B2	70.6	64.32	1.098	Shear then Yielding	Flexure+ shear
66	C451B3	67.1	64.32	1.043	Shear then Yielding	Flexure
67	C451B4	77.2	68.47	1.127	Shear then Yielding	Shear

B

Annex B

```
#Project Settings
newProject( "Directory/Name", 1000 )
setModelAnalysisAspects( [ "STRUCT" ] )
setModelDimension( "2D" )
setDefaultMeshOrder( "QUADRATIC" )
setDefaultMesherType( "HEXQUAD" )
setDefaultMidSideNodeLocation( "LINEAR" )
setUnit( "LENGTH", "MM" )
setUnit( "FORCE", "N" )

#Material Properties
#Concrete
E=26610.39              #Young's Modulus [MPa]
vc=0.2                  #Poisson Ratio [-]
MDensC=2.4e-09          #Mass Density [T/mm3]
fct=1.48                #Tensile Strength [MPa]
Gft=0.1239              #Tensile Fracture Energy [N/mm]
Gfc=30.99               #Compressive Fracture Energy [N/mm]
fc=18.96                #Compressive Strength [MPa]

#Reinforcement
Es=210000               #Young's Modulus [MPa]
vs=0.3                  #Poisson Ratio [-]
MdensR=7.85e-09         #Mass Density [T/mm3]
fy=550                  #Yield Strength [MPa]

#Interface Between Load/Support Plate and Beam
kn=8400                 #Normal Stiffness [N/mm3]
ks=84                   #Shear Stiffness [N/mm3]

#Geometry
#Beam and Reinforcement
Lbeam= 8000             #Length of the beam [mm]
Hbeam=300               #Height of the beam [mm]
width=300               #Width of the beam [mm]
d=270                   #Effective depth [mm]
As=603.19               #Area of reinforcement
Cbr= Hbeam-d            #Concrete Cover

#Support Plate
X1=1450                 #Start of the left support plate (X)
X2=1550                 #End of the left support plate (X)
Y1=-20                  #End of the support plate (Y)
Y2=0                    #Start of the support plate (Y)
Lspan=5000              #Clear Span of the Beam
Lsuppcent=1500          #Center of the left support
Rsuppcent=Lsuppcent+Lspan   #Center of the right support

#Load Plate
a=1100                  #Shear Span
Hplate=20               #Height of Load Plate
Lplatecent=Lsuppcent+a  #Center of the load plate

#Mesh
Elem=50                 #Mesh Size


#Layout of the Beam
createSheet( "Concrete beam", [[ 0, 0, 0 ],[ Lbeam, 0, 0 ],[ Lbeam, Hbeam, 0 ],[ 0,
Hbeam, 0 ]] )
createLine( "Bottom Rebar", [ 0, Cbr, 0 ], [ Lbeam, Cbr, 0 ] )
createLine( "Top Rebar", [ 0, d, 0 ], [ Lbeam, d , 0 ] )
createSheet( "L Supp plate", [[ X1, Y1, 0 ],[ X2, Y1, 0 ],[ X2, Y2, 0 ],[ X1, Y2, 0
]] )
createSheet( "R Supp plate", [[ X1+Lspan, Y1, 0 ],[ X2+Lspan, Y1, 0 ],[X2+Lspan ,
Y2, 0 ],[ X1+Lspan, Y2, 0 ]] )
createSheet( "Load plate", [[X1+a , Hbeam, 0 ],[ X2+a, Hbeam, 0 ],[ X2+a,
Hbeam+Hplate, 0 ],[ X1+a, Hbeam+Hplate, 0 ]] )
```

```
#Creating necessary vertex and lines
createPointBody( "Point body 1", [ Lsuppcent, Y1, 0 ] )
createPointBody( "Point body 2", [ Lplatecent, Hbeam+Hplate, 0 ] )
createPointBody( "Point body 3", [ Rsuppcent, Y1, 0 ] )
projection( "SHAPEEDGE", "L Supp plate", [[ Lsuppcent, Y1, 0 ]], [ "Point body 1"
], [ 0, 0, -1 ], True )
removeShape( [ "Point body 1" ] )
projection( "SHAPEEDGE", "Load plate", [[ Lplatecent, Hbeam+Hplate, 0 ]], [ "Point
body 2" ], [ 0, 0, -1 ], True )
removeShape( [ "Point body 2" ] )
projection( "SHAPEEDGE", "R Supp plate", [[ Rsuppcent, Y1, 0 ]], [ "Point body 3"
], [ 0, 0, -1 ], True )
removeShape( [ "Point body 3" ] )
createLine( "Line Lsupp", [ X1, Y2, 0 ], [ X2, Y2, 0 ] )
createLine( "Line Rsupp", [ X1+Lspan, Y2, 0 ], [ X2+Lspan, Y2, 0 ] )
projection( "SHAPEFACE", "Concrete beam", [[ Lbeam/2, Hbeam/2, 0 ]], [ "Line
Lsupp", "Line Rsupp" ], [ 0, 0, -1 ], True )
removeShape( [ "Line Lsupp", "Line Rsupp" ] )

#Support
addSet( "GEOMETRYSUPPORTSET", "Support" )
createPointSupport( "Lsupport", "Support" )
setParameter( "GEOMETRYSUPPORT", "Lsupport", "AXES", [ 1, 2 ] )
setParameter( "GEOMETRYSUPPORT", "Lsupport", "TRANSL", [ 1, 1, 0 ] )
setParameter( "GEOMETRYSUPPORT", "Lsupport", "ROTATI", [ 0, 0, 0 ] )
attach( "GEOMETRYSUPPORT", "Lsupport", "L Supp plate", [[ Lsuppcent, Y1, 0]])
createPointSupport( "Rsupport", "Support" )
setParameter( "GEOMETRYSUPPORT", "Rsupport", "AXES", [ 1, 2 ] )
setParameter( "GEOMETRYSUPPORT", "Rsupport", "TRANSL", [ 0, 1, 0 ] )
setParameter( "GEOMETRYSUPPORT", "Rsupport", "ROTATI", [ 0, 0, 0 ] )
attach( "GEOMETRYSUPPORT", "Rsupport", "R Supp plate", [[ Rsuppcent, Y1, 0 ]] )
addSet( "GEOMETRYSUPPORTSET", "load Support" )
createPointSupport( "Rxn @disp", "load Support" )
setParameter( "GEOMETRYSUPPORT", "Rxn @disp", "AXES", [ 1, 2 ] )
setParameter( "GEOMETRYSUPPORT", "Rxn @disp", "TRANSL", [ 0, 1, 0 ] )
setParameter( "GEOMETRYSUPPORT", "Rxn @disp", "ROTATI", [ 0, 0, 0 ] )
attach( "GEOMETRYSUPPORT", "Rxn @disp", "Load plate", [[ Lplatecent, Hbeam+Hplate,
0 ]] )

#Load
addSet( "GEOMETRYLOADSET", "Load" )
createPointLoad( "Point load", "Load" )
setParameter( "GEOMETRYLOAD", "Point load", "LODTYP", "DEFORM" )
setParameter( "GEOMETRYLOAD", "Point load", "DEFORM/TR/VALUE", -1 )
setParameter( "GEOMETRYLOAD", "Point load", "DEFORM/TR/DIRECT", 2 )
attach( "GEOMETRYLOAD", "Point load", "Load plate", [[ Lplatecent, Hbeam+Hplate, 0
]] )
addSet( "GEOMETRYLOADSET", "Self-weight" )
createModelLoad( "Self-weight", "Self-weight" )

#Material property
#Element data
addElementData( "Element data 1" )
setParameter( "DATA", "Element data 1", "./INTEGR", [] )
setParameter( "DATA", "Element data 1", "INTEGR", "HIGH" )
assignElementData( "Element data 1", "SHAPE", [ "Concrete beam" ] )
assignElementData( "Element data 1", "SHAPE", [ "L Supp plate" ] )
assignElementData( "Element data 1", "SHAPE", [ "Load plate" ] )
assignElementData( "Element data 1", "SHAPE", [ "R Supp plate" ] )

#Concrete
addMaterial( "Concrete", "CONCR", "TSCR", [] )
setParameter( "MATERIAL", "Concrete", "LINEAR/ELASTI/YOUNG", E )
setParameter( "MATERIAL", "Concrete", "LINEAR/ELASTI/POISON", vc )
setParameter( "MATERIAL", "Concrete", "LINEAR/MASS/DENSIT", MDensC )
setParameter( "MATERIAL", "Concrete", "TENSIL/TENCRV", "HORDYK" )
setParameter( "MATERIAL", "Concrete", "TENSIL/TENSTR", fct)
```

```
setParameter( "MATERIAL", "Concrete", "TENSIL/GF1", Gft)
setParameter( "MATERIAL", "Concrete", "TENSIL/POISRE/POIRED", "DAMAGE" )
setParameter( "MATERIAL", "Concrete", "COMPRS/COMCRV", "PARABO" )
setParameter( "MATERIAL", "Concrete", "COMPRS/COMSTR", fc )
setParameter( "MATERIAL", "Concrete", "COMPRS/GC", Gfc)
setParameter( "MATERIAL", "Concrete", "COMPRS/REDUCT/REDCRV", "VC1993" )
setParameter( "MATERIAL", "Concrete", "COMPRS/REDUCT/REDMIN", 0.4 )
setParameter( "MATERIAL", "Concrete", "COMPRS/CONFIN/CNFCRV", "VECCHI" )
setParameter( "MATERIAL", "Concrete", "SHEAR/SHRCRV", "DAMAGE" )
addGeometry( "Element geometry 1", "SHEET", "MEMBRA", [] )
rename( "GEOMET", "Element geometry 1", "Concrete" )
setParameter( "GEOMET", "Concrete", "THICK", width)
setParameter( "GEOMET", "Concrete", "LOCAXS", True )
setElementClassType( "SHAPE", [ "Concrete beam" ], "MEMBRA" )
assignMaterial( "Concrete", "SHAPE", [ "Concrete beam" ] )
assignGeometry( "Concrete", "SHAPE", [ "Concrete beam" ] )

#Reinforcement
addMaterial( "Reinforcement", "REINFO", "VMISES", [] )
setParameter( "MATERIAL", "Reinforcement", "LINEAR/ELASTI/YOUNG", Es )
setParameter( "MATERIAL", "Reinforcement", "PLASTI/YLDTYP", "EPSSIG" )
setParameter( "MATERIAL", "Reinforcement", "PLASTI/HARDI4/EPSSIG", [] )
setParameter( "MATERIAL", "Reinforcement", "PLASTI/HARDI4/EPSSIG", [ 0, 0,
0.002619, 550, 0.0157, 605 ] )
addGeometry( "Element geometry 4", "RELINE", "REBAR", [] )
rename( "GEOMET", "Element geometry 4", "Reinforcement" )
setParameter( "GEOMET", "Reinforcement", "REITYP", "REIEMB" )
setParameter( "GEOMET", "Reinforcement", "REIEMB/CROSSE", As )
setReinforcementAspects( [ "Top Rebar", "Bottom Rebar" ] )
assignMaterial( "Reinforcement", "SHAPE", [ "Top Rebar", "Bottom Rebar" ] )
assignGeometry( "Reinforcement", "SHAPE", [ "Top Rebar", "Bottom Rebar" ] )
assignElementData( "Element data 1", "SHAPE", [ "Top Rebar", "Bottom Rebar" ] )
setReinforcementDiscretization( [ "Top Rebar", "Bottom Rebar" ], "ELEMENT" )

#Steel plate
addMaterial( "Steel plate", "MCSTEL", "ISOTRO", [] )
setParameter( "MATERIAL", "Steel plate", "LINEAR/ELASTI/YOUNG", Es )
setParameter( "MATERIAL", "Steel plate", "LINEAR/ELASTI/POISON", vs )
setParameter( "MATERIAL", "Steel plate", "LINEAR/MASS/DENSIT", MdensR )
addGeometry( "Element geometry 3", "SHEET", "MEMBRA", [] )
rename( "GEOMET", "Element geometry 3", "Steel plate" )
setParameter( "GEOMET", "Steel plate", "THICK", width )
setParameter( "GEOMET", "Steel plate", "LOCAXS", True )
setElementClassType( "SHAPE", [ "L Supp plate", "Load plate", "R Supp plate" ],
"MEMBRA" )
assignMaterial( "Steel plate", "SHAPE", [ "L Supp plate", "Load plate", "R Supp
plate" ] )
assignGeometry( "Steel plate", "SHAPE", [ "L Supp plate", "Load plate", "R Supp
plate" ] )

#Interface
addMaterial( "Interface", "INTERF", "ELASTI", [] )
setParameter( "MATERIAL", "Interface", "LINEAR/IFTYP", "LIN2D" )
setParameter( "MATERIAL", "Interface", "LINEAR/ELAS2/DSNY", kn )
setParameter( "MATERIAL", "Interface", "LINEAR/ELAS2/DSSX", ks )
addGeometry( "Element geometry 4", "LINE", "STLIIF", [] )
rename( "GEOMET", "Element geometry 4", "Interface" )
setParameter( "GEOMET", "Interface", "LIFMEM/THICK", width )
setParameter( "GEOMET", "Interface", "LOCAXS", True )
createConnection( "Interface", "INTER", "SHAPEEDGE" )
setParameter( "GEOMETRYCONNECTION", "Interface", "MODE", "AUTO" )
attachTo( "GEOMETRYCONNECTION", "Interface", "SOURCE", "L Supp plate", [[
Lsuppcent, 0, 0 ]] )
attachTo( "GEOMETRYCONNECTION", "Interface", "SOURCE", "Concrete beam", [[
Lsuppcent, 0, 0 ]] )
attachTo( "GEOMETRYCONNECTION", "Interface", "SOURCE", "R Supp plate", [[
Rsuppcent, 0, 0 ]] )
attachTo( "GEOMETRYCONNECTION", "Interface", "SOURCE", "Concrete beam", [[
```

```
Rsuppcent, 0, 0 ]] )
attachTo( "GEOMETRYCONNECTION", "Interface", "SOURCE", "Load plate", [[ Lplatecent,
0, 0 ]] )
setElementClassType( "GEOMETRYCONNECTION", "Interface", "STLIIF" )
assignMaterial( "Interface", "GEOMETRYCONNECTION", "Interface" )
assignGeometry( "Interface", "GEOMETRYCONNECTION", "Interface" )
setParameter( "GEOMETRYCONNECTION", "Interface", "FLIP", False )
resetElementData( "GEOMETRYCONNECTION", "Interface" )

#Mesh
setElementSize( [ "Concrete beam" ], Elem, -1, True )
setMesherType( [ "Concrete beam" ], "HEXQUAD" )
setMidSideNodeLocation( [ "Concrete beam" ], "LINEAR" )
setElementSize( [ "Concrete beam" ], Elem, -1, True )
setMesherType( [ "Concrete beam" ], "HEXQUAD" )
setMidSideNodeLocation( [ "Concrete beam" ], "LINEAR" )
setElementSize( "Bottom Rebar", 1, [[ Lbeam/2, Cbr, 0 ]], Elem, 0, True )
setElementSize( "Top Rebar", 1, [[ Lbeam/2, Hbeam-Cbr, 0 ]], Elem, 0, True )
setElementSize( [ "L Supp plate", "R Supp plate", "Load plate" ], Elem, -1, True )
setMesherType( [ "L Supp plate", "R Supp plate", "Load plate" ], "HEXQUAD" )
setMidSideNodeLocation( [ "L Supp plate", "R Supp plate", "Load plate" ], "LINEAR"
)
generateMesh( [] )

#Analysis Commands
addAnalysis( "Analysis1" )
addAnalysisCommand( "Analysis1", "NONLIN", "Structural nonlinear" )
addAnalysisCommandDetail( "Analysis1", "Structural nonlinear", "EXECUT" )
addAnalysisCommand( "Analysis1", "PHASE", "Phased" )
setActivePhase( "Analysis1", "Phased" )
moveAnalysisCommand( "Analysis1", "Phased", "Structural nonlinear" )
setActivePhase( "Analysis1", "Phased" )
setActivePhase( "Analysis1", "Phased" )
setActiveInPhase( "Analysis1", "GEOMETRYSUPPORTSET", [ "load Support" ], [ "Phased"
], False )
setAnalysisCommandDetail( "Analysis1", "Structural nonlinear",
"EXECUT(1)/ITERAT/MAXITE", 100 )
removeAnalysisCommandDetail( "Analysis1", "Structural nonlinear", "EXECUT(2)" )
addAnalysisCommandDetail( "Analysis1", "Structural nonlinear",
"EXECUT(1)/LOAD/LOADNR" )
setAnalysisCommandDetail( "Analysis1", "Structural nonlinear",
"EXECUT(1)/LOAD/LOADNR", 2 )
addAnalysisCommand( "Analysis1", "PHASE", "Phased 1" )
setActivePhase( "Analysis1", "Phased 1" )
addAnalysisCommand( "Analysis1", "NONLIN", "Structural nonlinear 1" )
setActivePhase( "Analysis1", "Phased 1" )
setActivePhase( "Analysis1", "Phased 1" )
setAnalysisCommandDetail( "Analysis1", "Structural nonlinear 1", "EXECUT/EXETYP",
"START" )
swapAnalysisCommandDetails( "Analysis1", "Structural nonlinear 1", "EXECUT(2)",
"EXECUT(1)" )
swapAnalysisCommandDetails( "Analysis1", "Structural nonlinear 1", "EXECUT(1)",
"EXECUT(2)" )
swapAnalysisCommandDetails( "Analysis1", "Structural nonlinear 1", "EXECUT(2)",
"EXECUT(1)" )
setAnalysisCommandDetail( "Analysis1", "Structural nonlinear 1",
"EXECUT(1)/ITERAT/MAXITE", 100 )
setAnalysisCommandDetail( "Analysis1", "Structural nonlinear 1",
"EXECUT(1)/ITERAT/METHOD/METNAM", "SECANT" )
addAnalysisCommandDetail( "Analysis1", "Structural nonlinear 1",
"EXECUT(1)/ITERAT/LINESE" )
setAnalysisCommandDetail( "Analysis1", "Structural nonlinear 1",
"EXECUT(1)/ITERAT/LINESE", True )
addAnalysisCommandDetail( "Analysis1", "Structural nonlinear 1",
"EXECUT(1)/ITERAT/CONVER/ENERGY" )
setAnalysisCommandDetail( "Analysis1", "Structural nonlinear 1",
"EXECUT(1)/ITERAT/CONVER/ENERGY", True )
setAnalysisCommandDetail( "Analysis1", "Structural nonlinear 1",
```

```
"EXECUT(1)/ITERAT/CONVER/DISPLA", False )
setAnalysisCommandDetail( "Analysis1", "Structural nonlinear 1",
"EXECUT(1)/ITERAT/CONVER/ENERGY/TOLCON", 0.001 )
setAnalysisCommandDetail( "Analysis1", "Structural nonlinear 1",
"EXECUT(1)/ITERAT/CONVER/ENERGY/NOCONV", "CONTIN" )
setAnalysisCommandDetail( "Analysis1", "Structural nonlinear 1",
"EXECUT(1)/ITERAT/CONVER/FORCE/NOCONV", "CONTIN" )
setAnalysisCommandDetail( "Analysis1", "Structural nonlinear 1",
"EXECUT(2)/ITERAT/CONVER/FORCE", False )
addAnalysisCommandDetail( "Analysis1", "Structural nonlinear 1",
"EXECUT(2)/LOAD/LOADNR" )
setAnalysisCommandDetail( "Analysis1", "Structural nonlinear 1",
"EXECUT(2)/LOAD/LOADNR", 1 )
setAnalysisCommandDetail( "Analysis1", "Structural nonlinear 1",
"EXECUT(2)/LOAD/STEPS/EXPLIC/SIZES", "0.05(800)" )
setAnalysisCommandDetail( "Analysis1", "Structural nonlinear 1",
"EXECUT(2)/ITERAT/MAXITE", 10 )
addAnalysisCommandDetail( "Analysis1", "Structural nonlinear 1",
"EXECUT(2)/ITERAT/CONVER/ENERGY" )
setAnalysisCommandDetail( "Analysis1", "Structural nonlinear 1",
"EXECUT(2)/ITERAT/CONVER/ENERGY", True )
setAnalysisCommandDetail( "Analysis1", "Structural nonlinear 1",
"EXECUT(2)/ITERAT/CONVER/DISPLA", False )
setAnalysisCommandDetail( "Analysis1", "Structural nonlinear 1",
"EXECUT(2)/ITERAT/MAXITE", 100 )
setAnalysisCommandDetail( "Analysis1", "Structural nonlinear 1",
"EXECUT(2)/ITERAT/METHOD/METNAM", "SECANT" )
addAnalysisCommandDetail( "Analysis1", "Structural nonlinear 1",
"EXECUT(2)/ITERAT/LINESE" )
setAnalysisCommandDetail( "Analysis1", "Structural nonlinear 1",
"EXECUT(2)/ITERAT/LINESE", True )
setAnalysisCommandDetail( "Analysis1", "Structural nonlinear 1",
"EXECUT(2)/ITERAT/CONVER/ENERGY/TOLCON", 0.001 )
setAnalysisCommandDetail( "Analysis1", "Structural nonlinear 1",
"EXECUT(2)/ITERAT/CONVER/ENERGY/NOCONV", "CONTIN" )
setAnalysisCommandDetail( "Analysis1", "Structural nonlinear 1",
"EXECUT(2)/ITERAT/CONVER/FORCE/NOCONV", "CONTIN" )
swapAnalysisCommandDetails( "Analysis1", "Structural nonlinear 1", "EXECUT(1)",
"EXECUT(2)" )
swapAnalysisCommandDetails( "Analysis1", "Structural nonlinear 1", "EXECUT(2)",
"EXECUT(1)" )
setAnalysisCommandDetail( "Analysis1", "Structural nonlinear 1",
"EXECUT(2)/ITERAT/CONVER/FORCE", False )
setActivePhase( "Analysis1", "Phased 1" )
setAnalysisCommandDetail( "Analysis1", "Structural nonlinear 1",
"OUTPUT(1)/SELTYP", "USER" )
addAnalysisCommandDetail( "Analysis1", "Structural nonlinear 1", "OUTPUT(1)/USER" )
addAnalysisCommandDetail( "Analysis1", "Structural nonlinear 1",
"OUTPUT(1)/USER/DISPLA(1)/TOTAL/TRANSL/GLOBAL" )
addAnalysisCommandDetail( "Analysis1", "Structural nonlinear 1",
"OUTPUT(1)/USER/STRAIN(3)/TOTAL/GREEN/GLOBAL" )
setAnalysisCommandDetail( "Analysis1", "Structural nonlinear 1",
"OUTPUT(1)/USER/STRAIN(4)/TOTAL/GREEN/GLOBAL/LOCATI", "INTPNT" )
addAnalysisCommandDetail( "Analysis1", "Structural nonlinear 1",
"OUTPUT(1)/USER/STRESS(4)/TOTAL/CAUCHY/GLOBAL" )
setAnalysisCommandDetail( "Analysis1", "Structural nonlinear 1",
"OUTPUT(1)/USER/STRESS(4)/TOTAL/CAUCHY/GLOBAL/LOCATI", "INTPNT" )
setAnalysisCommandDetail( "Analysis1", "Structural nonlinear 1",
"OUTPUT(1)/USER/STRAIN(13)/CRACK/GREEN/LOCATI", "NODES" )
addAnalysisCommandDetail( "Analysis1", "Structural nonlinear 1",
"OUTPUT(1)/USER/STRAIN(15)/CRKWDT/GREEN/LOCAL" )
setAnalysisCommandDetail( "Analysis1", "Structural nonlinear 1",
"OUTPUT(1)/USER/STRAIN(16)/CRKWDT/GREEN/LOCAL/LOCATI", "INTPNT" )
addAnalysisCommandDetail( "Analysis1", "Structural nonlinear 1",
"OUTPUT(1)/USER/FORCE(1)/REACTI/TRANSL/GLOBAL" )
setAnalysisCommandDetail( "Analysis1", "Structural nonlinear 1",
"OUTPUT(1)/USER/STRAIN(13)/CRACK/GREEN/LOCATI", "INTPNT" )
addAnalysisCommandDetail( "Analysis1", "Structural nonlinear 1",
```

```
"OUTPUT(1)/USER/STRESS(5)/CRACK/CAUCHY/LOCAL" )
removeAnalysisCommandDetail( "Analysis1", "Structural nonlinear 1",
"OUTPUT(1)/USER/STRAIN(1)" )
removeAnalysisCommandDetail( "Analysis1", "Structural nonlinear 1",
"OUTPUT(1)/USER/STRAIN(3)" )
removeAnalysisCommandDetail( "Analysis1", "Structural nonlinear 1",
"OUTPUT(1)/USER/STRAIN(15)" )
removeAnalysisCommandDetail( "Analysis1", "Structural nonlinear 1",
"OUTPUT(1)/USER/STRESS(1)" )
addAnalysisCommandDetail( "Analysis1", "Structural nonlinear 1", "OUTPUT" )
setAnalysisCommandDetail( "Analysis1", "Structural nonlinear 1",
"OUTPUT(2)/DEVICE", "TABULA" )
setAnalysisCommandDetail( "Analysis1", "Structural nonlinear 1",
"OUTPUT(2)/SELECT/MODSEL", "USER" )
setAnalysisCommandDetail( "Analysis1", "Structural nonlinear 1",
"OUTPUT(2)/SELECT/NODES(1)/RNGNRS", "NONE" )
setAnalysisCommandDetail( "Analysis1", "Structural nonlinear 1",
"OUTPUT(2)/SELECT/ELEMEN(1)/RNGNRS", "NONE" )
setAnalysisCommandDetail( "Analysis1", "Structural nonlinear 1",
"OUTPUT(2)/SELTYP", "USER" )
addAnalysisCommandDetail( "Analysis1", "Structural nonlinear 1", "OUTPUT(2)/USER" )
addAnalysisCommandDetail( "Analysis1", "Structural nonlinear 1",
"OUTPUT(2)/USER/STRESS(1)/TOTAL/CAUCHY/LOCAL" )
setAnalysisCommandDetail( "Analysis1", "Structural nonlinear 1",
"OUTPUT(2)/USER/STRESS(1)/TOTAL/CAUCHY/LOCAL/COMP", [ "XX"] )
setAnalysisCommandDetail( "Analysis1", "Structural nonlinear 1",
"OUTPUT(2)/USER/STRESS(1)/TOTAL/CAUCHY/LOCAL/LOCATI", "INTPNT" )
addAnalysisCommandDetail( "Analysis1", "Structural nonlinear 1",
"OUTPUT(2)/USER/STRAIN(3)/TOTAL/GREEN/LOCAL" )
setAnalysisCommandDetail( "Analysis1", "Structural nonlinear 1",
"OUTPUT(2)/USER/STRAIN(3)/TOTAL/GREEN/LOCAL/COMP", [ "XX"] )
setAnalysisCommandDetail( "Analysis1", "Structural nonlinear 1",
"OUTPUT(2)/USER/STRAIN(3)/TOTAL/GREEN/LOCAL/LOCATI", "INTPNT" )
removeAnalysisCommandDetail( "Analysis1", "Structural nonlinear 1",
"OUTPUT(2)/USER/STRAIN(1)" )
saveProject(  )
```

C

Annex C

```
import math

#Project Settings
newProject( "Directory/Name", 1000 )
setModelAnalysisAspects( [ "STRUCT" ] )
setModelDimension( "2D" )
setDefaultMeshOrder( "QUADRATIC" )
setDefaultMesherType( "HEXQUAD" )
setDefaultMidSideNodeLocation( "LINEAR" )
setUnit( "LENGTH", "MM" )
setUnit( "FORCE", "N" )

#Material Properties
#Concrete
CG=65                       #Concrete Grade
fcmcubic=78.5               #Cubic Compressive Strength [MPa]
fc=0.8*fcmcubic             #Cylinder Compressive Strength [MPa]
fck=fc-8                    #Characteristic Strength [MPa]
if CG<=50 :
    fct=0.3*fc**(2/3)       #Tensile Strength [MPa]
else:
    fct= 2.12 * math.log(1+0.1*fc)
Ec=21500*(fc/10)**(1/3) #Young's Modulus [MPa]
vc=0.2                      #Poisson Ratio [-]
MDensC=2.4e-09              #Mass Density [T/mm3]
Gft=0.073*fc**0.18          #Tensile Fracture Energy [N/mm]
Gfc=250*Gft                 #Compressive Fracture Energy [N/mm]

#Reinforcement
Es=210000                   #Young's Modulus
MdensR=7.85e-09             #Mass Density [T/mm3]
n1=2                        #Number of Rebars with diameter_1
dia1=20                     #Diameter_1 of Reinforcement [mm]
n2=1                        #Number of Rebars with diameter_2
dia2=12                     #Diameter_2 of Reinforcement [mm]
pi=math.pi
vs=0.3                      #Poisson Ratio [-]
fy=550                      #Yield Strength [MPa]

#Interface Between Load/Support Plate and Beam
kn=8400                     #Normal Stiffness [N/mm3]
ks=84                       #Shear Stiffness [N/mm3]

#Mesh
Elem=25                     #Mesh Size

#Bond-slip Interface
bn=100*Ec/Elem              #Normal Stiffness of bond-slip interface [N/mm3]
bs=bn/10                    #Tangential Stiffness of bond-slip interface [N/mm3]

#Geometry
#Beam and Reinforcement
Lbeam= 8000                 #Length of the beam [mm]
Hbeam=300                   #Height of the beam [mm]
width=300                   #Width of the beam [mm]
d=270                       #Effective depth [mm]
As=(n1*pi*(dia1**2)/4)+(n2*pi*(dia2**2)/4)  #Area of Reinforcement
Cp=(n1*pi*dia1)+(n2*pi*dia2)                #Perimeter of Reinforcement
Cbr= Hbeam-d                #Concrete Cover

#Support Plate
X1=1450                     #Start of the left support plate (X)
X2=1550                     #End of the left support plate (X)
Y1=-20                      #End of the support plate (Y)
Y2=0                        #Start of the support plate (Y)
Lspan=5000                  #Clear Span of the Beam [mm]
Lsuppcent=1500              #Center of the left support [mm]
Rsuppcent=Lsuppcent+Lspan   #Center of the right support [mm]
```

```
#Load Plate
a=1100                  #Shear Span [mm]
Hplate=20               #Height of Load Plate [mm]
Lplatecent=Lsuppcent+a  #Center of the load plate [mm]

#Layout of the Beam
createSheet( "Concrete beam", [[ 0, 0, 0 ],[ Lbeam, 0, 0 ],[ Lbeam, Hbeam, 0 ],[ 0,
Hbeam, 0 ]] )
createLine( "Bottom Rebar", [ 0, Cbr, 0 ], [ Lbeam, Cbr, 0 ] )
createLine( "Top Rebar", [ 0, d, 0 ], [ Lbeam, d , 0 ] )
createSheet( "L Supp plate", [[ X1, Y1, 0 ],[ X2, Y1, 0 ],[ X2, Y2, 0 ],[ X1, Y2, 0
]] )
createSheet( "R Supp plate", [[ X1+Lspan, Y1, 0 ],[ X2+Lspan, Y1, 0 ],[X2+Lspan ,
Y2, 0 ],[ X1+Lspan, Y2, 0 ]] )
createSheet( "Load plate", [[X1+a , Hbeam, 0 ],[ X2+a, Hbeam, 0 ],[ X2+a,
Hbeam+Hplate, 0 ],[ X1+a, Hbeam+Hplate, 0 ]] )

#Creating necessary vertex and lines
createPointBody( "Point body 1", [ Lsuppcent, Y1, 0 ] )
createPointBody( "Point body 2", [ Lplatecent, Hbeam+Hplate, 0 ] )
createPointBody( "Point body 3", [ Rsuppcent, Y1, 0 ] )
projection( "SHAPEEDGE", "L Supp plate", [[ Lsuppcent, Y1, 0 ]], [ "Point body 1"
], [ 0, 0, -1 ], True )
removeShape( [ "Point body 1" ] )
projection( "SHAPEEDGE", "Load plate", [[ Lplatecent, Hbeam+Hplate, 0 ]], [ "Point
body 2" ], [ 0, 0, -1 ], True )
removeShape( [ "Point body 2" ] )
projection( "SHAPEEDGE", "R Supp plate", [[ Rsuppcent, Y1, 0 ]], [ "Point body 3"
], [ 0, 0, -1 ], True )
removeShape( [ "Point body 3" ] )
createLine( "Line Lsupp", [ X1, Y2, 0 ], [ X2, Y2, 0 ] )
createLine( "Line Rsupp", [ X1+Lspan, Y2, 0 ], [ X2+Lspan, Y2, 0 ] )
projection( "SHAPEFACE", "Concrete beam", [[ Lbeam/2, Hbeam/2, 0 ]], [ "Line
Lsupp", "Line Rsupp" ], [ 0, 0, -1 ], True )
removeShape( [ "Line Lsupp", "Line Rsupp" ] )

#Support
addSet( "GEOMETRYSUPPORTSET", "Support" )
createPointSupport( "Lsupport", "Support" )
setParameter( "GEOMETRYSUPPORT", "Lsupport", "AXES", [ 1, 2 ] )
setParameter( "GEOMETRYSUPPORT", "Lsupport", "TRANSL", [ 1, 1, 0 ] )
setParameter( "GEOMETRYSUPPORT", "Lsupport", "ROTATI", [ 0, 0, 0 ] )
attach( "GEOMETRYSUPPORT", "Lsupport", "L Supp plate", [[ Lsuppcent, Y1, 0]])
createPointSupport( "Rsupport", "Support" )
setParameter( "GEOMETRYSUPPORT", "Rsupport", "AXES", [ 1, 2 ] )
setParameter( "GEOMETRYSUPPORT", "Rsupport", "TRANSL", [ 0, 1, 0 ] )
setParameter( "GEOMETRYSUPPORT", "Rsupport", "ROTATI", [ 0, 0, 0 ] )
attach( "GEOMETRYSUPPORT", "Rsupport", "R Supp plate", [[ Rsuppcent, Y1, 0 ]] )
addSet( "GEOMETRYSUPPORTSET", "load Support" )
createPointSupport( "Rxn @disp", "load Support" )
setParameter( "GEOMETRYSUPPORT", "Rxn @disp", "AXES", [ 1, 2 ] )
setParameter( "GEOMETRYSUPPORT", "Rxn @disp", "TRANSL", [ 0, 1, 0 ] )
setParameter( "GEOMETRYSUPPORT", "Rxn @disp", "ROTATI", [ 0, 0, 0 ] )
attach( "GEOMETRYSUPPORT", "Rxn @disp", "Load plate", [[ Lplatecent, Hbeam+Hplate,
0 ]] )

#Load
addSet( "GEOMETRYLOADSET", "Load" )
createPointLoad( "Point load", "Load" )
setParameter( "GEOMETRYLOAD", "Point load", "LODTYP", "DEFORM" )
setParameter( "GEOMETRYLOAD", "Point load", "DEFORM/TR/VALUE", -1 )
setParameter( "GEOMETRYLOAD", "Point load", "DEFORM/TR/DIRECT", 2 )
attach( "GEOMETRYLOAD", "Point load", "Load plate", [[ Lplatecent, Hbeam+Hplate, 0
]] )
addSet( "GEOMETRYLOADSET", "Self-weight" )
createModelLoad( "Self-weight", "Self-weight" )
```

```
#Material property
#Element data
addElementData( "Element data 1" )
setParameter( "DATA", "Element data 1", "./INTEGR", [] )
setParameter( "DATA", "Element data 1", "INTEGR", "HIGH" )
assignElementData( "Element data 1", "SHAPE", [ "Concrete beam" ] )
assignElementData( "Element data 1", "SHAPE", [ "L Supp plate" ] )
assignElementData( "Element data 1", "SHAPE", [ "Load plate" ] )
assignElementData( "Element data 1", "SHAPE", [ "R Supp plate" ] )

#Concrete
addMaterial( "Concrete", "CONCR", "TSCR", [] )
setParameter( "MATERIAL", "Concrete", "LINEAR/ELASTI/YOUNG", Ec )
setParameter( "MATERIAL", "Concrete", "LINEAR/ELASTI/POISON", vc )
setParameter( "MATERIAL", "Concrete", "LINEAR/MASS/DENSIT", MDensC )
setParameter( "MATERIAL", "Concrete", "MODTYP/TOTCRK", "ROTATE" )
setParameter( "MATERIAL", "Concrete", "TENSIL/TENCRV", "HORDYK" )
setParameter( "MATERIAL", "Concrete", "TENSIL/TENSTR", fct)
setParameter( "MATERIAL", "Concrete", "TENSIL/GF1", Gft)
setParameter( "MATERIAL", "Concrete", "TENSIL/POISRE/POIRED", "DAMAGE" )
setParameter( "MATERIAL", "Concrete", "COMPRS/COMCRV", "PARABO" )
setParameter( "MATERIAL", "Concrete", "COMPRS/COMSTR", fc )
setParameter( "MATERIAL", "Concrete", "COMPRS/GC", Gfc)
setParameter( "MATERIAL", "Concrete", "COMPRS/REDUCT/REDCRV", "VC1993" )
setParameter( "MATERIAL", "Concrete", "COMPRS/REDUCT/REDMIN", 0.4 )
setParameter( "MATERIAL", "Concrete", "COMPRS/CONFIN/CNFCRV", "VECCHI" )
addGeometry( "Element geometry 1", "SHEET", "MEMBRA", [] )
rename( "GEOMET", "Element geometry 1", "Concrete" )
setParameter( "GEOMET", "Concrete", "THICK", width)
setParameter( "GEOMET", "Concrete", "LOCAXS", True )
setElementClassType( "SHAPE", [ "Concrete beam" ], "MEMBRA" )
assignMaterial( "Concrete", "SHAPE", [ "Concrete beam" ] )
assignGeometry( "Concrete", "SHAPE", [ "Concrete beam" ] )

#BS-Reinforcement
addMaterial( "BS-Reinforcement", "REINFO", "REBOND", [] )
setParameter( "MATERIAL", "BS-Reinforcement", "REBARS/ELASTI/YOUNG", Es )
setParameter( "MATERIAL", "BS-Reinforcement", "REBARS/MASS/DENSIT", MdensR )
setParameter( "MATERIAL", "BS-Reinforcement", "REBARS/PLATYP", "VMISES" )
setParameter( "MATERIAL", "BS-Reinforcement", "REBARS/PLASTI/TRESSH", "EPSSIG" )
setParameter( "MATERIAL", "BS-Reinforcement", "REBARS/PLASTI/EPSSIG", [] )
setParameter( "MATERIAL", "BS-Reinforcement", "REBARS/PLASTI/EPSSIG", [ 0, 0,
0.002619, 550, 0.0157, 605, 0.0159, 1 ] )
setParameter( "MATERIAL", "BS-Reinforcement", "RESLIP/SHFTYP", "BONDS4" )
setParameter( "MATERIAL", "BS-Reinforcement", "RESLIP/SHFTYP", "BONDS5" )
setParameter( "MATERIAL", "BS-Reinforcement", "RESLIP/SHFTYP", "BONDS4" )
setParameter( "MATERIAL", "BS-Reinforcement", "RESLIP/BONDS4/DIAMET",20 )
setParameter( "MATERIAL", "BS-Reinforcement", "RESLIP/BONDS4/SLPVAL", fc )
setParameter( "MATERIAL", "BS-Reinforcement", "RESLIP/BONDS4/SLPVAL", fc)
setParameter( "MATERIAL", "BS-Reinforcement", "RESLIP/DSNY", bn )
setParameter( "MATERIAL", "BS-Reinforcement", "RESLIP/DSSX", bs )
setParameter( "MATERIAL", "BS-Reinforcement", "RESLIP/DSSX", bs )
setParameter( "MATERIAL", "BS-Reinforcement", "RESLIP/DSNY", bn )
setParameter( "MATERIAL", "BS-Reinforcement", "RESLIP/SHFTYP", "BONDS6" )
setParameter( "MATERIAL", "BS-Reinforcement", "RESLIP/SHFTYP", "BONDS3" )
setParameter( "MATERIAL", "BS-Reinforcement", "RESLIP/BONDS3/DISTAU", [] )
setParameter( "MATERIAL", "BS-Reinforcement", "RESLIP/BONDS3/DISTAU", [0    ,  0   ,
0.011927684    ,  2.658832327    ,  0.023855367    ,  3.50835029 ,  0.047710735
,  4.629295961    ,  0.071566102    ,  5.444417869    ,  0.09542147 ,  6.108392642
,  0.119276837    ,  6.678684847    ,  0.143132205    ,  7.183952447    ,
0.166987572    ,  7.640858635    ,  0.19084294 ,  8.060072413    ,  0.214698307
,  8.448895772    ,  0.238553675    ,  8.812577489    ,  0.286264409    ,  0.01   ,
3  ,  0.01
])
addGeometry( "Element geometry 2", "RELINE", "REBAR", [] )
rename( "GEOMET", "Element geometry 2", "BS-Reinforcement" )
setParameter( "GEOMET", "BS-Reinforcement", "REITYP", "REITRU" )
setParameter( "GEOMET", "BS-Reinforcement", "REITRU/CROSSE", As )
```

```
setParameter( "GEOMET", "BS-Reinforcement", "REITRU/PERIME", Cp )
addElementData( "Element data 2" )
setReinforcementAspects( [ "Bottom Rebar", "Top Rebar" ] )
assignMaterial( "BS-Reinforcement", "SHAPE", [ "Bottom Rebar", "Top Rebar" ] )
assignGeometry( "BS-Reinforcement", "SHAPE", [ "Bottom Rebar", "Top Rebar" ] )
assignElementData( "Element data 2", "SHAPE", [ "Bottom Rebar", "Top Rebar" ] )
setReinforcementDiscretization( [ "Bottom Rebar", "Top Rebar" ], "ELEMENT" )
setParameter( "DATA", "Element data 2", "./ALMANS", [] )
removeParameter( "DATA", "Element data 2", "ALMANS" )
setParameter( "DATA", "Element data 2", "./INTERF", [] )
setParameter( "DATA", "Element data 2", "INTERF", "TRUSS" )

#Steel plate
addMaterial( "Steel plate", "MCSTEL", "ISOTRO", [] )
setParameter( "MATERIAL", "Steel plate", "LINEAR/ELASTI/YOUNG", Es )
setParameter( "MATERIAL", "Steel plate", "LINEAR/ELASTI/POISON", vs )
setParameter( "MATERIAL", "Steel plate", "LINEAR/MASS/DENSIT", MdensR )
addGeometry( "Element geometry 3", "SHEET", "MEMBRA", [] )
rename( "GEOMET", "Element geometry 3", "Steel plate" )
setParameter( "GEOMET", "Steel plate", "THICK", width )
setParameter( "GEOMET", "Steel plate", "LOCAXS", True )
setElementClassType( "SHAPE", [ "L Supp plate", "Load plate", "R Supp plate" ],
"MEMBRA" )
assignMaterial( "Steel plate", "SHAPE", [ "L Supp plate", "Load plate", "R Supp
plate" ] )
assignGeometry( "Steel plate", "SHAPE", [ "L Supp plate", "Load plate", "R Supp
plate" ] )

#Interface
addMaterial( "Interface", "INTERF", "ELASTI", [] )
setParameter( "MATERIAL", "Interface", "LINEAR/IFTYP", "LIN2D" )
setParameter( "MATERIAL", "Interface", "LINEAR/ELAS2/DSNY", kn )
setParameter( "MATERIAL", "Interface", "LINEAR/ELAS2/DSSX", ks )
addGeometry( "Element geometry 4", "LINE", "STLIIF", [] )
rename( "GEOMET", "Element geometry 4", "Interface" )
setParameter( "GEOMET", "Interface", "LIFMEM/THICK", width )
setParameter( "GEOMET", "Interface", "LOCAXS", True )
createConnection( "Interface", "INTER", "SHAPEEDGE" )
setParameter( "GEOMETRYCONNECTION", "Interface", "MODE", "AUTO" )
attachTo( "GEOMETRYCONNECTION", "Interface", "SOURCE", "L Supp plate", [[
Lsuppcent, 0, 0 ]] )
attachTo( "GEOMETRYCONNECTION", "Interface", "SOURCE", "Concrete beam", [[
Lsuppcent, 0, 0 ]] )
attachTo( "GEOMETRYCONNECTION", "Interface", "SOURCE", "R Supp plate", [[
Rsuppcent, 0, 0 ]] )
attachTo( "GEOMETRYCONNECTION", "Interface", "SOURCE", "Concrete beam", [[
Rsuppcent, 0, 0 ]] )
attachTo( "GEOMETRYCONNECTION", "Interface", "SOURCE", "Load plate", [[ Lplatecent,
0, 0 ]] )
setElementClassType( "GEOMETRYCONNECTION", "Interface", "STLIIF" )
assignMaterial( "Interface", "GEOMETRYCONNECTION", "Interface" )
assignGeometry( "Interface", "GEOMETRYCONNECTION", "Interface" )
setParameter( "GEOMETRYCONNECTION", "Interface", "FLIP", False )
resetElementData( "GEOMETRYCONNECTION", "Interface" )

#Mesh
setElementSize( [ "Concrete beam" ], Elem, -1, True )
setMesherType( [ "Concrete beam" ], "HEXQUAD" )
setMidSideNodeLocation( [ "Concrete beam" ], "LINEAR" )
setElementSize( [ "Concrete beam" ], Elem, -1, True )
setMesherType( [ "Concrete beam" ], "HEXQUAD" )
setMidSideNodeLocation( [ "Concrete beam" ], "LINEAR" )
setElementSize( "Bottom Rebar", 1, [[ Lbeam/2, Cbr, 0 ]], Elem, 0, True )
setElementSize( "Top Rebar", 1, [[ Lbeam/2, Hbeam-Cbr, 0 ]], Elem, 0, True )
setElementSize( [ "L Supp plate", "R Supp plate", "Load plate" ], Elem, -1, True )
setMesherType( [ "L Supp plate", "R Supp plate", "Load plate" ], "HEXQUAD" )
setMidSideNodeLocation( [ "L Supp plate", "R Supp plate", "Load plate" ], "LINEAR"
)
```

```
generateMesh( [] )

#Analysis Commands
addAnalysis( "Analysis1" )
addAnalysisCommand( "Analysis1", "NONLIN", "Structural nonlinear" )
addAnalysisCommandDetail( "Analysis1", "Structural nonlinear", "EXECUT" )
addAnalysisCommand( "Analysis1", "PHASE", "Phased" )
setActivePhase( "Analysis1", "Phased" )
moveAnalysisCommand( "Analysis1", "Phased", "Structural nonlinear" )
setActivePhase( "Analysis1", "Phased" )
setActivePhase( "Analysis1", "Phased" )
setActiveInPhase( "Analysis1", "GEOMETRYSUPPORTSET", [ "load Support" ], [ "Phased"
], False )
setAnalysisCommandDetail( "Analysis1", "Structural nonlinear",
"EXECUT(1)/ITERAT/MAXITE", 100 )
removeAnalysisCommandDetail( "Analysis1", "Structural nonlinear", "EXECUT(2)" )
addAnalysisCommand( "Analysis1", "PHASE", "Phased 1" )
setActivePhase( "Analysis1", "Phased 1" )
addAnalysisCommand( "Analysis1", "NONLIN", "Structural nonlinear 1" )
setActivePhase( "Analysis1", "Phased 1" )
setActivePhase( "Analysis1", "Phased 1" )
setAnalysisCommandDetail( "Analysis1", "Structural nonlinear 1", "EXECUT/EXETYP",
"START" )
swapAnalysisCommandDetails( "Analysis1", "Structural nonlinear 1", "EXECUT(2)",
"EXECUT(1)" )
swapAnalysisCommandDetails( "Analysis1", "Structural nonlinear 1", "EXECUT(1)",
"EXECUT(2)" )
swapAnalysisCommandDetails( "Analysis1", "Structural nonlinear 1", "EXECUT(2)",
"EXECUT(1)" )
setAnalysisCommandDetail( "Analysis1", "Structural nonlinear 1",
"EXECUT(1)/ITERAT/MAXITE", 100 )
setAnalysisCommandDetail( "Analysis1", "Structural nonlinear 1",
"EXECUT(1)/ITERAT/METHOD/METNAM", "SECANT" )
addAnalysisCommandDetail( "Analysis1", "Structural nonlinear 1",
"EXECUT(1)/ITERAT/LINESE" )
setAnalysisCommandDetail( "Analysis1", "Structural nonlinear 1",
"EXECUT(1)/ITERAT/LINESE", True )
addAnalysisCommandDetail( "Analysis1", "Structural nonlinear 1",
"EXECUT(1)/ITERAT/CONVER/ENERGY" )
setAnalysisCommandDetail( "Analysis1", "Structural nonlinear 1",
"EXECUT(1)/ITERAT/CONVER/ENERGY", True )
setAnalysisCommandDetail( "Analysis1", "Structural nonlinear 1",
"EXECUT(1)/ITERAT/CONVER/DISPLA", False )
setAnalysisCommandDetail( "Analysis1", "Structural nonlinear 1",
"EXECUT(1)/ITERAT/CONVER/ENERGY/TOLCON", 0.001 )
setAnalysisCommandDetail( "Analysis1", "Structural nonlinear 1",
"EXECUT(1)/ITERAT/CONVER/ENERGY/NOCONV", "CONTIN" )
setAnalysisCommandDetail( "Analysis1", "Structural nonlinear 1",
"EXECUT(1)/ITERAT/CONVER/FORCE/NOCONV", "CONTIN" )
addAnalysisCommandDetail( "Analysis1", "Structural nonlinear 1",
"EXECUT(2)/LOAD/LOADNR" )
setAnalysisCommandDetail( "Analysis1", "Structural nonlinear 1",
"EXECUT(2)/LOAD/LOADNR", 1 )
setAnalysisCommandDetail( "Analysis1", "Structural nonlinear 1",
"EXECUT(2)/LOAD/STEPS/EXPLIC/SIZES", "0.05(900)" )
setAnalysisCommandDetail( "Analysis1", "Structural nonlinear 1",
"EXECUT(2)/ITERAT/MAXITE", 10 )
addAnalysisCommandDetail( "Analysis1", "Structural nonlinear 1",
"EXECUT(2)/ITERAT/CONVER/ENERGY" )
setAnalysisCommandDetail( "Analysis1", "Structural nonlinear 1",
"EXECUT(2)/ITERAT/CONVER/ENERGY", True )
setAnalysisCommandDetail( "Analysis1", "Structural nonlinear 1",
"EXECUT(2)/ITERAT/CONVER/DISPLA", False )
setAnalysisCommandDetail( "Analysis1", "Structural nonlinear 1",
"EXECUT(2)/ITERAT/MAXITE", 100 )
setAnalysisCommandDetail( "Analysis1", "Structural nonlinear 1",
"EXECUT(2)/ITERAT/METHOD/METNAM", "SECANT" )
addAnalysisCommandDetail( "Analysis1", "Structural nonlinear 1",
```

```
"EXECUT(2)/ITERAT/LINESE" )
setAnalysisCommandDetail( "Analysis1", "Structural nonlinear 1",
"EXECUT(2)/ITERAT/LINESE", True )
setAnalysisCommandDetail( "Analysis1", "Structural nonlinear 1",
"EXECUT(2)/ITERAT/CONVER/ENERGY/TOLCON", 0.001 )
setAnalysisCommandDetail( "Analysis1", "Structural nonlinear 1",
"EXECUT(2)/ITERAT/CONVER/ENERGY/NOCONV", "CONTIN" )
setAnalysisCommandDetail( "Analysis1", "Structural nonlinear 1",
"EXECUT(2)/ITERAT/CONVER/FORCE/NOCONV", "CONTIN" )
swapAnalysisCommandDetails( "Analysis1", "Structural nonlinear 1", "EXECUT(1)",
"EXECUT(2)" )
swapAnalysisCommandDetails( "Analysis1", "Structural nonlinear 1", "EXECUT(2)",
"EXECUT(1)" )
setActivePhase( "Analysis1", "Phased 1" )
setAnalysisCommandDetail( "Analysis1", "Structural nonlinear 1",
"OUTPUT(1)/SELTYP", "USER" )
addAnalysisCommandDetail( "Analysis1", "Structural nonlinear 1", "OUTPUT(1)/USER" )
addAnalysisCommandDetail( "Analysis1", "Structural nonlinear 1",
"OUTPUT(1)/USER/DISPLA(1)/TOTAL/TRANSL/GLOBAL" )
addAnalysisCommandDetail( "Analysis1", "Structural nonlinear 1",
"OUTPUT(1)/USER/STRAIN(3)/TOTAL/GREEN/GLOBAL" )
setAnalysisCommandDetail( "Analysis1", "Structural nonlinear 1",
"OUTPUT(1)/USER/STRAIN(4)/TOTAL/GREEN/GLOBAL/LOCATI", "INTPNT" )
addAnalysisCommandDetail( "Analysis1", "Structural nonlinear 1",
"OUTPUT(1)/USER/STRESS(4)/TOTAL/CAUCHY/GLOBAL" )
setAnalysisCommandDetail( "Analysis1", "Structural nonlinear 1",
"OUTPUT(1)/USER/STRESS(4)/TOTAL/CAUCHY/GLOBAL/LOCATI", "INTPNT" )
setAnalysisCommandDetail( "Analysis1", "Structural nonlinear 1",
"OUTPUT(1)/USER/STRAIN(13)/CRACK/GREEN/LOCATI", "NODES" )
addAnalysisCommandDetail( "Analysis1", "Structural nonlinear 1",
"OUTPUT(1)/USER/STRAIN(15)/CRKWDT/GREEN/LOCAL" )
setAnalysisCommandDetail( "Analysis1", "Structural nonlinear 1",
"OUTPUT(1)/USER/STRAIN(16)/CRKWDT/GREEN/LOCAL/LOCATI", "INTPNT" )
addAnalysisCommandDetail( "Analysis1", "Structural nonlinear 1",
"OUTPUT(1)/USER/FORCE(1)/REACTI/TRANSL/GLOBAL" )
setAnalysisCommandDetail( "Analysis1", "Structural nonlinear 1",
"OUTPUT(1)/USER/STRAIN(13)/CRACK/GREEN/LOCATI", "INTPNT" )
addAnalysisCommandDetail( "Analysis1", "Structural nonlinear 1",
"OUTPUT(1)/USER/STRESS(5)/CRACK/CAUCHY/LOCAL" )
removeAnalysisCommandDetail( "Analysis1", "Structural nonlinear 1",
"OUTPUT(1)/USER/STRAIN(3)" )
removeAnalysisCommandDetail( "Analysis1", "Structural nonlinear 1",
"OUTPUT(1)/USER/STRAIN(4)" )
removeAnalysisCommandDetail( "Analysis1", "Structural nonlinear 1",
"OUTPUT(1)/USER/STRAIN(15)" )
removeAnalysisCommandDetail( "Analysis1", "Structural nonlinear 1",
"OUTPUT(1)/USER/STRESS(1)" )
setAnalysisCommandDetail( "Analysis1", "Structural nonlinear 1",
"OUTPUT(1)/USER/STRAIN(1)/TOTAL/GREEN/GLOBAL/LOCATI", "INTPNT" )
addAnalysisCommandDetail( "Analysis1", "Structural nonlinear",
"EXECUT(1)/LOAD/LOADNR" )
setAnalysisCommandDetail( "Analysis1", "Structural nonlinear",
"EXECUT(1)/LOAD/LOADNR", 2 )
addAnalysisCommandDetail( "Analysis1", "Structural nonlinear 1",
"OUTPUT(1)/USER/STRESS(6)/TOTAL/TRACTI/LOCAL" )
addAnalysisCommandDetail( "Analysis1", "Structural nonlinear 1",
"OUTPUT(1)/USER/STRAIN(17)/TOTAL/TRACTI/LOCAL" )
addAnalysisCommandDetail( "Analysis1", "Structural nonlinear 1",
"OUTPUT(1)/USER/STRAIN(18)/TOTAL/GREEN/GLOBAL" )
addAnalysisCommandDetail( "Analysis1", "Structural nonlinear 1",
"OUTPUT(1)/USER/STRAIN(19)/TOTAL/GREEN/PRINCI" )
setAnalysisCommandDetail( "Analysis1", "Structural nonlinear 1",
"OUTPUT(1)/USER/STRAIN(19)/TOTAL/GREEN/PRINCI/LOCATI", "INTPNT" )
setAnalysisCommandDetail( "Analysis1", "Structural nonlinear 1",
"OUTPUT(1)/USER/STRAIN(19)/TOTAL/GREEN/PRINCI/LOCATI", "NODES" )
addAnalysisCommandDetail( "Analysis1", "Structural nonlinear 1",
"OUTPUT(1)/USER/STRAIN(20)/TOTAL/GREEN/LOCAL" )
setAnalysisCommandDetail( "Analysis1", "Structural nonlinear 1",
```

```
"OUTPUT(1)/USER/STRAIN(20)/TOTAL/GREEN/LOCAL/LOCATI", "NODES" )
addAnalysisCommandDetail( "Analysis1", "Structural nonlinear 1",
"OUTPUT(1)/USER/STRESS(7)/TOTAL/CAUCHY/PRINCI" )
addAnalysisCommandDetail( "Analysis1", "Structural nonlinear 1",
"OUTPUT(1)/USER/STRESS(8)/TOTAL/CAUCHY/LOCAL" )
addAnalysisCommandDetail( "Analysis1", "Structural nonlinear 1",
"OUTPUT(1)/USER/STRESS(9)/TOTAL/CAUCHY/GLOBAL" )
addAnalysisCommandDetail( "Analysis1", "Structural nonlinear 1",
"OUTPUT(1)/USER/STRESS(10)/TOTAL/TRACTI/LOCAL" )
addAnalysisCommandDetail( "Analysis1", "Structural nonlinear 1",
"OUTPUT(1)/USER/STRESS(11)/TOTAL/SHEAR/LOCAL" )
addAnalysisCommandDetail( "Analysis1", "Structural nonlinear 1",
"OUTPUT(1)/USER/STRAIN(21)/TOTAL/GREEN/LOCAL" )
setAnalysisCommandDetail( "Analysis1", "Structural nonlinear 1",
"OUTPUT(1)/USER/STRAIN(21)/TOTAL/GREEN/LOCAL/LOCATI", "INTPNT" )
addAnalysisCommandDetail( "Analysis1", "Structural nonlinear 1",
"OUTPUT(1)/USER/STRESS(12)/TOTAL/CAUCHY/LOCAL" )
setAnalysisCommandDetail( "Analysis1", "Structural nonlinear 1",
"OUTPUT(1)/USER/STRESS(12)/TOTAL/CAUCHY/LOCAL/LOCATI", "INTPNT" )
saveProject(  )
```

D

Annex D

```
import openpyxl
from openpyxl.utils.cell import coordinate_from_string,
column_index_from_string
from openpyxl import Workbook
#Insert the name of the excel file
wb = openpyxl.load_workbook('DI trial.xlsx')
Sheet = wb['Sheet2']

rowexx = []
rowsxx = []

rowexxS = []
rowsxxS= []
for rowOfCellObjects in Sheet['D1':'D'+ str(Sheet.max_row)]:
     for cellObj in rowOfCellObjects:
        if cellObj.value == 'Exx':
            xy = coordinate_from_string(cellObj.coordinate)
            rowexx1 = xy[1]
            rowexx.append(rowexx1)
            rowexxS1 = xy[1]
            rowexxS.append(rowexxS1)
        if cellObj.value == 'Sxx':
            xy = coordinate_from_string(cellObj.coordinate)
            rowsxx1 = xy[1]
            rowsxx.append(rowsxx1)
            rowsxxS1 = xy[1]
            rowsxxS.append(rowsxxS1)

rowsxx[:] = [a-1 for a in rowsxx]
#print(rowsxx)
Exxbook = Workbook()
Exxsheet = Exxbook.active
#this is to fill the element number in the new excel file
Exxbook
elemnum = []

for i, j in zip(rowexx, rowsxx):
    for rowOfCellObjects in Sheet['B' + str(i):'B' + str(j)]:
        for cellObj in rowOfCellObjects:
            elemnum1 = cellObj.value
            elemnum.append(elemnum1)

Len = len(elemnum)
for a, b in zip(range(1, Len), range(0, Len)):
    c = Exxsheet.cell(row=a, column=1)
    c.value = elemnum[b]

print("Length of elemnum for Exx =", Len)
#this is to fill the intg points in the new excel file
intgpt = []
```

```
for i, j in zip(rowexx, rowsxx):
    for rowOfCellObjects in Sheet['c' + str(i):'c' + str(j)]:
        for cellObj in rowOfCellObjects:
            intgpt1 = cellObj.value
            intgpt.append(intgpt1)


Lenintgpt = len(intgpt)
for a, b in zip(range(1, Lenintgpt), range(0, Lenintgpt)):
    d = Exxsheet.cell(row=a, column=2)
    d.value = intgpt[b]

#this is to fill the Exx in the new excel file
Exx = []
for i, j in zip(rowexx, rowsxx):
    for rowOfCellObjects in Sheet['D' + str(i):'D' + str(j)]:
        for cellObj in rowOfCellObjects:
            Exx1 = cellObj.value
            Exx.append(Exx1)
LenExx = len(Exx)
for a, b in zip(range(1, LenExx), range(0, LenExx)):
    e = Exxsheet.cell(row=a, column=3)
    e.value = Exx[b]

#FOR SXX : FOR SXX  : FOR SXX
LenrowexxS = len(rowexxS)
rowexxSS = []         # this is so the row of Exx except the
first row can be stored
for b in range(1, LenrowexxS):
    rowexxSS1 = rowexxS[b]
    rowexxSS.append(rowexxSS1)
rowexxSS[:] = [a-1 for a in rowexxSS]
elemnumS = []
for i, j in zip(rowexxSS, rowsxxS):
    for rowOfCellObjects in Sheet['B' + str(j):'B' + str(i)]:
        for cellObj in rowOfCellObjects:
            elemnumS1 = cellObj.value
            elemnumS.append(elemnumS1)

LenE = len(elemnumS)
for a, b in zip(range(1, Len), range(0, LenE)):
    c = Exxsheet.cell(row=a, column=6)
    c.value = elemnumS[b]

print("Length of elemnum for Sxx =", Len)
#this is to fill the integration points in the new excel file
intgptS = []

for i, j in zip(rowexxSS, rowsxxS):
    for rowOfCellObjects in Sheet['c' + str(j):'c' + str(i)]:
        for cellObj in rowOfCellObjects:
```

```
            intgptS1 = cellObj.value
            intgptS.append(intgptS1)


LenintgptS = len(intgptS)
for a, b in zip(range(1, LenintgptS), range(0, LenintgptS)):
    d = Exxsheet.cell(row=a, column=7)
    d.value = intgptS[b]

#this is to fill the Exx in the new excel file
Sxx = []
for i, j in zip(rowexxSS, rowsxxS):
    for rowOfCellObjects in Sheet['D' + str(j):'D' + str(i)]:
        for cellObj in rowOfCellObjects:
            Sxx1 = cellObj.value
            Sxx.append(Sxx1)
LenSxx = len(Sxx)
for a, b in zip(range(1, LenSxx), range(0, LenSxx)):
    e = Exxsheet.cell(row=a, column=8)
    e.value = Sxx[b]

#  For the Sxx of the LAST STEP there is a separate loop for
element number, integration points & Sxx
LenrowsxxS = len(rowsxxS)
rowsxxSS = []
for x in range(1, LenrowsxxS):
    rowsxxSS = rowsxxS[x]

elemnumSL = []
for rowOfCellObjects in Sheet['B' + str(rowsxxSS):'B' +
str(Sheet.max_row)]:
        for cellObj in rowOfCellObjects:
            elemnumSL1 = cellObj.value
            elemnumSL.append(elemnumSL1)

Len = len(elemnumSL)
Q = LenE +1
R = Len + LenE
for a, b in zip(range(Q, R), range(0, Len)):
    c = Exxsheet.cell(row=a, column=6)
    c.value = elemnumSL[b]

print("Length of elemnum for last Sxx =", Len)
#this is to fill the integration points in the new excel file
intgptSL = []

for rowOfCellObjects in Sheet['c' + str(rowsxxSS):'c' +
str(Sheet.max_row)]:
        for cellObj in rowOfCellObjects:
            intgptSL1 = cellObj.value
            intgptSL.append(intgptSL1)
```

```
LenintgptSL = len(intgptSL)

Q = LenintgptS +1
R = LenintgptSL + LenintgptS
for a, b in zip(range(Q, R), range(0, LenintgptSL)):
    d = Exxsheet.cell(row=a, column=7)
    d.value = intgptSL[b]

#this is to fill the Exx in the new excel file
SxxL = []
for rowOfCellObjects in Sheet['D' + str(rowsxxSS):'D' +
str(Sheet.max_row)]:
        for cellObj in rowOfCellObjects:
            SxxL1 = cellObj.value
            SxxL.append(SxxL1)

LenSxxL = len(SxxL)
Q = LenSxx + 1
R = LenintgptSL + LenSxx
for a, b in zip(range(Q, R), range(0, LenSxxL)):
    e = Exxsheet.cell(row=a, column=8)
    e.value = Sxx[b]

Exxbook.save("Exx & Sxx book.xlsx")
```

Bibliography

[1] Beatrice Belletti, Rita Esposito, and Joost Walraven. Shear capacity of normal, lightweight, and high-strength concrete beams according to model code 2010. ii: Experimental results versus nonlinear finite element program results. *Journal of Structural Engineering*, 139(9):1600–1607, 2012.

[2] Morten Engen, Max AN Hendriks, Jochen Köhler, Jan Arve Øverli, and Erik Åldstedt. A quantification of the modelling uncertainty of non-linear finite element analyses of large concrete structures. *Structural Safety*, 64:1–8, 2017.

[3] P Evangeliou. Probabilistic nonlinear finite element analysis of reinforced concrete beams without shear reinforcement. 2016.

[4] FIB. Model code 2010, 2010.

[5] PG Gambarova. Sulla trasmissione del taglio in elementi bidimensionali piani di ca fessurati. *Proc., Giornate AICAP*, pages 141–156, 1983.

[6] Max AN Hendriks, Ane de Boer, and Beatrice Belletti. Guidelines for nonlinear finite element analysis of concrete structures. *Rijkswaterstaat Technisch Document (RTD), Rijkswaterstaat Centre for Infrastructure, RTD*, 1016:2012, 2012.

[7] YR Rashid. Ultimate strength analysis of prestressed concrete pressure vessels. *Nuclear engineering and design*, 7(4):334–344, 1968.

[8] Jan Gerrit Rots. Computational modeling of concrete fracture. 1988.

[9] Joost Cornelis Walraven. Aggregate interlock: a theoretical and experimental analysis. 1980.

[10] Yuguang Yang and R.T. Koekoek. Measurement report on the transition between flexural and shear failure of rc beams without shear reinforcement. Technical report, 2017.

[11] Yuguang Yang, Joop den Uijl, and Joost Walraven. Critical shear displacement theory: on the way to extending the scope of shear design and assessment for members without shear reinforcement. *Structural Concrete*, 322(10):891–921, 2016.